



MONASH MOTORSPORT FINAL YEAR THESIS COLLECTION

DESIGN, MANUFACTURE AND TESTING OF SUSPENSION FOR A FORMULA SAE CAR

Adam Mapson - 2011

The Final Year Thesis is a technical engineering assignment undertaken by students of Monash University. Monash Motorsport team members often choose to conduct this assignment in conjunction with the team.

The theses shared in the Monash Motorsport Final Year Thesis Collection are just some examples of those completed.

These theses have been the cornerstone for much of the team's success. We would like to thank those students that were not only part of the team while at university but also contributed to the team through their Final Year Thesis.

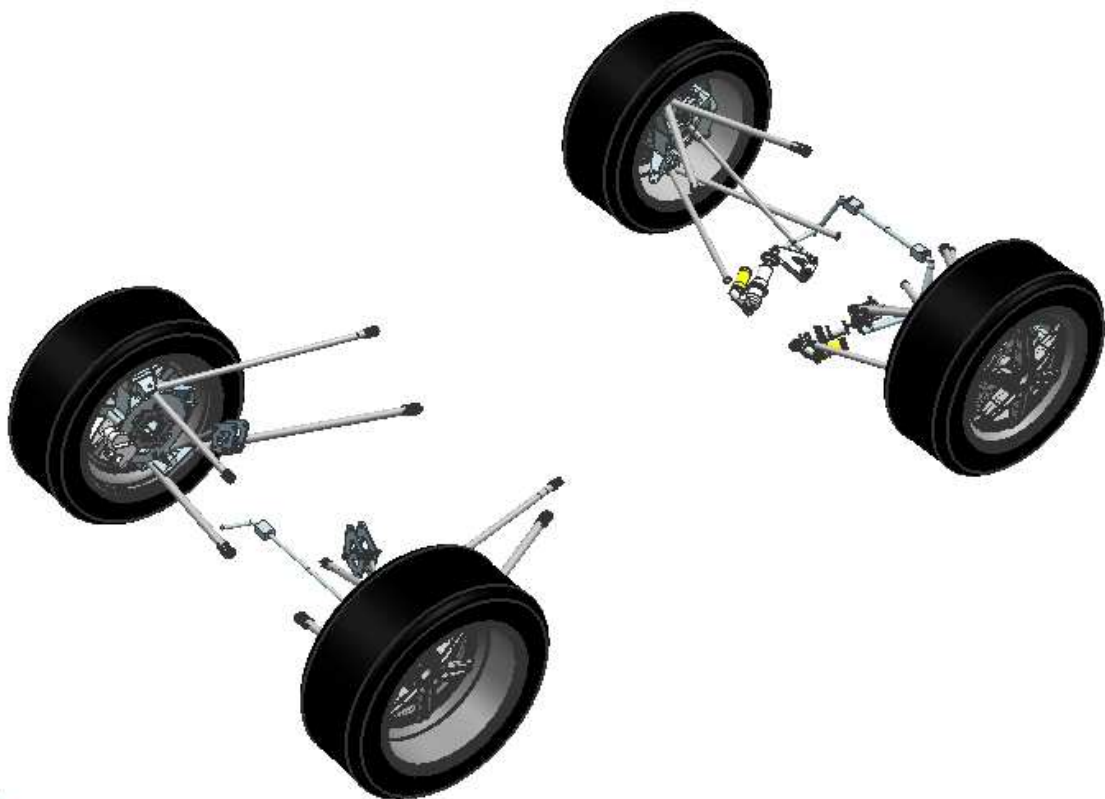
The purpose of the team releasing the Monash Motorsport Final Year Thesis Collection is to share knowledge and foster progress in the Formula Student and Formula-SAE community.

We ask that you please do not contact the authors or supervisors directly, instead for any related questions please email info@monashmotorsport.com

DESIGN, MANUFACTURE AND TESTING OF SUSPENSION FOR A FORMULA SAE CAR

ADAM MAPSON

SUPERVISED BY: DR SCOTT WORDLEY



SUMMARY

This report details the design, manufacturing and testing of a suspension system for Monash's 2011 Formula SAE car. The car was a 'clean sheet' design, built around parameters determined through a newly devised simulation. The resulting package was smaller and lighter than previous designs, with a significant increase in aerodynamic downforce. A suspension system had to be designed to suit, with a strong focus on manufacturability to meet a strict and early deadline. An appropriate degree of analysis was carried out to generate a reliable, nearly trouble free system. Testing to date has shown a marked performance improvement through suspension testing, and the completed car promises to be Monash's most competitive to date.

TABLE OF CONTENTS

1.	Introduction	5
2.	Competition Overview	6
3.	Vehicle Dynamics	6
	3.1 Car Axes	6
	3.2 Tyres	7
	3.3 Suspension Kinematics	13
	3.4 Overview of Suspension Layouts	17
	3.5 Springs and Dampers	20
	3.6 Inertial Effects	21
	3.7 Design Compromises	21
4.	Design Goals	23
	4.1 Lap Simulation and Concept Generation	23
	4.2 Load Cases	25
	4.3 Analysis Methods	26
	4.4 Reliability	27
	4.5 Adjustment and Serviceability	27
	4.6 Weight	28

5.	Design Constraints	29
5.1	Manufacturing	29
5.2	Competition Rules	31
6.	Design Outline	32
6.1	Tyre Choice	32
6.2	Layout	37
6.3	Kinematics	37
7.	Component Design	39
7.1	Damper Choice	39
7.2	Uprights and Hubs	41
7.3	Brake System	47
7.4	Wishbones	51
7.5	Bellcranks	53
7.6	Anti Roll Bars	55
8.	Testing	55
8.1	Shakedown Testing	56
8.2	Steady State Tuning	56
8.3	Damper Testing	56
9.	Failures and Suggested Improvements	56
10.	Conclusions	58
11.	Acknowledgements	58
12.	References	58
13	Appendices	59
13.1	Appendix A: 3D Vector Force Analysis	60
13.2	Appendix B: Relevant Suspension Rules	65

13.3	<i>Appendix C: MATLAB Tyre Data Treatment</i>	68
13.4	<i>Appendix D: Wishbone Stress Calculations</i>	77
13.5	<i>Appendix E: Hub Calculations</i>	83
13.6	<i>Appendix E: Brake Calculations</i>	84

1. INTRODUCTION

Formula SAE is the world's foremost student engineering design competition. Monash University has fielded an entry in the Australasian competition every year since the inaugural competition in 2000, recently achieving wins in the 2009 and 2010 competitions.

The role of suspension on a Formula SAE car, or any race car for that matter, is to control the angle, position and velocity of each wheel to maintain a high value of mechanical grip, while transmitting the forces generated by the tyres to the chassis. The handling of the car can be modified by subtly changing the kinematics of the suspension linkages and relative stiffnesses of springs, bars and dampers (Smith 1995, p64.) Formula SAE is held on tight, winding tracks, making the handling of the car, and by extension the suspension, critical in gaining competition points.

The major parts of the suspension system on almost every Formula SAE car are the tyres, wheels wishbones, uprights, hubs, push and pull rods, bell cranks, springs, dampers and anti roll bars. All these parts vary in the degree of difficulty to design and manufacture, but failure in almost any of them could have serious consequences. The design of these parts must therefore be undertaken in the knowledge that the safety of drivers depends on the job being done well.

In recent years, the focus of the competition has changed in accordance with societal demands for greater fuel efficiency and sustainable technology. To this end, the Society of Automotive Engineers (SAE) have increased the points value of fuel economy in the 'endurance' part of the competition, a move that favours lightweight cars with small capacity engines, in contrast to the relatively heavy and high powered cars that have proved successful for Monash in recent competitions. The competition organisers have also changed the rules to reduce the limitations on cars using aerodynamic enhancements, with substantial implications for Monash as one of the leading 'wing car' teams.

2010 saw the team develop a basic Excel based competition points simulator (Webb, 2012) to allow a reasonable comparison between different concepts. Based on the results of this simulator the team chose to use a single cylinder KTM 450 SX-F engine to power the car for the 2011 season and several seasons beyond, replacing the Honda CBR 600RR four cylinder engine used in every Monash car to date. The narrower footprint of this engine has allowed the team to reduce the overall width of the car, which can show a measurable time advantage through the tight slaloms and lane changes of typical Formula SAE tracks. Despite the drag penalty, it can be shown downforce can be increased to a very high level before drag and the consequently increased fuel consumption start to detract from its traction advantages in overall points terms. The team will therefore be taking full advantage of the more liberal 2011 aero rules and increasing downforce by a factor of approximately two.

These and other fundamental changes from the previous car required a completely new suspension design to suit. This report reviews the large body of vehicle dynamics theory that has built up since the invention of the automobile, then focuses on the mechanical layout of modern suspension systems. The report then goes through the aims and constraints of the project, detailing the design process for each major part in turn. The report concludes by analysing the successes and failures of the completed system in practice, and suggests improvements for future designs.

2. COMPETITION OVERVIEW

Formula SAE is an engineering design competition for tertiary students. Competing university teams design and construct small scale racecars to race in a sanctioned competition at the end of the school year. The competition involves almost 500 teams worldwide, and takes place in a number of countries, including Australia. The enduring success of the competition comes from its foundation in motorsport; racing the cars on track provides an objective measure of the quality of the design work put into each entry, and frames the work in an exciting medium.

The stated aim of the competition is to design an autocross style racecar for the amateur weekend racer. The nature of the competition and the rules imposed on the teams cause entries to deviate slightly from this aim in many cases, and Formula SAE cars have developed into a wide range of layouts.

The competition is split into two parts - static and dynamic events. In the static events, each team's car is judged as a commercial manufactured product. Cars score points for their design justifications, marketing, and cost and manufacturing considerations. The static events had relatively little effect on the design of the car in 2011, although reducing costs and improving the appearance of the cars can offer some advantage. The dynamic events are all timed motorsport events, including a 75m acceleration run, skidpan, short circuit time trial and a 22km endurance run. The endurance run is a particularly effective test for vehicles - in the 2010 Australasian competition, only ten entrants out of 27 finished the endurance event. Monash entries have finished every event, including endurance, in every competition entered for the last eight years running.

To ensure safety, the competition organisers control competition speeds by laying out tracks with a large number of tight obstacles, such as slaloms, lane changes and hairpins; these features also match the 'autocross' style of competition set out by the rules. This places a strong emphasis on transient and ultimate cornering performance, and requires a car which doesn't require too much physical effort to drive; hundreds of tight corners in an endurance run can take a toll on drivers. To add some complexity and modern relevance to the competition, an increasing emphasis is being placed on rewarding teams with points for fuel economy in the endurance event. This requires careful consideration of the overall design of the car, where power must be traded off for weight and fuel economy.

3. VEHICLE DYNAMICS

3.1 Car Axes

For many explanations throughout this report, it is convenient to describe directions in terms of a common set of coordinates. As is conventional in vehicle dynamics, this report will use a set of Cartesian coordinates with the longitudinal x axis aligned front to rear, y axis from right to left and z axis positive upward. The origin of this coordinate system is placed along the front axle line, in the middle of the front tyres, at ground level. This is shown in figure 1.



Figure 1: CAD model of the 2011 car with x, y and z axes.

3.2 Tyres

3.2.1 Physical Behaviour

The mechanisms by which tyres generate grip are complex, and cannot be ignored in the design of any vehicle suspension. The contact patch of a tyre is the portion of the tyre in contact with the ground at any point in time. The tyre does more than just 'flatten' at the contact patch; it deforms laterally, longitudinally and torsionally in response to the loads applied to it. In the contact patch itself, the tread deforms in a characteristic way. Figure 2 shows a view of a contact patch as it might be seen from below.

Tread begins deforming before it enters the contact patch. Within the contact patch, the tread is aligned with the slip angle of the tyre; this is never the same angle as the orientation of the tyre as long as the tyre is generating lateral grip. The deflection of the tread is at its highest value at the rear of the contact patch, and as the tread is lifted out of the contact patch by the rotation of the wheel, the tread 'snaps back', giving a sharp angle to the trailing tread deformation. On racing tyres, the slip angle can increase to angles of ten degrees before the tyre reaches its peak lateral force; to an observer, a car with such a high slip angle would appear to be sliding, despite gripping the road as hard as is possible.

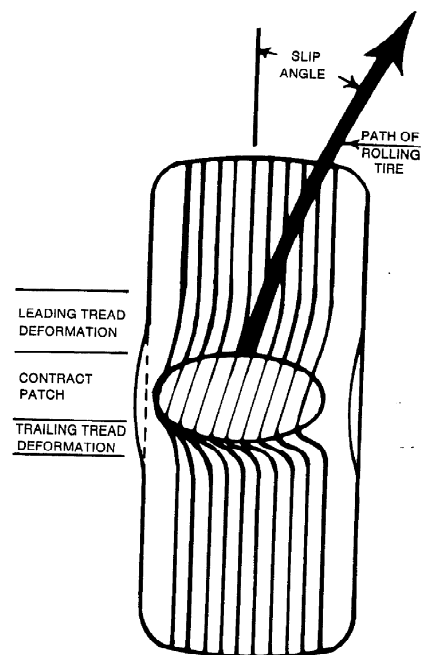


Figure 2: Tyre producing lateral grip, as seen from below. The definition of slip angle is represented here; it is the difference between the steered angle of the tyre and the actual path followed by the tyre. (Smith, p28)

Deforming the tread in this way obviously results in a lateral reaction force (in figure 2, the force applied to the tyre by the ground is to the right of the diagram). Less obviously, the deformation and resulting force is greater towards the rear of the contact patch, resulting in a moment in the opposite sense to the rotation of the wheel - this is usually termed 'self aligning torque'. This has significant implications for driver effort and feedback.

A similar mechanism of grip generation occurs in the longitudinal sense; a degree of longitudinal 'slip' is required to generate longitudinal grip in acceleration or braking, called the slip ratio.

Camber is the inclination of the tyre with respect to the ground, as shown in figure 3.

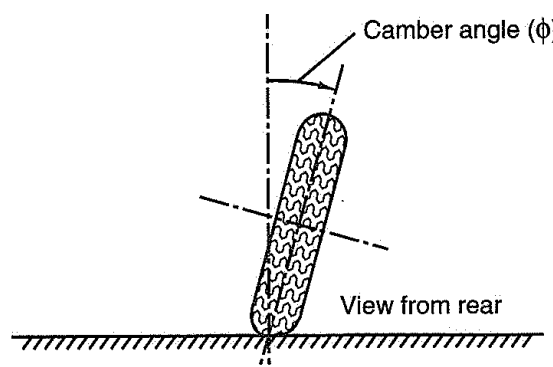
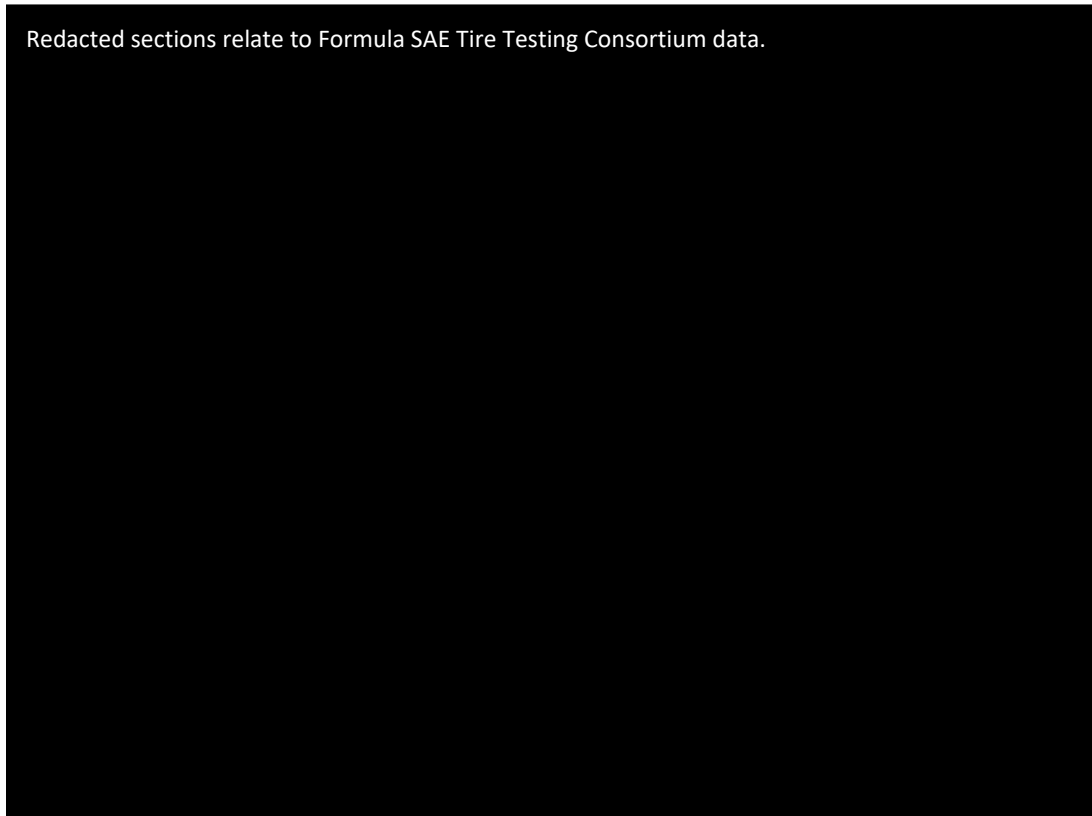


Figure 3: A cambered tyre. Although unclear in this diagram, it is conventional to define camber angle as negative toward the centre of the car. (Milliken, p47)

A rolling tyre set at a nonzero camber angle will generate a thrust in the direction of its lean. This is useful to a designer, as the thrust is roughly proportional to the normal load on the tyre, and as weight

transfers to the outside wheels in a maneuver this can provide increased overall cornering potential. There is a trade off here - a cambered tyre will not provide as much longitudinal thrust as an uncambered one, and this is important when choosing a suspension type for a particular application. Camber thrust peaks at a particular slip angle depending on the tyre, and will then reduce with further increasing angle. Figure 4 gives an example from the tyre data treatment in a later section of the report.

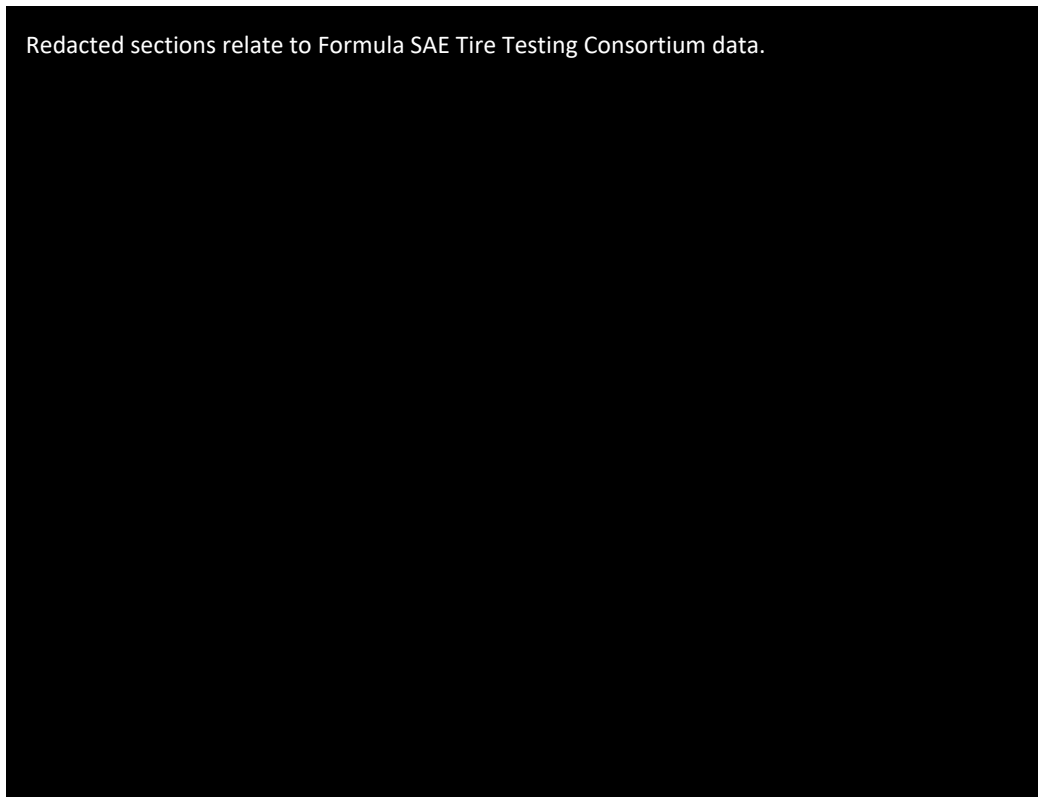
Figure 4: Effect of inclination angle on peak lateral force (Goodyear D2696)



Tyre performance is often quoted in terms of coefficient of friction; a dimensionless quantity relating peak lateral or longitudinal force generated by a tyre to a normal load acting upon it. Much of the scope for tuning a race car comes from the inherent load sensitivity of the tyres - the coefficient of grip is not a constant but a function of normal load, and is almost always a decreasing function.. Figure 5 shows this effect for the Goodyear D2696:

All tyres are temperature sensitive; racing tyres in particular are designed to work towards the limit of their performance most of the time, and will produce substantially less grip before they are heated up to their operating temperature. Race tyres generally wear much more quickly than road tyres.

Figure 5: Effect of normal load on peak coefficient of friction, as seen in constrained testing.



3.2.2 Modelling Literature

A large volume of literature is dedicated to reconciling the real physical behaviour of tyres with mathematical and computational models that can be easily extended to simulations. The reasons for this are obvious; being able to accurately simulate the behaviour of the tyre in the context of a whole car (or bicycle, truck, or aircraft) allows designers to make design decisions without the need for extensive prototyping and physical testing. Hans Pacejka, a prominent name in the theory, testing and modelling of tyre behaviour, categorises tyre models according to their degree of empirical and theoretical focus in figure 6 below.

In the same order as Pacejka presents them, the categories of model are:

From experimental data only: Predictions about tyre performance are based only on curve fits on experimental data. These methods have a very high level of fidelity, as every model prediction is based directly on empirical data. These methods are limited, however, as no inferences are made about tyre behaviour with input conditions outside of those tested; a vehicle simulation model based off empirical curve fits would have to use data points from a very large number of tests, or suffer from poor resolution. As laboratory tyre testing is very expensive, the latter issue could be expected to be the limiting factor.

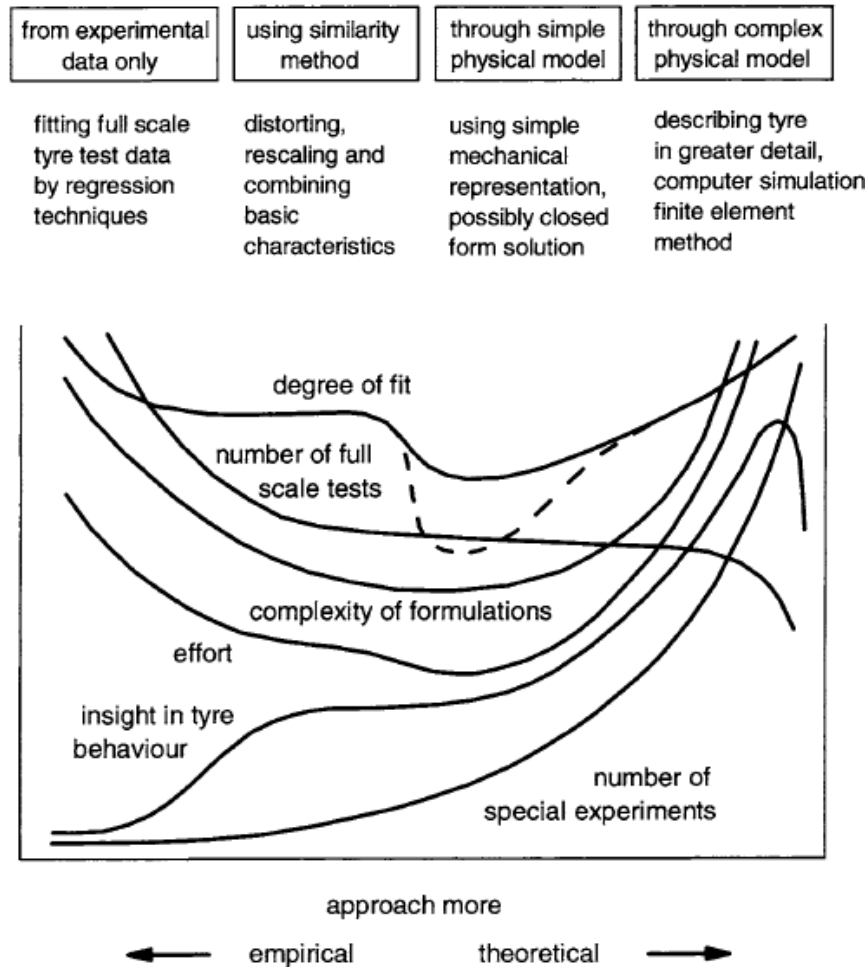


Figure 6: Characteristics of different methods of tyre modelling, sketched quantitatively (Pacejka, p82)

Using similarity method: These models are also based off curve fits of empirical data. Test costs can be reduced by relating tyre forces and moments to slip variables using scaling factors; these factors are tyre characteristics such as cornering stiffness and peak values. The results can thus be reduced to a set of data to which a single curve can be fit, for a range of input conditions such as normal loads and camber angles. Condensing the data in this way reduces the fidelity of the model output, as scaling factors can't account perfectly for every difference in tyre response to input conditions. However, this type of model provides a function output that is continuous with respect to inputs, and is thus ideally suited to the pseudo steady state analysis of a full car. This is the type of tyre data treatment favoured by Milliken (Milliken, p473).

Through simple physical model: It can be advantageous to reduce a real tyre to a simple physical model that can be interrogated to make predictions. The brush type model (Svendenius & Gafvert 2004, Sorniotti & Velardocchia 2008) has been popular for decades, and provides good insight and moderately good performance predictions. The string type model (Liu et al 2007) is of similar use. A particular advantage of this type of modelling is the ability to make predictions about the dynamic behaviour of

tyres, which the empirical models lack. Trevorrow (2006), an alumnus of Monash's Formula SAE team, developed one such model for his PhD thesis.

Through complex physical model: The rapid contemporary improvements in finite element analysis make it possible to accurately predict the behaviour of tyres under steady state and dynamic conditions (Narasimha et al 2007). This can be done with an enormous degree of insight into the true physical behaviour of the tyres and its causes; however, a large degree of computational power is required to solve these simulations, and they are less amenable to full car modelling than empirical or simple physical models.

Of these types, the first two are of interest to Monash in 2011. A large volume of high quality tyre data is available to the team, acquired through the Calspan tyre test facility. This facility is described below:

3.2.3 Calspan Tyre Testing Facility

The Calspan tyre research facility (TIRF) is a test rig consisting of a steel belt moving between two large diameter rollers. The facility is one of very few flat belt tyre testers in the world, and has been used for decades in analysing tyres for the aerospace and ground transport industries. The tyre being tested is mounted on a steel rim, with the height of the rim and its angle controlled in three dimensions. The belt can be covered with friction altering materials, including stones to represent reasonably realistic road conditions, and water to a depth of 10mm.



Figure 7, Calspan tyre test rig (left) and wheel being tested (right). Note the rotary union connected to control tyre pressure.

The rig is equipped with 21 sensor channels, able to measure forces and moments in three dimensions, as well as wheel speed, tyre temperatures across the tread, ambient temperatures, and tyre pressures. Some of these sensors form part of control systems that maintain applied forces, moments, angles and tyre pressures at desired level, usually set to match a test matrix.

Despite efforts to simulate realistic road conditions with the test belt, even with a simulated 'stoned' surface, the data produced by Calspan predict a significantly higher level of performance than is ever seen in practice. The data must therefore be used with some care. The similarity method described in the previous section provides some scope to scale the data to more typical values, but some fidelity is lost in this process.

The tyre data obtained from the Calspan facility is provided to students as raw ASCII and Matlab data, with accompanying analysis for some rounds. The data can be used in a wide variety of ways - tyre choice, determining kinematic parameters, and performing full vehicle performance simulations are chief among them.

3.3 Suspension Kinematics

The motion of the car is intimately related to the position and angle of the linkages through which tyre forces react. Some of the more relevant suspension kinematic parameters and their effects are listed below:

3.3.1 Roll Centre

The roll centre is so named as it is the geometric point in the y-z plane about which the sprung mass of the car rotates as the car rolls. The physical implication of this is that this is also the point into which forces from the tyres react into the chassis; this is an obvious phenomenon in beam axle type suspensions, where the roll centre is the point where the Panhard rod or Watt's linkage attaches to the chassis, shown in figure 8 below;

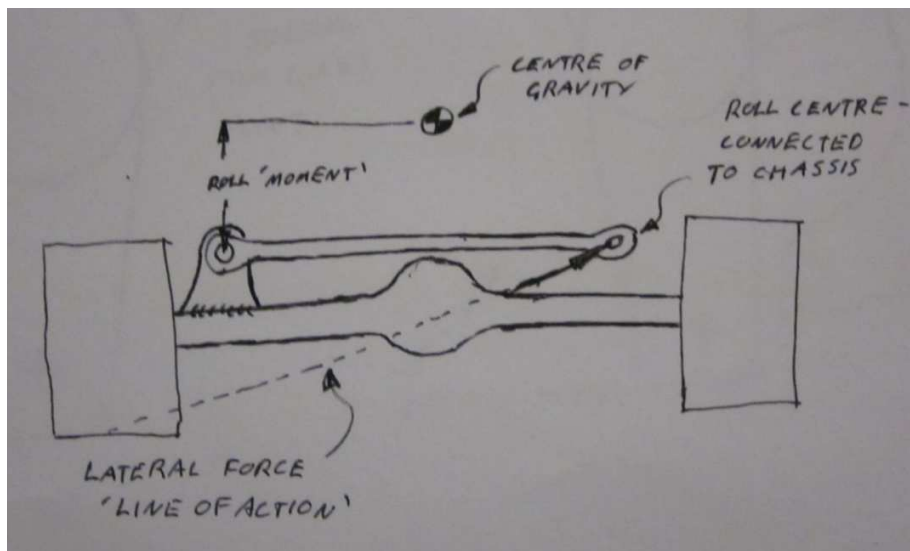


Figure 8: Roll centre and roll moment on a vehicle equipped with a beam axle located with a Panhard rod.

Note that in figure 8, the Panhard rod is reacting the tyre load at a fairly high point in the chassis, above the axle line (it's more likely that this point would be as close as possible to the axle line to minimise lateral movement of the beam). This implies a high roll centre, which necessarily imposes an extra

vertical 'jacking' force onto the chassis. This would cause the chassis to lift in a cornering maneuver, raising the CG height of the chassis and in turn reducing the stability and overall grip of the car.

Note also that roll centre is very close to the CG in the z direction. This vertical difference between these two points is often referred to as the 'roll moment' in vehicle dynamics literature (Smith, p30); this can be misleading, as the moment acting on the chassis is in fact the product of this distance and the lateral force being reacted. The relatively small roll moment in figure 8 would generate a small roll angle as the car corners; this equates to a relatively responsive car, as it would spend little time in a transient mode as the car assumes its 'steady state' roll angle. The tradeoff to this is that the angle of the linkage would couple the vertical motion of the sprung and unsprung masses more than it would if it were horizontal; importantly, this means that the suspension links take some of the vertical load in cornering, adding of element of 'geometric weight transfer' and reducing elastic weight transfer; that is, load that transfers through the springs. The consequence of this is a reduction of the responsiveness of the suspension to changes in the road and a reduction in the overall mechanical grip in cornering. This vertical load also has the effect of lifting the chassis, increasing the CG height and usually to the detriment of the car's kinematics.

Although less obvious, an analogous point exists for all suspension arrangements, including modern double wishbone suspension. This point is usually found geometrically as in figure 9.

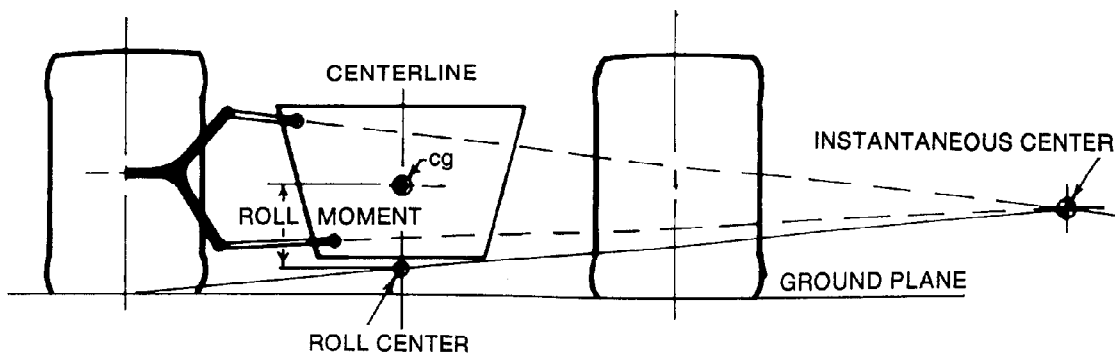


Figure 9: Geometric determination of the roll centre and roll moment for a double wishbone suspension system with equal wheel displacements (Smith, p30)

In the case of double wishbones, it should be noted that the roll centre moves laterally and vertically relative to the chassis as the suspension members move. Too much roll centre migration can cause the car to feel unpredictable and difficult to control; tracking the motion of roll centres in all but the simplest suspension layouts is no simple matter, and a range of kinematic software now exists to aid designers.

3.3.2 Pitch Centre

The pitch centre is the longitudinal analogue of the roll centre. This point defines how the car dives and squats in response to acceleration and braking manoeuvres. As with roll centres, the location of the pitch centre relative to the centre of gravity of the car controls the total dive or squat angle in steady state, as well as the relative amounts of elastic and geometric weight transfer.

In the case of double wishbones, inclining the wishbones to converge toward the centre of the car in the longitudinal plane generates so called 'anti squat' and 'anti dive' geometry when applied to the front and rear of the car respectively. Reducing the squat and dive behaviour of the car makes a car respond more quickly to changes in acceleration, in the same way as a high roll centre in the lateral plane. This must be considered against the effect of supporting part of the car's mass directly through the suspension links, reducing the overall mechanical grip of the vehicle and translating to a large degree of harshness felt by the driver.

3.3.3 Virtual Swing Arm Length

Swing axle type suspension, as discussed in section 3.3.2, pivot about a single point on the chassis in the lateral plane. The distance between the centre of the wheel and the pivot is referred to as the swing arm length, and the relationship between the length of this arm and the tyre camber is obvious - camber change for a given degree of wheel movement is inversely proportional to the arm length.

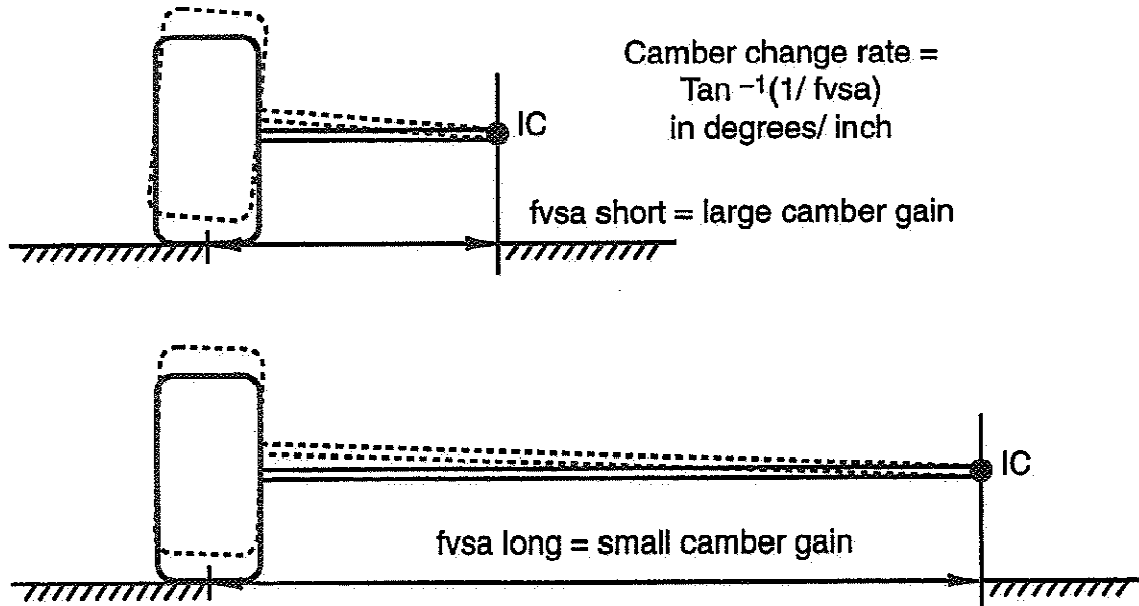


Figure 10: Camber change as a function of swing arm length for a pure swing axle setup (Milliken, p380)

An analogous value can be assigned to other suspension types, referred to as virtual swing arm length or VSAL. This must be designed with consideration of roll centres and CG height to ensure that appropriate camber is maintained on each wheel in cornering maneuvers. Virtual swing arm lengths, in combination

with spring and pitch centre settings, determine the degree of camber gained or lost by the wheels in longitudinal manoeuvres. As with any independent suspension, a rear wheel drive will experience camber gain under acceleration, usually an undesirable side effect of the configuration.

3.3.4 Steering Geometry

The front steering geometry has an important role to play in the transient response of the racecar, as well as the feedback received by the driver from the road. These three kinematic attributes are heavily dependent upon one another, as shown in figure 11:

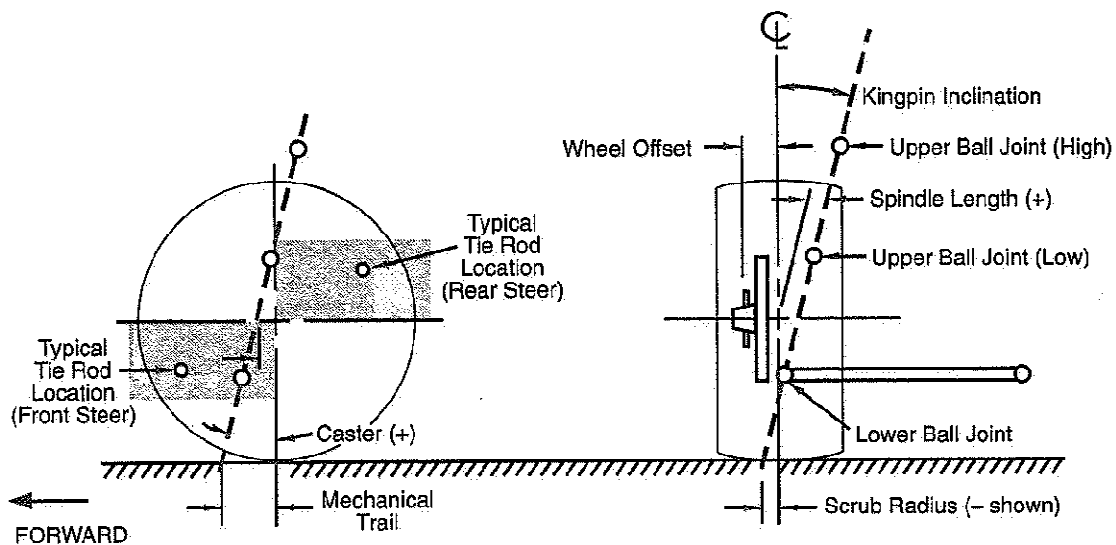


Figure 11: Front steering geometry, shown from the side and rear of the car. The proximity of the parts in this diagram demonstrates some of the packaging compromises that have to be reached with the front suspension (Milliken, p710)

The effect of kingpin inclination is to cause the front of the car to lift as the wheels are steered. It is therefore inevitable that kingpin inclination contributes to steering effort; the weight of the car centres the wheels. Large kingpin inclinations are usually the result of a packaging compromise. Kingpin inclination also results in camber loss at the front wheels as they are steered, a condition which is almost always undesirable. The scrub radius adds a self a further self centering effect to the steering.

Caster is the kingpin analogue in the longitudinal plane, and results in camber gain in cornering; thus if packaging constraints force a non zero kingpin inclination, caster angle can be used to offset the camber loss. Unlike kingpin inclination, scrub radius has an opposite jacking effect on each front wheel - the inside wheel lifts while the outside wheel is forced down (assuming positive scrub radius.) Caster therefore generates diagonal weight transfer, unloading the inside rear wheel in cornering. Positive mechanical trail, as positive scrub radius, increases steering self centering.

3.3.5 Ackerman Steering Geometry

As a car steers, at all times it is rotating about some point towards to inside of the turn. At low speeds, and for anything but a very large radius turn, having the front wheels parallel to one another will create drag that opposes their motion. This can be offset by introducing dynamic toe out to the steering system. This can be accomplished by inclining the steering arms inwards towards the rear of the car in plan view.

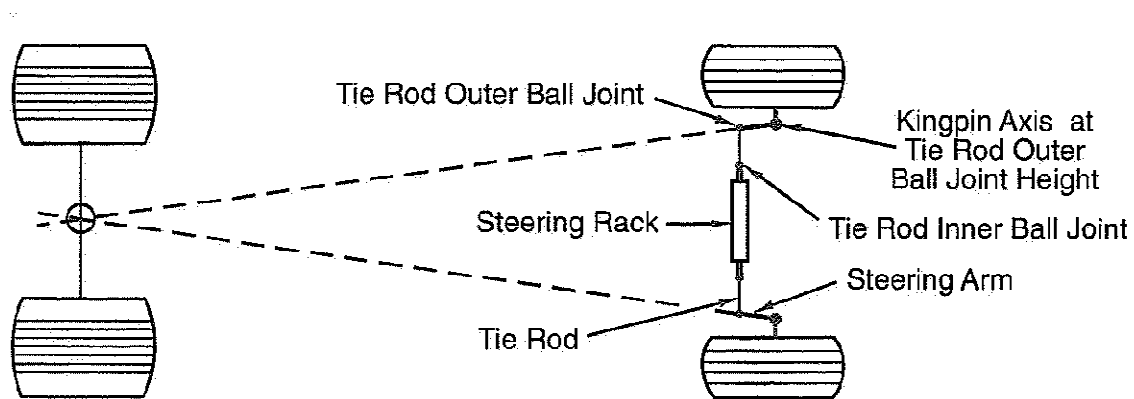


Figure 12: Pure Ackerman steering geometry. Steering wheels of this geometry will cause a larger angular change on the inside than the outside wheel. (Milliken, p720)

If the axis of the steering arms meet at the rear axle line of the car in an unsteered state, both front wheels can negotiate a corner without sliding (for small steering angles). This is usually referred to as Ackerman geometry. Under racing conditions, the large slip angles assumed by the tyres make this goal relatively meaningless; instead, Ackerman style steering is used to improve the transient response of the car and maintain appropriate steered wheel angles in steady state conditions. Typically, as the vertical load on a tyre is increased, as is the case for an outside tyre in a corner, the slip angle at which it generates a peak lateral force decreases. It is therefore optimal to have the outside wheel at a lower slip angle than the inside wheel in steady state cornering. Steering geometry is often referred to in terms of '% Ackerman'; the definition of this varies between sources.

3.4 Overview of Suspension Layouts

Innovation over more than a century of automotive development has led to a variety of suspension types in common use. The only common feature is that each type must constrain each wheel in six degrees of freedom - six translational, and six rotational. One of these constraints includes a spring and damper to control wheel movement.

3.4.1 Beam Axle

The beam axle is a carryover from centuries of horse drawn cart design. The front and rear wheel pairs are fixed to one another by means of a solid structure, or 'beam'. The beam can include the differential carrier and driveshafts, as is common in rear suspension designs, or can be a completely independent structure. Beam axles must be located laterally with respect to the chassis, often with a Watts linkage or Panhard rod. Longitudinal location is accomplished with an axial link on each side of the beam, and the beam is further connected to the chassis through a pair of springs and dampers; often longitudinal or transverse leaf springs are used, but coil springs are equally applicable.

Generally, beam axles react lateral force at axle height, causing the roll centre to lie at the same height. This can generate substantial jacking forces, causing the chassis to 'lift' in a cornering maneuver. Due to the springing action of the tyres, the beam axle is able to roll to a small extent in cornering, causing the outside wheel to go into positive camber and lose overall grip. Beam axles, particularly rear axles which include a differential, add substantial unsprung weight to the wheel pair, reducing the ability of the wheels to respond dynamically to variations in the road surface. Any bump in the track disturbs the pair of wheels, rather than one as with independent suspension. The advantage of beam axles is in simplicity of manufacture (only six accurate chassis points are needed per end, rather than ten), a low parts count, and being able to move through a very long range of wheel travel without the extreme kinematic changes that could be expected with other suspension types. Beam axles nearly eliminate camber change in longitudinal manoeuvres, which can be an advantage.

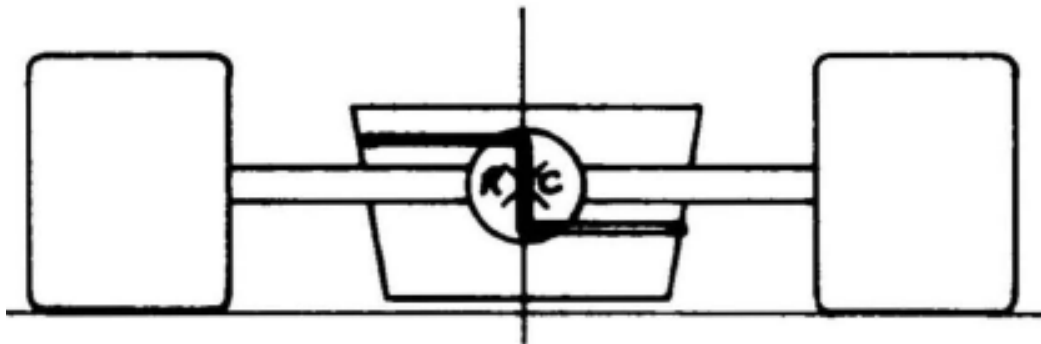


Figure 13: A beam axle with lateral location provided by a Watt's link. The roll centre is located in the centre of the middle bar (Staniforth, p61)

De Dion type suspension is a slight variation on the beam axle, in which the differential is hard mounted to the chassis and drive is transferred through halfshafts to the wheels. This allows the beam to be mounted lower on the car, reducing the roll height. The wheels can also be mounted to the beam with a degree of negative camber, making up for the positive camber usually encountered in roll on a beam axle.

3.4.2 Swing Axle

An early form of independent suspension, the swing axle forms a structure that connects each wheel to the chassis through a single pivoting axis. Swing axles have a fearsome reputation for their poor

handling qualities; typically they generate very high jacking forces due to their high roll centre, experience large and nonlinear camber and track changes, and in extreme cases, can have the wheel 'tuck under' in cornering (Smith, p41). Mounting the swing axle low on the chassis can solve some of these problems; however, this suspension type has been largely abandoned in favour of double wishbones.

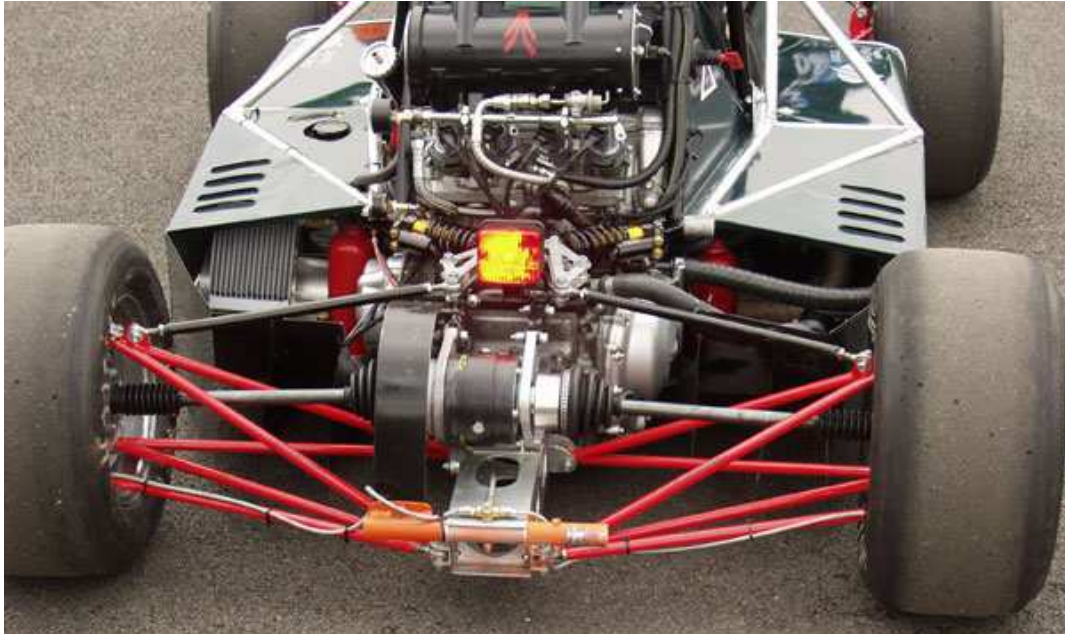


Figure 14: Low mounted swing axles on the rear suspension of Lancaster University's entry in the 2010 Formula Student UK competition. Swing axles are very unusual in student competitions.

3.4.3 Macpherson/Chapman Strut

The Macpherson strut arrangement (Chapman strut when used on the rear of the car) has the lower section of the damper strut integral with the upright, such that it moves with the wheel in the y-z plane. The Macpherson strut is favoured among passenger cars for its ability to package neatly into the corner of a sedan, leaving more room for passengers and luggage. For racing, however, the strut cannot package easily into wide racing wheels; particularly on a front suspension design, this forces a large scrub radius or kingpin inclination to be imposed, to the detriment of steering effort and drivability. Macpherson struts also carry the penalty of a high centre of gravity, and a requirement for the damper to actuate despite a large bending load across the seals; this can be expected to result in a heavy assembly.

3.4.4 Double Wishbone

Invented in the early part of the 20th century, the double wishbone suspension arrangement became the performance car standard after the 1950s, when Chapman and Broadley recognised the need to make wishbones unequal length and non parallel to extract the full potential of the arrangement. With appropriately selected dimensions, the double wishbone arrangement allows excellent control of

camber change in roll, low roll centres, minimal scrub (track change in bump) and reasonably linear behaviour throughout its range of motion. As with all but the beam axle suspension arrangement, a car with double wishbones will experience camber change during acceleration and braking manoeuvres. Some considerations in the design of such a system are:

-Longer wishbones are preferable; shorter wishbones will cause a large change in track width or camber, depending on the relative lengths of the upper and lower wishbones, while longer wishbones are more immune to this problem.

-Wishbones that are near parallel will experience a large change in roll centre during roll. Inclining the lower wishbone upwards to compensate for this leads to a high roll centre, thus in most cases the upper wishbone is inclined downwards to prevent this problem.

-Careful positioning of the axial toe link is needed to prevent bump steer - a change in toe with wheel displacement.

3.5 Springs and Dampers

Springs and dampers, or 'shocks' as they are commonly referred to in motoring literature, play a vital role in controlling the motion of the car. Each quarter of the car can be modeled as a pair of masses connected by a spring and damper. The tyre, wheel, upright, hubs, brakes (if mounted outboard) and some portion of the links are referred to as the unsprung mass, although the tyre acts as a spring element to some degree. The remainder of the mass of the car is referred to as the sprung mass. The spring and damper connect the two masses in parallel. The first function of this arrangement is to isolate the sprung mass from disturbances in the road; an improperly tuned system would allow a large variation in normal load on the tyre, reducing its grip. The measure of this behaviour is transmissibility - the degree to which the motion of one mass affects the other. Large values of transmissibility correspond with large variations in tyre normal load.

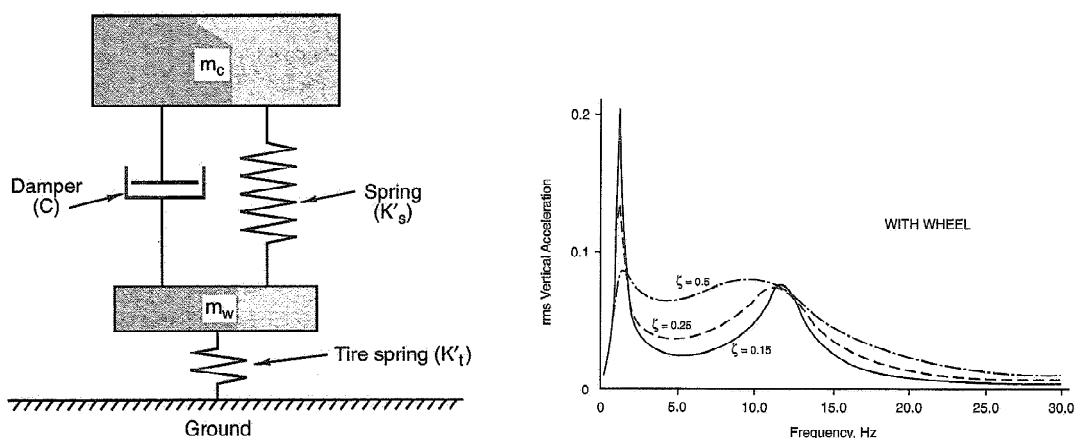


Figure 15: Schematic representation of the sprung mass and unsprung mass connected to the ground through spring and damper elements. The unsprung mass of a Formula SAE car is typically one quarter of the total mass,

making a large pair of transmissivity peaks inevitable. The second peak represents high speed transmissivity, which contributes to the 'harshness' felt by drivers of high performance cars.

With negligible unsprung mass, the frequency response of the quarter car model has a single peak, as is the case for the familiar spring-mass-damper system. The peak corresponds with an oscillatory (ringing) response from the system, which is damaging to grip. The inclusion of a second, unsprung, mass introduces a second degree of freedom, with an accompanying frequency response peak. With increasing unsprung mass, it becomes more difficult to find a good compromise between the two damaging peaks. A peak in transmissivity is impossible to avoid with any reasonable damping ratio. For racing applications, the dampers are usually set up such that the high transmissivity occurs at frequencies above those representative of large scale road undulations (typically 1-2Hz). This leads to a level of 'harshness' due to the high transmissivity at frequencies representing road surface roughness.

Dampers are not used in isolation, and the response of all four corners of the car as a whole system have a significant effect on the transient behaviour of the car. As the car changes direction, the response of the springs is proportional to displacement - this means that the spring's contribution to the normal load on the tyre and the final attitude of the car will not be felt until steady state is reached. The response of the damper depends on the velocity of the unsprung assembly relative to the chassis, so its effect is immediate. Adjustment of the dampers can therefore affect the balance of grip between the front and rear wheel pairs during transients, and corner entry understeer and oversteer can be controlled in this way.

3.6 *Inertial Effects*

The mass of a car has a large influence on its behaviour. Heavier cars, when not constrained by the grip limits of the tyres, will accelerate more slowly for a given amount of power, as a simple rearrangement of Newton's 3rd law can show. Mass also limits ultimate cornering and braking acceleration, although the cause is less obvious; the relationship between normal force and coefficient of friction is discussed in section 3.2.1. Because of this the mass of racecars is kept to a reasonable minimum.

The static weight of the car is distributed over all four wheels, and the distribution changes with vehicle motion. Cornering manoeuvres, for example, increase the load on the tyres on the outside of the corner while proportionally decreasing the load on the inside tyres. Braking and accelerating manoeuvres have a similar effect. The total load transfer experienced by the car is directly proportional to the height of its centre of gravity, and its effect is always a reduction in overall grip due to tyre load sensitivity, thus a low CG height is desirable in a performance car.

The moment of inertia of the car about its centre of gravity provides a measure of its resistance to changes in direction. Locating the mass of the car as centrally as possible minimizes the MOI (or yaw inertia) but there are obvious tradeoffs with mass, CG height and other concerns such as packaging.

3.7 *Design Compromises*

The suspension system of any racecar has to fulfil several distinct functions, while minimising its negative impact on other car subsystems.

As discussed in section 3.2.2, the behaviour of tyres is physically complex; while it can be analytically convenient to treat tyre forces as a point load, the effect of suspension kinematics on the position and motion of tyres and the resulting three dimensional moments and forces cannot be ignored.

In a racecar, driver comfort is not a high priority; however, it is still important to minimize the transmission of shocks from the road surface to the sprung chassis. This is a grip consideration; inappropriate spring and damper settings can cause the normal load on the tyre to vary significantly with asperities in the road surface, reducing the effective grip of the tyre. While more mechanical grip can be generated using relatively soft springs and anti-roll bars, there is a penalty to be paid in responsiveness and undesirable kinematic characteristics. A 'soft' car setup will change direction more slowly than a 'stiff' setup, and wheel displacements will often occur outside the linear range of suspension movement, causing a loss of grip and control.

To allow the car to perform to its limit in a controllable manner, the driver must be considered to be a part of the system - driver feedback and fatigue is thus a priority. Self aligning torque generally reaches a peak at a slip angle just before the total lateral grip reaches a maximum value. This causes a loss of torque at the steering wheel, giving the driver an indication of the limits of the tyres. Poor geometry choices can mask this feedback, making the car feel 'dead'. This will be discussed in more detail in the kinematic design section.

Driver fatigue can arise from poor ergonomics and suspension geometry. Good ergonomics require the shape of the cockpit and layout of controls to work well with the biomechanics of the driver; this subject is worthy of a project in itself, but will not be discussed further in this report. The tradeoff between feedback and driver effort must be considered carefully when deciding on geometry.

As with all car components, the weight of suspension components has a negative effect on the performance of the car. To further complicate matters, the location of component mass is also an important factor - in some cases, it is worthwhile to increase the weight of a component to be able to position it lower and/or more centrally in the car. The centre of gravity height is important as it is directly proportional to the amount of vertical load transferred between wheels in a maneuver, and transferring load reduces the overall grip of the car. Locating vehicle mass centrally reduces the yaw inertia of the car; yaw acceleration is inversely proportional to yaw inertia, so the reduction of yaw inertia increases the manoeuvrability of the car.

Apart from the obvious considerations of robustness, weight reduction must be weighed up against the effect of compliance. Lightweight parts generally exhibit more compliance than their heavier counterparts; this can cause undesirable kinematic changes, and adds undamped spring effects to the system. Drivers feel this as instability, and although the effects are hard to quantify directly, it is common wisdom that excessive compliance is very undesirable in racecar suspension.

To further complicate matters, the budget of the Monash team is relatively low. Spending a sizeable part of the budget on an expensive outsourced process, high performance material or a well regarded off-the-shelf part is a matter of competing for resources; the decision must be weighed up against investment in other areas where greater gains are to be made. This must be considered, in turn, against

the cost of an in house part or process in terms of manpower - although Monash is a large team, labour resources are finite.

4. DESIGN GOALS

4.1 Lap Simulation and Concept Generation

After winning two Australian championships, the Monash team had enough sponsor support and drive to build its first 'from scratch' car since 2006. A large part of the motivation to follow a new approach was the changing face of the competition; the value of fuel economy in the competition increased significantly, to force a greater emphasis on environmental considerations in the design. Although the team had had great success using a four cylinder engine of the maximum capacity allowed in the rules, it was understood that such a large engine may not have fit into an 'ideal' overall concept.

Evaluating different vehicle designs against each other was challenging, given the competing and contradictory priorities imposed by the competition. The team's approach was to write a lap simulator, that represented the car as a particle on a one dimensional path around a typical track. By estimating coefficients of friction, engine and drivetrain efficiency, drag and downforce, estimated times and scores for each event could be generated for any different concept. There was also a significant emphasis placed on generating estimates of the closest reasonable racing line through the tight slaloms of the course, as it was expected that a car with a narrower track width may have a significant advantage through these sections. This lap simulator is still being developed as the subject of a final year project to be completed mid 2012; some of the significant car parameters were based on an early version of this project.

Some significant results from the lap simulation are summarised in Figure 16 - these are sensitivities of the points generated by the car to several parameters. Much of this was already known anecdotally; for example, the success of any given design is very sensitive to lateral grip, but a Formula SAE car can tolerate a large loss of power without being overly disadvantaged in the competition. One of the more surprising results in figure 16 is the high track width sensitivity - although some advantage was expected, the gradient of 3.5 points/%change suggests that this could unlock many points in a new design.

The other significant result from this study was quantifying the effect of aerodynamic downforce. The result of 1.3 points/%change is consistent with many years' worth of testing by the Monash team - substantial points gains can be made by adding aerodynamic devices to a Formula SAE car, even at the low speeds these cars experience. It should be noted that this gain includes the effect of drag and the associated increased fuel consumption, and the extra weight of the wings - reasonably accurate estimates could be made for both values, thanks to Monash's experience with these components. The rules regarding aerodynamics became more liberal in 2011, as shown in table 1

After careful consideration, a final layout was decided upon. The 2011 car would utilise a lightweight single cylinder dirtbike engine (expected weight 30kg) packaged in a car with a wheelbase approaching the minimum needed to avoid rolling. The small size of the engine was important in the selection of

Figure 16: The effect on points of a 10% improvement in each of several parameters.

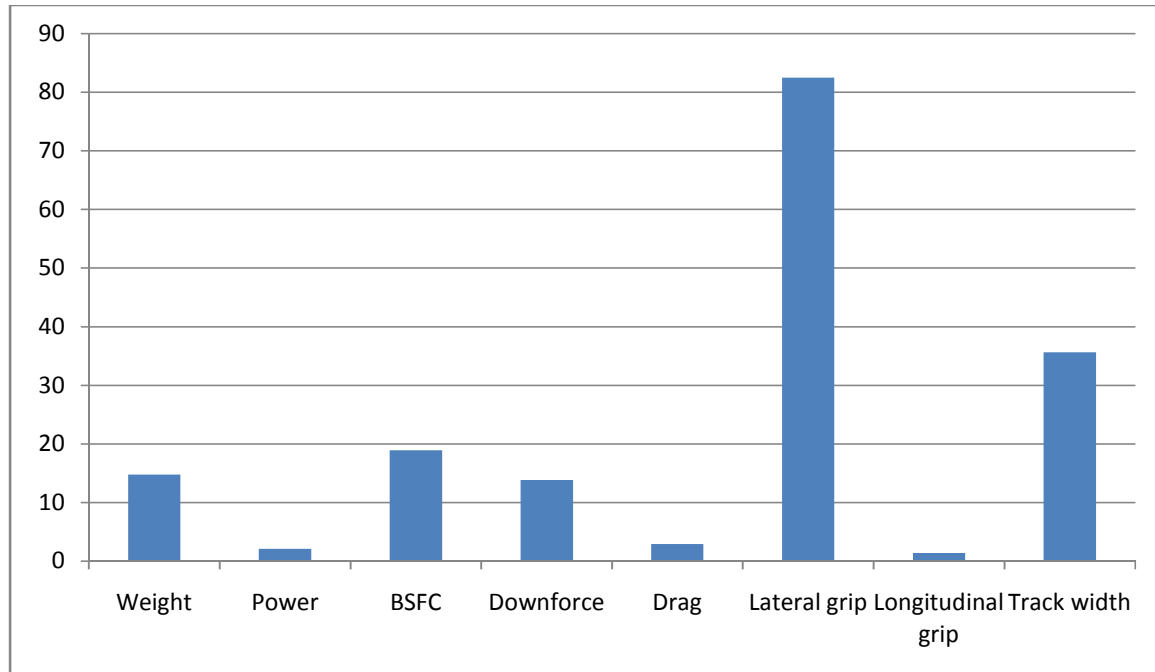


Table 1: Changes in aerodynamic packaging rules from the 2010 to 2011 competitions.

Parameter	2010 Rules	2011 Rules
Front wing packaging space (in front of wheel)	460mm	762mm
Rear wing packaging space (behind wheel)	0mm	305mm

track width - its narrow footprint allowed the chassis width to be small enough to mount wishbones that would not be excessively short. The wheelbase was chosen as 1530mm, 5mm from the smallest value allowed in the rules - although it is hard to quantify, short wheelbases are common in FSAE due to reduced yaw inertia and increased maneuverability. A large aerodynamics package was chosen to make the most of the new, liberal aero rules. A weight target was set at 185kg; this was considered reasonable for the rest of the car parameters and the design time allocated to the components. These parameters defined the starting point for the suspension design project.

4.2 Load Cases

A common set of load cases was chosen for all parts of the car. The loads were defined in terms of the peak accelerations of the car under various conditions. Predicting the performance of the car in order to determine cornering, braking, acceleration and combined cases required some informed guesswork; the performance of the 2009 car in competition was captured with accelerometer data, but the new car would not be directly comparable.

A set of conservative estimates was used:

- 25.4ms⁻² (2.5G) steady state lateral acceleration, and combined lateral/braking acceleration (applied at 45deg)
- 19.6ms⁻² (2G) braking acceleration
- 11.6ms⁻² (1.2G) forward acceleration
- 29.4ms⁻² (3G) bump

All parts were required to withstand the loads generated by these accelerations, with appropriate safety factors. For every suspension part the loads had to start at the tyre, so calculating loads in three dimensions at the contact patch was appropriate at this point.

The following calculations assumed equal assume that tyre loads are independent of car setup, a reasonable assumption as an appropriately designed Formula SAE car will see little difference in the loads on front and rear wheels due to setup.

The 'base' load on each wheel, for a car with a 50:50 weight distribution, is

$$F_{Z,base} = \frac{m_{car}g}{4} + \frac{F_{aero}}{4}$$

$$\Delta_{Lateral,front} = \frac{-m_{car} \cdot h_{cg} \cdot a_{lateral} \cdot \%k_{roll}}{100T}$$

$$\Delta_{Lateral,rear} = \frac{-m_{car} \cdot h_{cg} \cdot a_{lateral} \cdot (100 - \%k_{roll})}{100T}$$

where Δ is load transfer T is the track width of the car and $\%k_{roll}$ is the relative front roll stiffness distribution.

$$\Delta_{Longitudinal} = \frac{-m_{car} \cdot h_{cg} \cdot a_{longitudinal}}{W}$$

where W is the wheelbase. The total normal load on each wheel for the four load cases based on these equations, for a 185kg car with 70kg driver, CG of 310mm and 45% front roll stiffness distribution are summarised in table 3.

Table 3: Loads applied to the contact patch

	Front			Rear		
	x	y	z	x	y	z
Lateral	0	2984.01	1652.68	0	3513.48	1945.93
Braking	-2299.77	0	1447.40	505.89	0	318.39
Combined	2385.16	2385.16	1876.43	1499.49	1499.49	1179.67
Acceleration	0	0	574.99	1530.36	0	1190.81

4.3 Analysis Methods

The Formula SAE competition presents component designers with an open ended problem, part of which is the choice of method to analyse their parts. Design tasks frequently reach the limit of the university curriculum, where similar problems are often solved using significant simplifications. Complex 3D geometries and contact conditions are encountered, and failure to analyse the effect of loads under these conditions can cause significant damage to the car and danger to the driver.

Finite element analysis has been used extensively in this project where hand calculations alone were judged to be inadequate. Some previous FEA analyses were subject to the problem often referred to as 'rubbish in, rubbish out'; loads and boundary conditions were imposed without careful consideration of physical reality, and the resulting output tended to be given more credibility than was reasonable.

In terms of the suspension system, this issue has manifested itself in a set of assumptions do not properly represent the behaviour of the car on track. In previous projects, it has been assumed that the car rarely or never encounters combined cornering and braking or acceleration manoeuvres; the team has a large volume of on track data to show otherwise. The contact patch has often been treated as a fixed point in the centre of the tyre, sometimes producing zero loads in suspension links - this does not accurately reflect the complexity of the tyre/road interaction.

To correct these issues and improve the accuracy of FEA and hand calculation results, an Excel spreadsheet was written to provide a more thorough estimate of loads at relevant points in the system. The fundamental difference between this and previous solutions is that it doesn't require the geometry and loads to be simplified to give solvable two dimensional free body diagrams; instead it solves a free body diagram in three dimensions in a quasi static sense (see appendix A for details). The solution that this produces can account for unusual link angles, combined cornering and acceleration/braking conditions, and a contact patch 'point' that can be moved to account for complex tyre behaviour, such as self aligning torque.

Geometrical external forces				Solution (forces acting on upright)				Magnitude
Lower wishbone (pullrod) <i>Outboard</i> g z 9.35 -529.23 139.39 <i>Fore</i> g z -150 -100 104.94 <i>Aft</i> g z 163.63 -136.23 113.39	Upper wishbone (pullrod) <i>Outboard</i> g z 40.21 -511.73 359.02 <i>Fore</i> g z -163.15 -229.51 282.3 <i>Aft</i> g z 152.18 -264.11 287.54	Tie rod/toe link <i>Outboard</i> g z 80.24 -521.62 179.39 <i>Inboard</i> g z 80.02 -150 140	Contact patch <i>Location</i> g z 0 -550 0 <i>Force (acting DMCP)</i> g z 2231.144 2231.144 1939.058	Lower wishbone g z -3340.194203 -2840.153447 146.81396 Upper Wishbone g z 1108.682323 1230.267276 -2211.7227 Tie rod/toe link g z 0.367786296 -621.2579235 65.8504645 Magnitude 4386.903607 2763.051118 624.7382063				
Upper normal - 3D g z 2378.87 -8458.046 -128846	Orientation - fore g z 203.36 -282.22 76.72 Unit orientation - fore g z 0.570891 -0.79227 0.215375 Orientation - aft g z -111.97 -247.62 71.48 Unit orientation - aft g z -0.39847 -0.8812 0.254375	Hub <i>Outboard</i> g z 0 -1 0 <i>Inboard</i> g z 0 0 0 Shaft torque Viewed from outboard * value for counterclockwise 0	Shock/pushrod/pullrod <i>Outboard</i> g z 30 -490 340 <i>Inboard</i> g z -88.11 -103.33 88.64	Solution (axial wishbone force) Lower Fore Aft 3116.380432 -6192.632821 Upper Fore Aft -4060.389875 -306.6700996 Pull Rod 5783.47787				
Orientation - fore g z 159.35 -429.23 34.45 Unit orientation - fore g z 0.347055 -0.8348386 0.07503 Orientation - aft g z -154.28 -393 26 Unit orientation - aft g z -0.36473 -0.8290824 0.061466	Orientation - tie/foe g z 0.22 -371.62 38.09 Unit Orientation g z 0.000589 -0.99443 0.105405	Orientation - hub g z 0 -1 0 Unit Orientation g z 0 -1 0	Orientation g z RR ll -386.67 259.36 Unit Orientation g z 0.18788 -0.81568 0.547117					

Figure 17: Spreadsheet used to calculate loads acting on suspension components based on the method outlined in appendix A.

This approach gave the team much greater confidence in the results of their simulations and hand calculations. The resulting suspension structures are extremely robust and reliable by Formula SAE standards, allowing long test days with very few failures (see section 9 for details).

4.4 Reliability

One of the greatest challenges facing any student team is ensuring reliability in their vehicle. In the 2010 Australasian competition, only 10 out of 27 teams completed the endurance event - worth 400 points out of 1000 available. Technical failures put a podium position firmly out of reach of the other 17 teams. Monash aimed to finish the car within a very ambitious timeline; late July was chosen as the earliest realistic date for the car to be driving, partly to minimise the risk of failure of insufficiently tested components at competition. This timeline was overshoot by only a fortnight, leaving over four months of testing time available to detect and resolve technical issues. This rapid design and manufacturing process is partly as a result of a component design philosophy which favoured robust simplicity over the ultra lightweight and often difficult to manufacture designs favoured by many teams.

The use of composite materials in safety critical structures was to be avoided; it was considered that the team does not have sufficient knowledge and experience of composites and bonding methods to produce reliable parts in this way. Similarly, the team was very cautious about any parts that utilised welding on aluminium, as a history of failures had shown that the heat effects tended to have a catastrophic effect on the properties of this base material.

4.5 Adjustment and Serviceability

In a similar vein, the Monash team recognised that significant testing is necessary to realise the full potential of a prototype racecar. This is another reason for imposing an early driving deadline. Effective

testing also requires suitable adjustments to be built into most parts. Finite adjustments were used where possible for easy adjustment and repeatability; however, the steel tubes used for many suspension components were more conducive to the use of threaded adjusters in some places. Suspension setup changes also require ease of changing springs and anti-roll bars between events, which required some forethought given to bolt access. The planned adjustable parameters included:

- Inboard pickup points (affecting roll, pitch centre locations, anti squat and anti dive characteristics)
- Push and pull rod lengths (affecting ride height, corner weight)
- Some wishbone lengths (affecting caster, kingpin inclination)
- Camber shim stack depth (affecting camber)
- Steering/toe rod lengths (affecting toe)
- Damper high speed/low speed bump/rebound damping
- Spring stiffnesses
- Anti roll bar stiffnesses

In the unfortunately common scenario of a major component failure, it is critical to be able to remove components quickly and easily to effect a repair. Bolt access is thus a high priority, as is minimising the number of different tools required. A pertinent example of this occurred on the driveline on Monash's 2009 car - after the flange bolts failed, the rear end of the car was completely removed in order to repair it, then reinstalled in time to drive in the endurance event and take out an overall win.

Keeping all fasteners to a small number of standard sizes was a high priority; this would allow the car to be worked on unimpeded by the need to find and share specific tools.

4.6 Weight

A realistic weight goal could only be set based on benchmarking of previous cars. The 2009 car was broken down to parts for shipping from the UK competition in 2010, and so could be weighed piece by piece on its return. The weight of each component is tabulated against the weight target for the 2011 car, with accompanying comments:

Table 4: Weight breakdown and targets of 2009 and 2011 cars respectively.

	Qty	2009 weight (g)	2011 target weight	Comment
Rear Brake Rotor	2	430	400	Change to two rotors, can reduce weight slightly
Front Brake Rotor	2	558	600	Not appropriate to save weight here
Brake Pads	8	62	80	
Tyre (New)	4	5099	4000	Goodyear D2704 - significantly lighter than Avon
Wheels	4	2528	2528	Similar rims, wheel centre
Springs	4	866	500	Lighter springs suited to

				smaller dampers
Front Upright, Hub & Caliper	2	2200	2200	Very time consuming to save significant weight
Rear Upright, Hub & Caliper	2	3400	3400	
Front Upper Wishbone	2	500	600	Needs to take bending load
Front Lower Wishbone	2	630	400	Pure axial loading
Rear Upper Wishbone	2	620	400	Overdesigned in 2009, easy to save weight
Rear Lower Wishbone	2	615	600	Bending load
Front Antiroll Bar	1	0	700	No front ARB on 2009 car
Rear Antiroll Bar	1	1120	700	Simpler design - can be lighter
Dampers	4	1650	450	Can be lighter with inboard design
Front Bellcranks	2	0	300	No bellcranks on 2009 car
Rear Bellcranks	2	0	300	

5. DESIGN CONSTRAINTS

5.1 Manufacturing

Each Formula SAE team must work within the constraints imposed by the resources (or lack of them) available. Monash's team is very fortunate to have a well outfitted workshop with a welder, milling machine, lathe and a wide selection of hand tools with which to fabricate parts. The team is also heavily supported by Chisolm TAFE in Dandenong, where qualified instructors teach team members welding and machining skills, and supervise the production of parts on their own machines. The TAFE also houses several CNC lathes and milling machines, and teaches NC programming to students with the MasterCam software package.

5.1.1 Welding

Welding was used throughout the car to manufacture most components, from tube and sheet stock. All structural parts were TIG welded, using a range of different machines as constant failures plagued the project.

The standard of steel welding within the team is high enough that failures of welded joints are extremely uncommon, but care was taken throughout the design phase to apply a high safety factor to the material properties of all welded parts. ANSI grade 4130 sheet and tube was used for most steel parts; this material combines a yield strength double that of mild steel (~500MPa, depending on thickness) with high weldability, and an excellent response to heat treatment.

Jigs and fixtures for welding were all either manually machined or laser cut.



Figure 18: Simple rectangular hollow section fixture used for welding wishbones.

5.1.2 Laser Cutting

Monash Motorsport is supported by an excellent laser cutting sponsor, so a large part of the manufacturing involved laser cut parts in some way. Flat aluminium and steel sheet of between 1mm and 10mm was utilised throughout the project to take advantage of this resource.



Figure 19: Laser cut sheet metal components.

5.1.3 Manual Machining

Manual machining, particularly lathe work, was used to produce small, simple parts throughout the car. Components such as ferrules, used to capture spherical bearings in clevises, could be made in the hundreds by beginners with only basic skills. Welding fixtures were mostly manufactured on a milling machine.

One improvement on the 2011 design would be to better utilise the large pool of machining skills and resources in future cars - team members would often run out of work during compulsory TAFE machining sessions.

5.1.4 NC Machining

NC machining was used for a wide range of components, particularly those that combined complex geometry with tight tolerances. A three and five axis mill, EDM wirecutter and NC lathe were available at Chisolm TAFE.

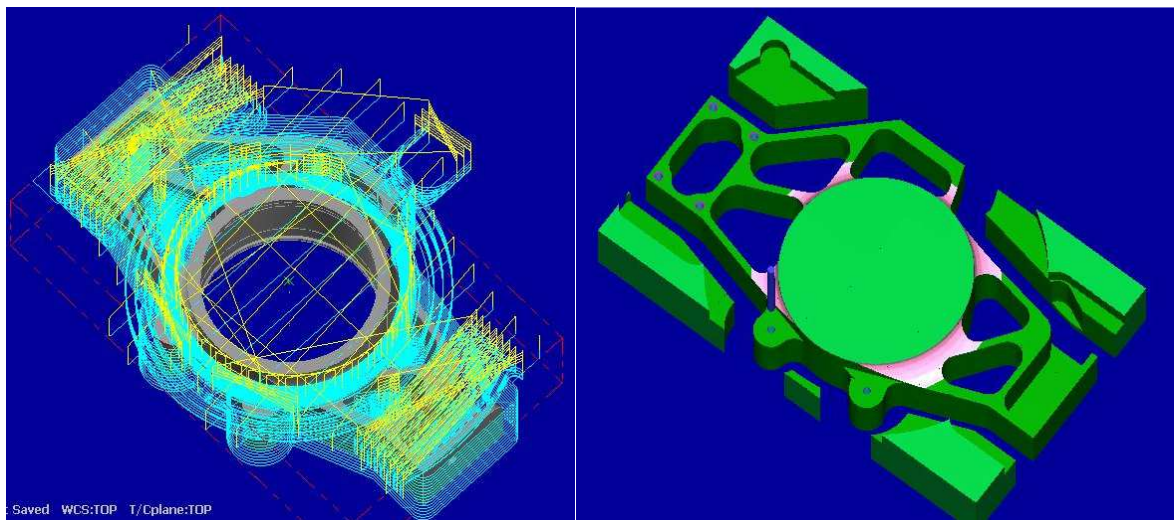


Figure 20: Toolpaths used for the machining operation used to generate the outer profile and pockets of the rear uprights, simulated with MasterCam X4 software. The blue lines represent cutting toolpaths, while the yellow lines represent rapid movements.

5.2 Competition Rules

The Formula SAE rules are mostly designed to control the safety aspect of the competition; trying to ensure equality between vehicles would be contrary to the aims of the competition. Given this emphasis on safety, it is surprising that the rules that directly affect the design of the suspension system are relatively few. Appendix B lists all of these relevant rules; those that have a significant effect on the design are discussed below.

B2.3 Wheelbase

The car must have a wheelbase of at least 1525 mm (60 inches). The wheelbase is measured from the center of ground contact of the front and rear tires with the wheels pointed straight ahead.

B2.4 Vehicle Track

The smaller track of the vehicle (front or rear) must be no less than 75% of the larger track.

B6.7 Rollover Stability

B6.7.1 *The track and center of gravity of the car must combine to provide adequate rollover stability.*

B6.7.2 *Rollover stability will be evaluated on a tilt table using a pass/fail test. The vehicle must not roll when*

*tilted at an angle of sixty degrees (60°) to the horizontal in either direction, corresponding to 1.7 G's.
The tilt test will be conducted with the tallest driver in the normal driving position.*

These rules impact the basic vehicle parameters. The wheelbase was chosen as the minimum of this rule, with an extra 5mm added to ensure compliance. The track was chosen based on stability considerations given the minimum expected achievable CG height (310mm). A tilt test rig is currently being constructed to test check compliance with section B6.7.2.

B6.1 Suspension

B6.1.1 The car must be equipped with a fully operational suspension system with shock absorbers, front and rear, with usable wheel travel of at least 50.8 mm (2 inches), 25.4 mm (1 inch) jounce and 25.4 mm (1 inch) rebound, with driver seated. The judges reserve the right to disqualify cars which do not represent a serious attempt at an operational suspension system or which demonstrate handling inappropriate for an autocross circuit.

The suspension travel was designed to exceed this requirement, with 30mm bump and 40mm rebound travel; this was a roadholding rather than rules decision.

6. DESIGN OUTLINE

6.1 Tyre Choice

It is a generally accepted view that tyres, moreso than any other component, define the performance limits of a racecar (Milliken, p14). Tyres are complex to understand and simulate; they are a composite of rubber and carcass material, and even the forces and moments generated by tyres in a simplified 'steady state' condition are a nonlinear function of normal load, camber angle, slip angle, slip ratio, tyre temperature and the properties of the surface on which the tyres are running (see appendix C). Transient properties of tyres present an even higher level of complexity - see the tyre data treatment section for a summary of some work in this area.

Students in the Formula SAE competition are not restricted to a 'control' tyre as is common in many forms of motorsport. Tyre choice is therefore left as a part of the overall design problem. In 2005, several prominent people in the Formula SAE community recognised that extensive tyre testing is excessively laborious and expensive for most student teams, and in response formed a consortium in which teams pooled resources to conduct tests through the commercial tyre testing facility, Calspan. The result is the Formula SAE tyre testing consortium, which Monash chose to join in 2011.

For several years, Monash has driven on the Avon A45 20.0x7.2 13" tyre. The choice at the time was based on the detailed investigation of Nick Trevorrow, a team member who graduated to pursue a PhD based on tyre modelling. The results of (Trevorrow, 2006) clearly showed that the Avon was a good choice at the time; however, in the intervening years several manufacturers produced tyres specifically for Formula SAE, and the test procedures and analysis required to replicate Trevorrow's tests were considered too expensive (new tyres would need to be bought and cut into strips) and laborious to

properly analyse the new tyres. The team recognised that there were gains to be made by choosing a new tyre, and the one off cost of \$500 USD to join the consortium was seen as an economical way of making and justifying a change. It was therefore an important part of this overall project to find an objective way to analyse the data and make a new tyre choice.

The apparatus used to test the tyres is described in section 3.2.3. Each tyre is subject to two test matrices. The first is a freerolling test, wherein no torque is applied to the spindle of the test machine. Normal load and inclination angle are varied in increments, while the slip angle is varied continuously. Forces and moments generated by the tyre are measured throughout. The second test matrix is a combined brake/drive/cornering test, wherein the inclination angle, slip angle and normal load are varied incrementally while slip ratio is varied continuously. The changes in variables are timed in such a way that each combination of variables receives reasonable testing time.

6.1.1 Performance Envelopes

The performance of a tyre is often discussed in terms of its performance envelope, the range of loads the tyre is able to generate in the lateral and longitudinal directions and the full range of angles in between, for a range of normal loads on the tyre. This can be plotted as a cartesian or polar plot, analogous to the g-g diagram often used to describe the acceleration potential of a car under a range of conditions.

Generating such plot from the Calspan tyre data required the manipulation of the data from the free rolling (cornering performance) test and the combined brake/drive/cornering test for each tyre. The free rolling data showed good correlation with Pacejka's 'magic formula'. The MATLAB code written to find useful peaks worked through the following procedure:

- Label each data point in terms of nominal inclination angle and normal load*
- Group the data correlating to each combination of inclination angle and normal load, and relate lateral force and slip angle for each combination using the Pacejka magic formula*
- For each curve fit, find the peak lateral force. For each normal load, store the highest peak value as the maximum lateral force (this will correspond to one inclination angle).*

The complete code is included in appendix C. This method is limited in that it performs no interpolation between the peaks generated at different inclination angles. However, free rolling tests are performed with steps of inclination angle of only one degree, which is small enough that interpolation is not considered necessary.

The remainder of the polar plot must be obtained through examination of the combined brake/drive/cornering data. Three variables are varied discretely in this test; inclination angle, slip angle and normal load, in three, three and four steps respectively. This would require a total of 36 curve fits, with multiple force peaks present in some. Figure 21 shows one of the 36 curve fits applied to a Goodyear D2696 tyre at 12psi.

Redacted sections relate to Formula SAE Tire Testing Consortium data.

Figure 21: Lateral and longitudinal force for a constant inclination angle, slip angle and normal load, with varying slip ratio. A Pacejka 'magic formula' fit is applied to FX, while FY is represented by a second order hyperbola.

Note that the magic formula could not be applied to the FY curve in this case. A bell shaped curve was required to match the characteristic shape of this data. Although no physical basis existed for it, a second order hyperbola was found to provide a sufficiently good fit.

Two maxima would be obtained from the $|FX+FY|$ curve, representing two forces of similar magnitude at two different angles. Repeating this for each of the 36 curve fits would produce a polar plot with some points lying within the envelope of each normal load. This is considered acceptable for the purpose of creating a visual aid to tyre selection. The code for this section works as

- Label each data point in terms of nominal inclination angle, slip angle and normal load*
- Group the data correlating to each combination of inclination angle, slip angle and normal load, relate longitudinal force and slip ratio for each combination using the Pacejka magic formula, and relate lateral force and slip ratio using a second order hyperbola*
- Find the vector sum of the lateral and longitudinal forces, and find all peaks in this curve. Relate these peaks to the angle of the two dimensional force vector*
- Plot force as a function of angle and normal load on a polar chart*

The Goodyear D2696 and Hoosier R25B, both mounted on 7" wide rims, are compared in this report. Figure 22 shows the friction ellipses generated for both tyres: the convhull command was used in MATLAB to give a linear interpolating curve that connected the outermost peak points at each normal load.

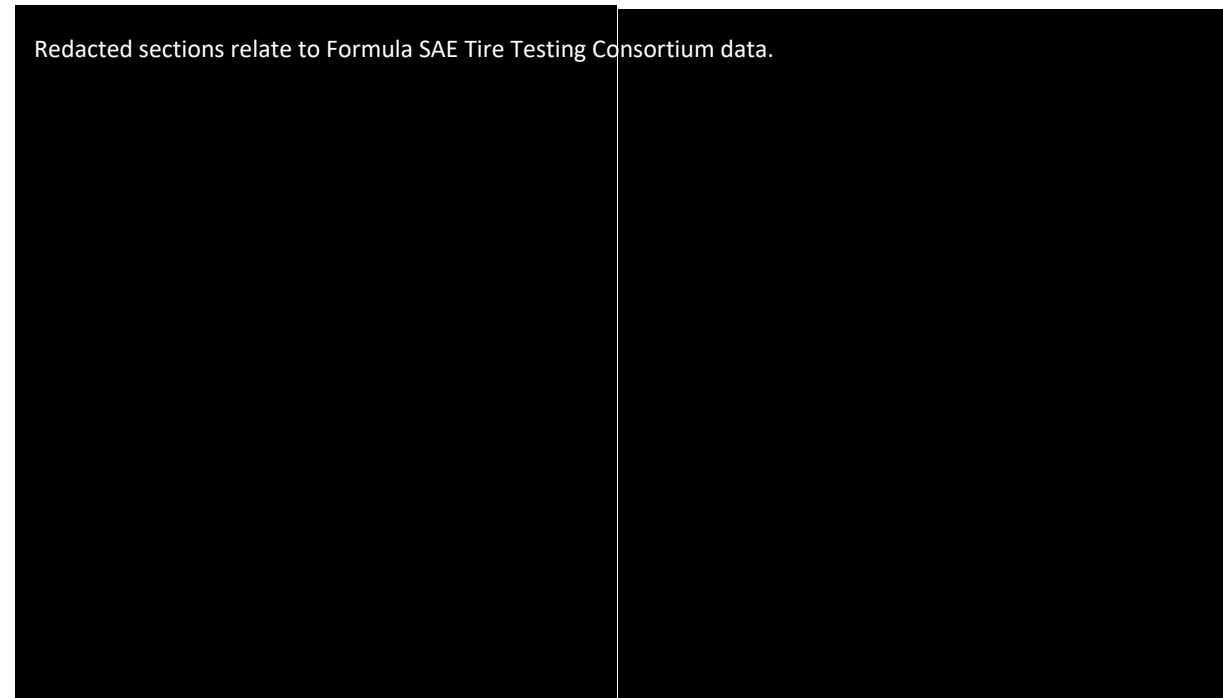


Figure 22: Friction ellipses for the Hoosier R25B and Goodyear D2696 tyres

The limitations of this method are immediately obvious. While the plot does contain some useful information, it is incomplete. There are no data available for combinations of high lateral force and low longitudinal force, because the correct conditions were never tested - the combined brake/drive/cornering tests only tested slip angles of 0, 3 and 6 degrees, while peak cornering forces were typically seen at closer to 10 degrees. As calculating performance envelopes in this way does not provide a complete picture of tyre performance, other metrics would need to be developed.

Peak lateral force and corresponding slip angle: The peak lateral force provided by a given tyre is proportional to the cornering acceleration it can deliver. The relevant peak should correspond to the normal load and inclination (camber) angle likely to be seen in a typical FSAE cornering maneuver - here they are compared at 1° negative camber, with a normal load of 1100N, in pure slip (no driving/braking torque). The corresponding slip angle gives some sense of how 'pointy' a tyre is; tyres that generate their peak load at small slip angles can be expected to respond quickly to driver input, as slip angles take some time to develop. This is a particularly important characteristic in Formula SAE, which emphasises change in direction.

Cornering stiffness: Gauging the dynamic responsiveness of a tyre by the slip angle corresponding to the peak lateral force is flawed, in that some tyres can have a very 'flat' force curve at higher slip angles, making the peak slip angle somewhat arbitrary. Small angle cornering stiffness is the ratio of cornering force/slip angle for small slip angles, and it provides an indicator of tyre 'pointiness' without this flaw.

Load sensitivity: Load sensitivity is a phenomenon observed in all real tyres, wherein the coefficient of friction (peak load/normal load) tends to decrease with an increasing normal load. Tyres with a high load

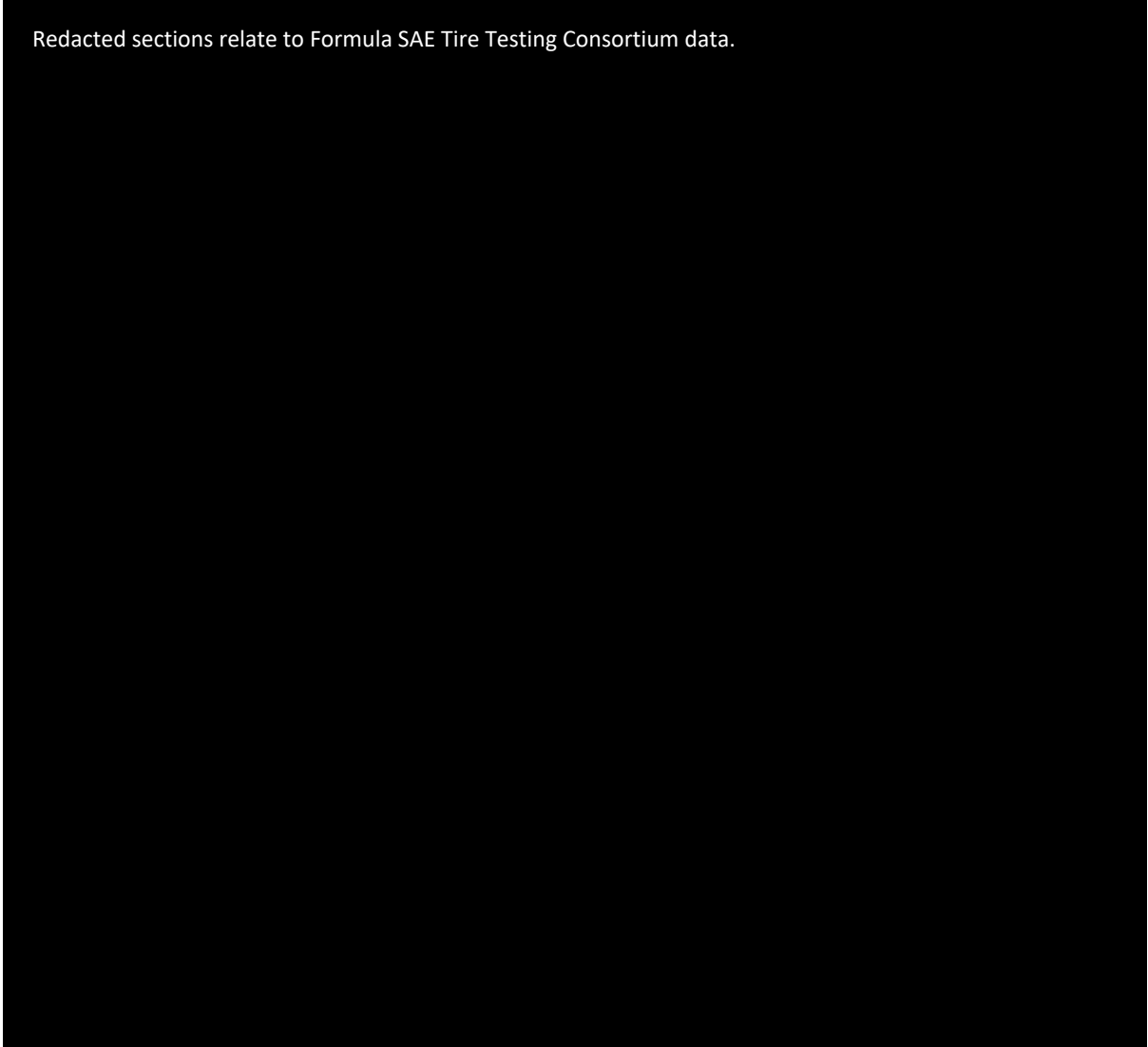
Final Year Project 2011
Final Report

sensitivity will see the greatest deterioration in performance with a narrow track width and/or high centre of gravity, factors that increase the load on the tyres. Load sensitivity is presented in the decision as a proportion of friction coefficient lost across the free rolling results

Cost: Cost varies significantly between popular Formula SAE tyres. The impact of tyre choice is such that the benefits of a more expensive tyre can easily outweigh the monetary cost, but the limitations of the team's resources ensure that this is still an important metric.

Table 5: Summary of tyre properties

Redacted sections relate to Formula SAE Tire Testing Consortium data.



6.2 Layout

The choice of the 450cc KTM engine to power the new car, and the use of relatively small Ohlins dampers posed a new packaging challenge. The previous generation of Monash cars used large Ohlins ST44 dampers, which were very suitable for mounting directly between the wishbones and the chassis. This was an elegant, albeit heavy solution. Implementing a similar layout on the 2011 car with the smaller dampers would have required the use of extensions, or a chassis with significant overhang. Instead, it was decided to use linkages to actuate the springs and dampers indirectly.

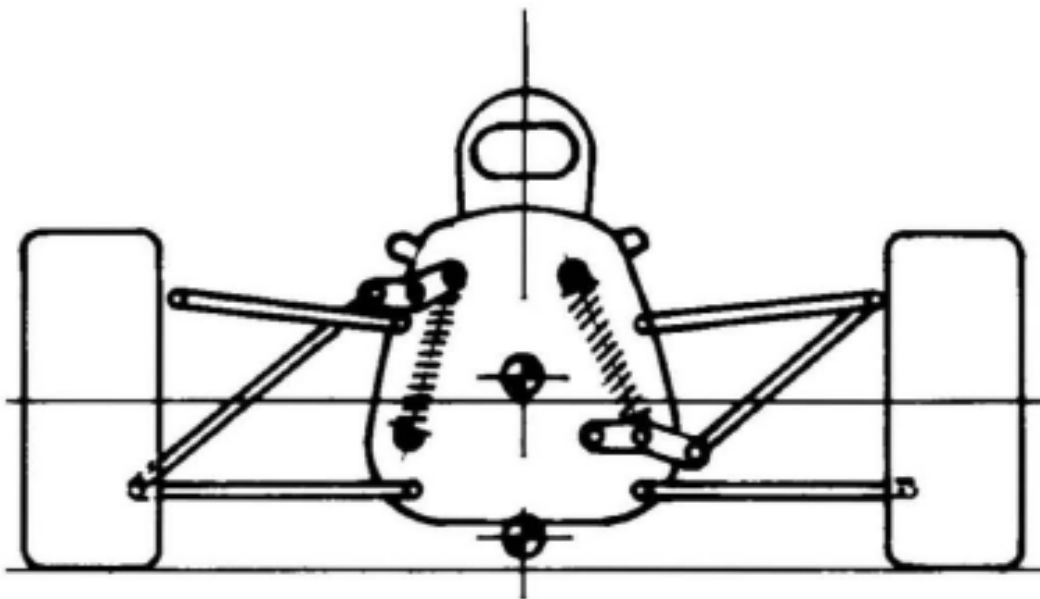


Figure 23: Pushrod (left) and pullrod (right) arrangements on a double wishbone suspension setup (McBeath, p47)

This allowed a great deal of flexibility in the placement of the springs and dampers. The lack of packaging space around the engine made a conventional pushrod arrangement convenient on the rear of the car; the pushrods, bellcranks, shocks and engine mounting plate formed a neat planar mechanism. On the front, there was sufficient room to mount the spring and damper units low to the ground, and central on the chassis, in a pull rod and bellcrank arrangement.

6.3 Kinematics

The kinematic properties of the 2011 suspension system were adapted from the previous system to suit the new layout.

6.3.1 Roll centres & VSAL

Roll centres of 30mm and 55mm were chosen for the front and rear suspension respectively. These values had been found to produce an acceptable compromise between jacking forces, roll angles and inelastic weight transfer. Testing showed that the narrower track had increased the jacking forces to an unacceptable level (see section 9); however, the adjustable wishbone pickup height allowed them to be lowered enough to compensate. VSAL was chosen as 930mm, generating relatively large camber gain appropriate for the Avon A45. The Goodyear D2696 has an extremely low camber sensitivity, so no change was necessary for testing on the team's set of these tyres.

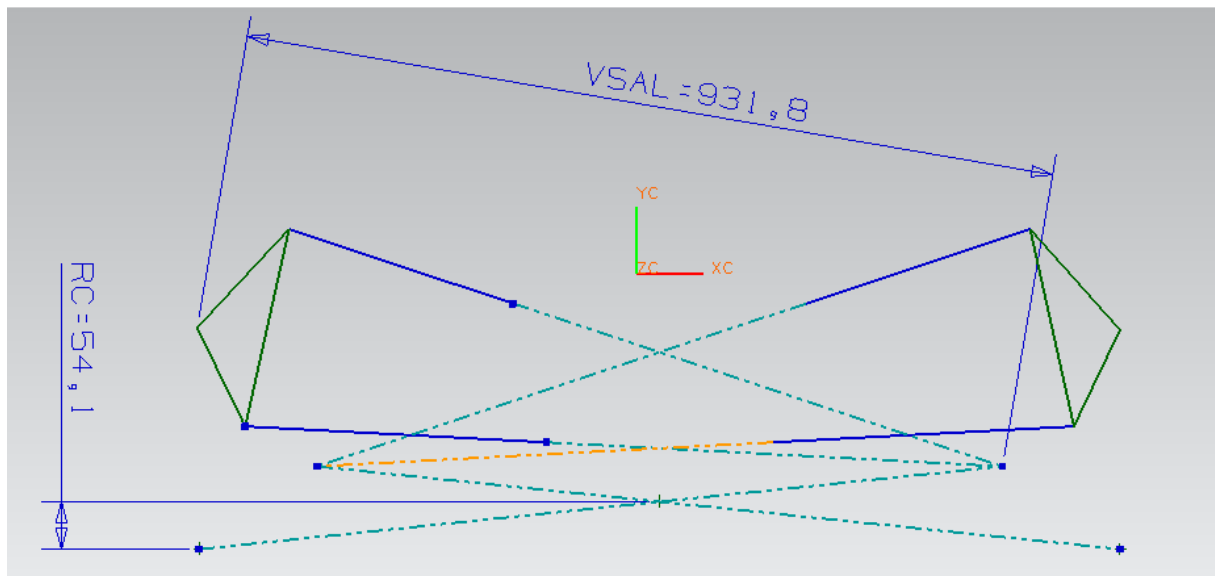


Figure 24: Rear suspension geometry in the Y-Z plane

6.3.2 Pitch centres

The pitch centre was left at ground level - the default condition for wishbones that are not inclined in the longitudinal plane. The pitching motion of the car was not seen as an issue worthy of sacrificing roadholding under acceleration and braking conditions.

6.3.3 Steering geometry

The caster angle was originally set at 8 degrees, with 15mm positive offset. This was intended to promote diagonal weight transfer when the wheels were steered, lifting the inside rear wheel to minimize turn in understeer with a spool setup. The purchase of the differential partway through the year removed this need, but initial testing was done with significant caster on the front wheels.

In an effort to reduce the high steering effort seen in the previous two cars, scrub radius was kept to a reasonable minimum of 10mm. This would require a change in the front wheel offset, and new rims would have to be spun for this purpose.

Kingpin inclination was set at four degrees, sufficient to prevent excessive camber gain by the front wheels during steering. Ackerman was set at 130%; - this was originally set for the characteristics for the Avon A45 tyre, but proved equally appropriate for the Goodyear D2696 tyre.

6.4 Wheel Sizing

With very few exceptions, Formula SAE cars are built around standard 13" and 10" rim diameters. 10" wheels and tyres offer an opportunity to save a meaningful amount of weight from the unsprung assembly, and were seriously considered for the 2011 car. However, the tyre selection for the smaller wheel size was very limited, and the team had serious concerns about overheating with the lower thermal mass of these tyres. The smaller wheels were also expected to worsen the compromise between packaging and clearance for wheel movement, and the smaller wishbone base would have amplified compliance issues. Considering these issues, and several years of trouble free design using 13" wheels and tyres, the larger wheel size was chosen.

7. COMPONENT DESIGN

7.1 Damper Choice

For several years, Monash has used direct acting suspension for the sake of simplicity, a lower part count and improved serviceability compared to the more complex linkages common in the competition. Due to packaging constraints, this required a relatively large damper to be used (Ohlins ST44, designed for larger formula cars). Preserving the 2010 car for driver training and testing gave the team a chance to reassess this choice, and the decision was made to use a smaller damper in conjunction with bellcranks and push/pull rods, for a meaningful weight saving and reduction in yaw inertia. Three options were considered, and are summarised in table 2 below:

Table 6: Comparison of popular Formula SAE damper options

Model	Cost (\$AUD) per shock	Weight (g)	Stroke (mm)	Adjustment	Single/double tube	Cost/spring (\$AUD, as part of a spring kit)
Ohlins TTX 25 MkII FSAE	610	448	57	4 way	Double	\$14
Kaz Penske 7800 series FSAE	675	412	50 or 75mm versions	2 way	Single	\$45
Sachs Formula Matrix	Unknown (custom)	480	Unknown (custom)	4 way	Double	Unknown

The adjustability of the damper is a key feature. The four way adjustable dampers allow low and high speed damping to be adjusted independently, which gives greater control over the transient response of the car. The Sachs damper is only available as a customised unit, and is expected to be considerably more expensive than the other options. The cheapest option, the Ohlins damper, has greater adjustability than the Kaz Penske, as well as a substantially lower cost for matching spring. The construction of the Ohlins damper is shown in figure 25 below; the four hex headed adjusters are easily accessible on the damper body.

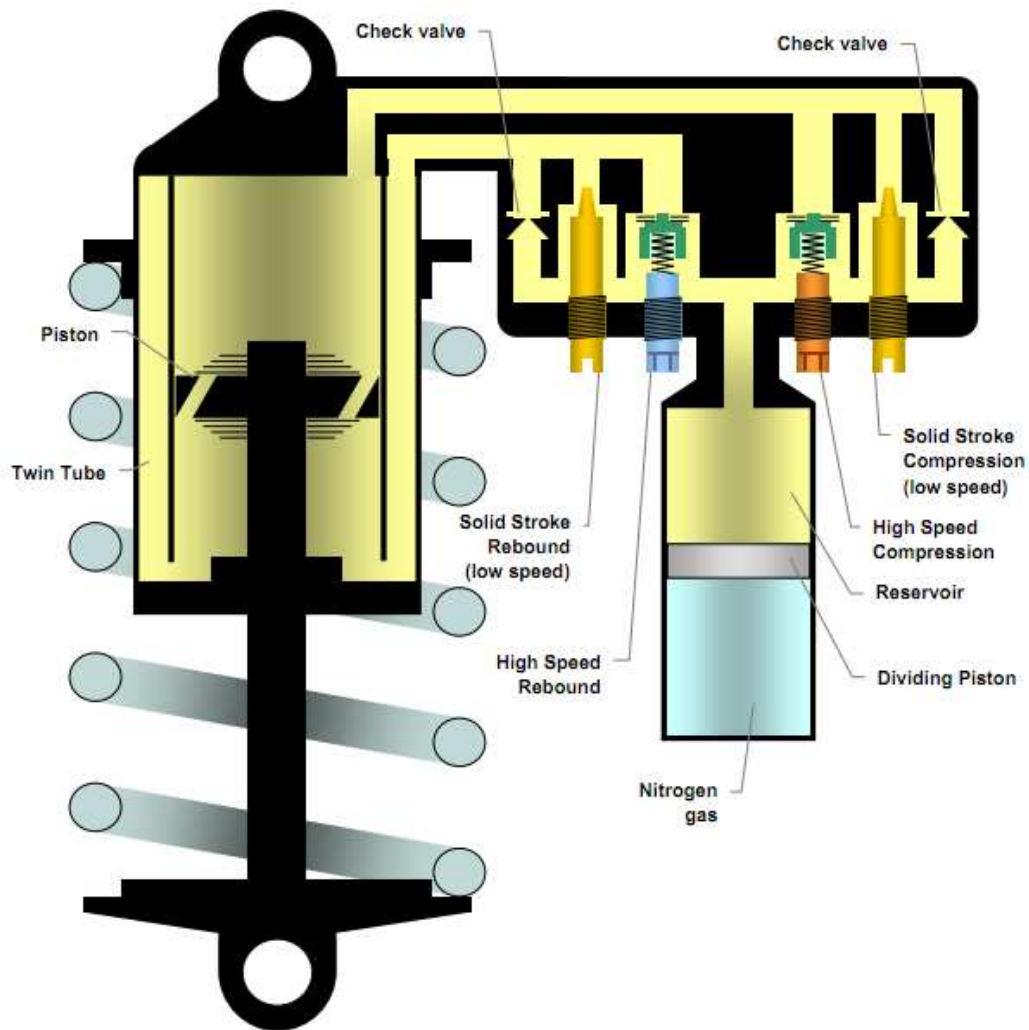


Figure 25: Layout of the Ohlins TTX 25 MkII damper (courtesy Ohlins USA)

The force-velocity data for this damper is available from the Ohlins website for the full range of adjustment. Figure 26 shows a set of example plots with a range of different low and high speed settings.

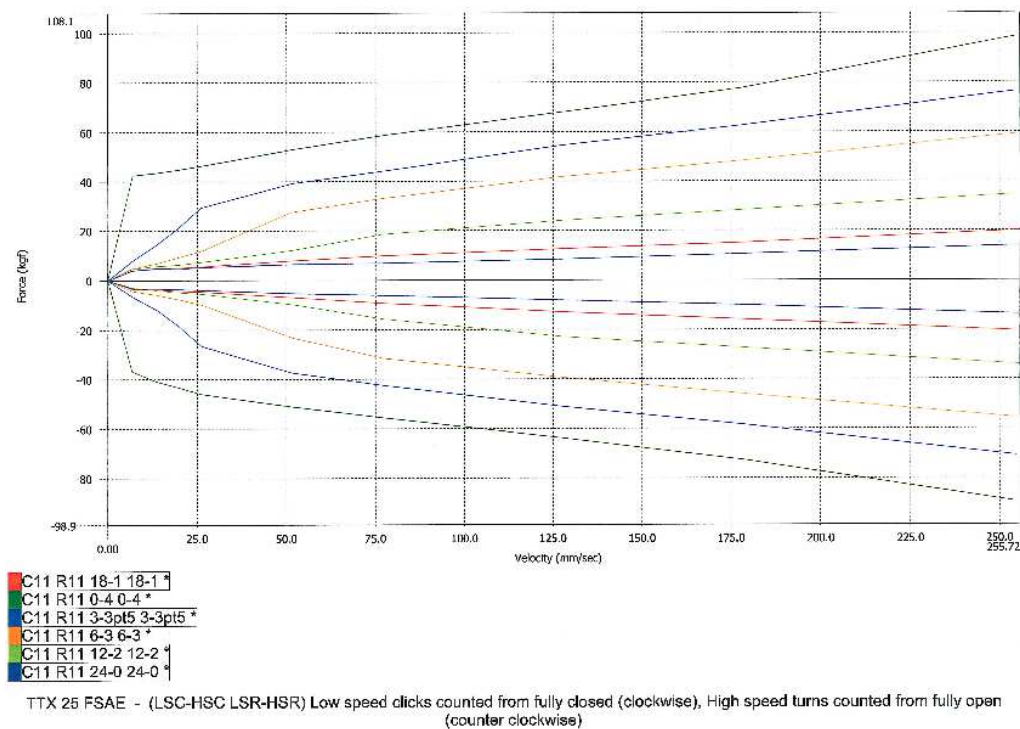


Figure 26: Force-velocity plots for a range of damper settings. Rebound settings are mirrored to appear below the bump settings, as is conventional for these plots. Note the 'knee' point where the high speed valves open.

7.2 Uprights and Hubs

The uprights and hub have many design interactions, and will therefore be discussed together. These parts are subject to a complex combination of loadings, reacting bending loads from acceleration, braking, and cornering, brake torque and torsion from the steering arms; often several of these loads occur simultaneously. The hub and upright must have sufficient stiffness to react these loads without any significant deterioration of handling, and enough strength to avoid a component failure which could have catastrophic consequences for the driver and car.

These requirements lend themselves to a design with a significant three dimensional aspect, in contrast to most of the slender axially loaded members making up a modern double wishbone system. The constraints imposed by packaging these components into the wheels through their full range of motion while retaining a high installed stiffness required a particular sequence of design steps. These are listed below:

7.2.1 Wheel offset and caliper selection

The selection of brake caliper and suspension layout determined the selection of wheel offset. In packaging the caliper, it is advantageous to place it close to the spokes of the wheel centre, to minimise the length of the hub and in doing so increase its bending stiffness. When an appropriate clearance is given between the caliper and wheel, the centreline of the brake rotor is defined in terms of a y

coordinate. This is a less important consideration where the brakes are mounted on the inboard side of the upright, as was the case on the rear of the 2011 car.

7.2.2 Selection of bearing arrangement

The brake rotor placement defined the furthest outboard location of one of the two bearings needed to constrain the hub. The location of the inboard bearing controlled the maximum loading seen by each bearing. Spacing them further apart reduced the loading allowing smaller bearings to be used, at the expense of increased length of the hub and depth of the upright needed to support them, and the consequent weight increase. A spreadsheet was written to perform calculations according to the NSK catalogue (reference). For the front suspension, several iterations were performed with different hub and bearing arrangements, comparing the component weights needed to achieve a safety factor of 1.4.

The lightest feasible solution for the front suspension was found to be 40mm ID tapered roller bearings arranged back to back, with 500mm spacing. The constraint of including the outer part of the CV joint within the rear hub forced an internal diameter of 80mm; deep groove bearings were chosen for this purpose, with bearing centre spacing of 40mm. Appendix E includes details of the calculations used to come to these conclusions.

7.2.3 Brake mounting & steering arm

The brake caliper can be mounted at any point in the 360 degree rotation of the rotor; the steering mounting point must be selected based on the steering pickup point, adjustment and packaging considerations. The basic shape of each upright in the x-z plane was generated by drawing straight lines connecting upper and lower pickup points with the bearing cup. The 2011 car utilizes a rear steering arrangement, with the steering point behind the upright and between the lower wishbone mount and hub on the z axis; it was convenient to have a long bolt on steering arm connecting directly to one of the walls defined by this outline. (see figure 27). To minimise the CG height of the whole arrangement, the front calipers were mounted on the opposite side of the upright, as low as possible without interfering with the upright outline. This solution required one of the brake mounting lugs on a cantilever; this issue is discussed in more detail in section 7.3.

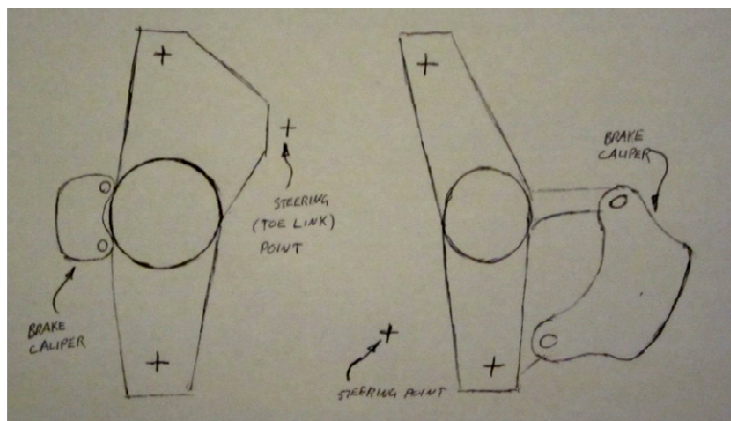


Figure 27: Basic shape of rear (left) and front (right) uprights

The same method applied to the rear upright defined a much larger package, and keeping the brake calipers low in the same way as the front would have been impossible without using a large brake rotor or creating a torturous load path to react the brake torque to the wishbones. For this reason the brake caliper was mounted at 90 degrees to the steering axis, towards the rear of the car; the steering arm was required to be located at the front of the upright to accommodate the four wheel steering package in front of the engine shear plate.

7.2.4 Camber adjustment method

As mentioned in section 4.5, finite adjustment was favoured wherever possible to ensure consistency and repeatability of suspension adjustments. The easiest way to achieve this for camber adjustment was to use shims of known thickness between the uprights and wishbone pickups. It was decided early on to use a bolt on clevis on the front lower and rear upper pickup points - this prevented the weight of the car from being carried through the shim pack, which would introduce extra bending loads.

With these details confirmed, the design could be 'fleshed out' in CAD. Team experience had shown that fabricated steel uprights could be manufactured more quickly and reliably than previous CNC machined uprights; however, the CNC uprights designed by previous Monash team members included complex three dimensional shapes, and required several machine setups and a range of tools to make. It was determined that if the shapes of the uprights were simplified with careful consideration of machining strategy, this disadvantage could be overcome, and NC machining could be used instead of labour intensive fabrication.

The uprights were initially laid out in a two dimensional sketch in CAD to provide triangulation between all load application points on the upright, including the bearing cup, wishbone pickups, steering arm pickup and brake mounting points. The wall thickness at all points was initially set to 4mm; this was a manufacturing consideration, as thinner walls would increase the tendency of the workpiece to 'chatter' during machining, reducing the quality of the surface finish or otherwise requiring a very slow machining process to offset it.

The resulting two dimensional shapes were then extruded to form the basic three dimensional shape of the uprights. It was found that extruding the sketches to the full depth of the bearing cups caused clearance issues during suspension movement; this was corrected by creating 'steps' in the uprights, with a ball nose cutter used to create smooth, stress concentration free transitions between the levels, as shown in figure 28.

The design was iterated through finite element analysis. To allow rapid iterations the finite element model was simplified, with some bolted connections replaced with perfectly bonded surfaces, and others with integral cylinders to allow loads to be applied in a representative way.

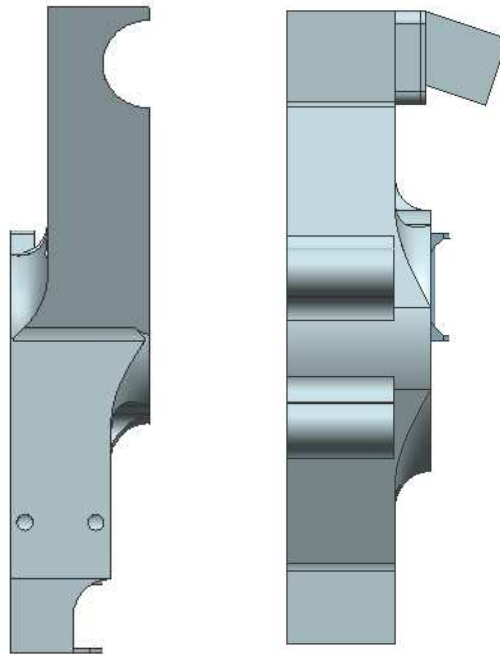


Figure 28: Stepped upright design

The uprights were constrained at the bearing surfaces, using a 'pinned' constraint (all degrees of freedom constrained but rotation; this did not fully account for the compression only behaviour of the bearing/upright interaction). This model was considered sufficient to model the transmission of loads through the bulk of the upright material, while the inaccurate results immediately adjacent to the loaded and constrained points were ignored. A safety factor of two was applied to the yield strength of the aluminium - a formal fatigue study was not done, but this safety factor was applied with fatigue in mind.

Based on the results of each FEA run, the wall thicknesses in different parts of the uprights were increased only where appropriate. It was found that, for all but the walls carrying the majority of the brake load in each upright, the strength and stiffness of the uprights far exceeded that required by the safety factor. As the limit on wall thickness was imposed by machining considerations, it was decided to remove the stiffening webs on the back face of the uprights - although this reduced the overall efficiency of the structure, it was seen as the most sensible way to reduce the weight of the components.

After six iterations, the final design of the uprights was locked in, barely missing the 'design freeze' deadline imposed by management.

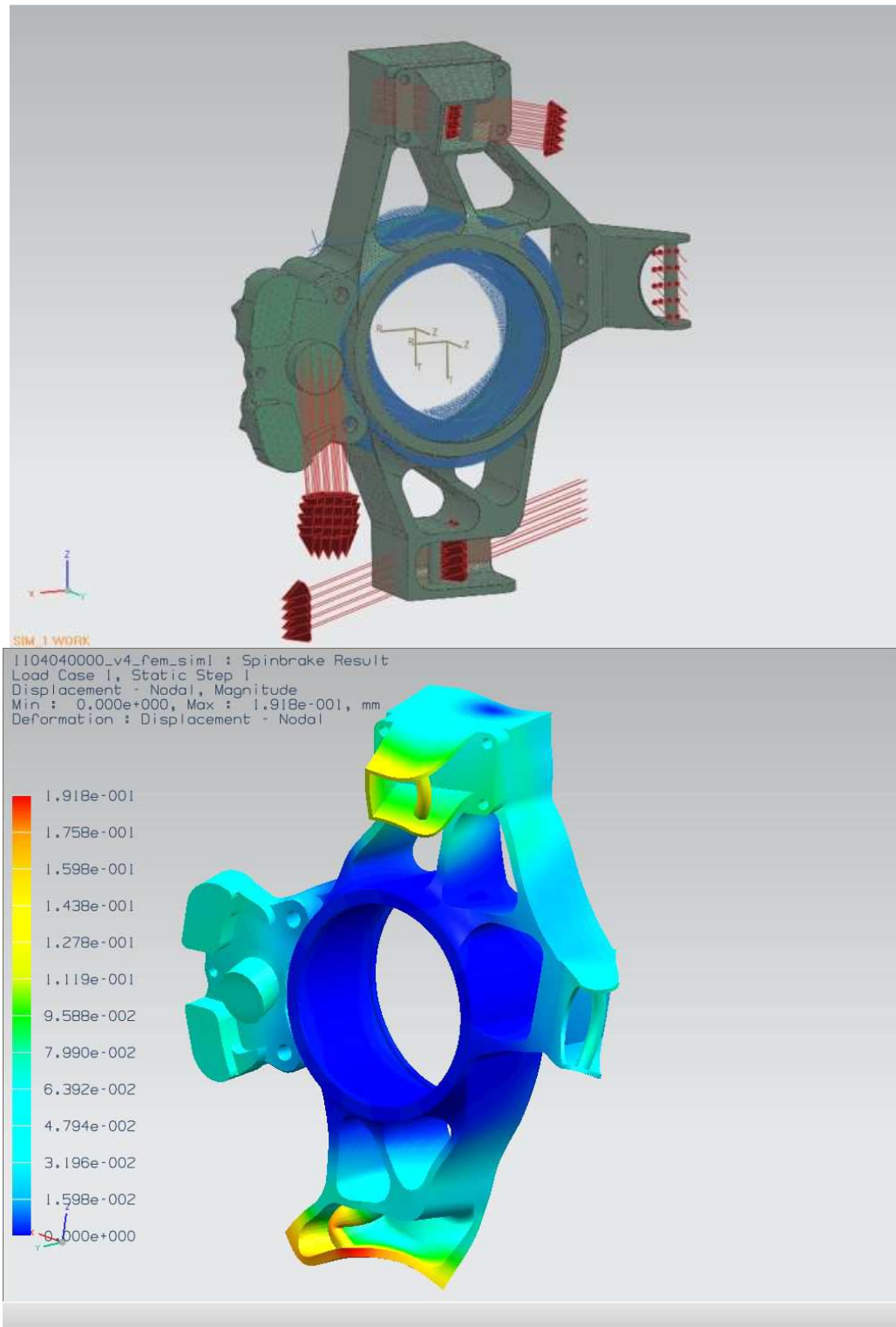


Figure 27: FEA setup (top) and solution (bottom) as used in the iterative design of the rear upright. Note the simplifications used - all parts are bonded, and the loads are applied uniformly over bolts. The bearing surfaces have a pinned constraint applied to them, with one degree of freedom.

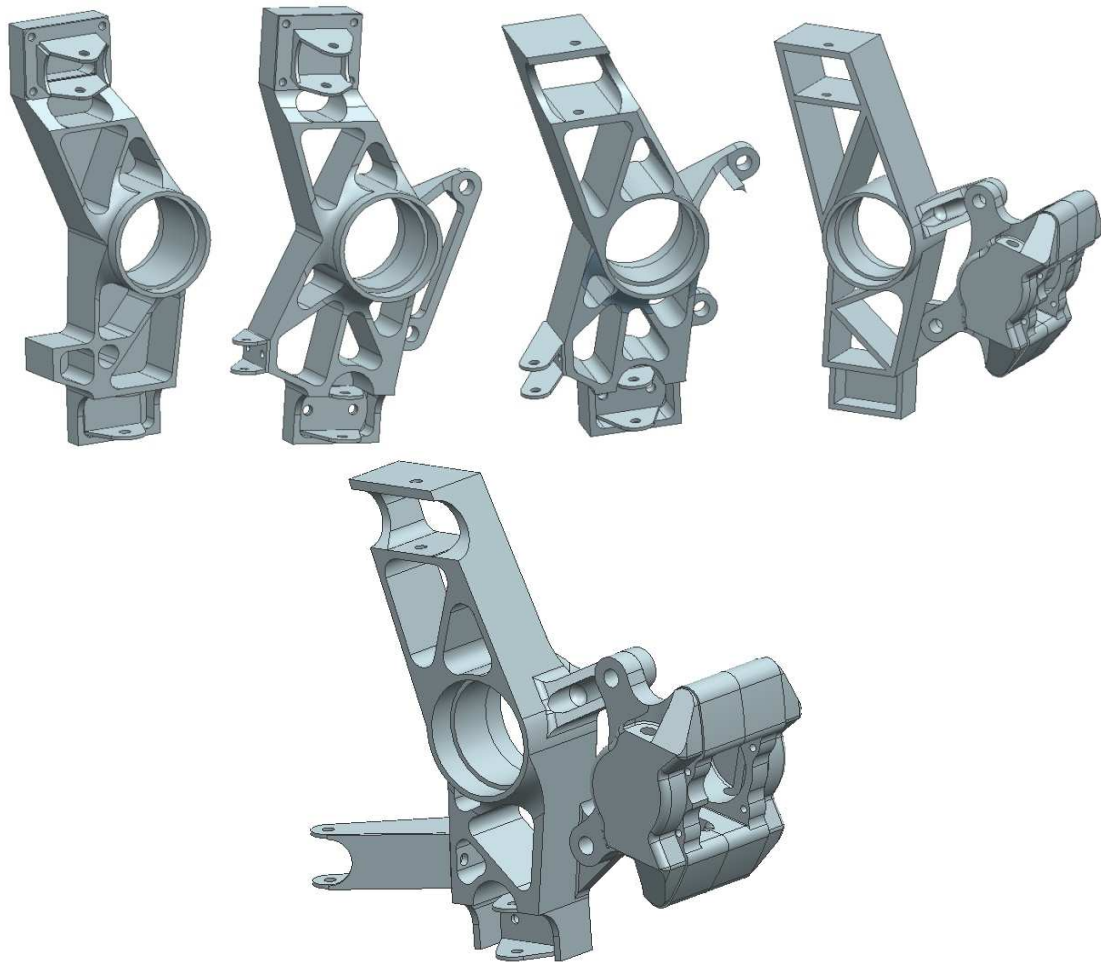


Figure 29: Front upright design iterations

Between accommodating the outboard CV joint, wheel centre and brake spider, and the minimum spacing required for bearings, the shape of the rear hubs was almost completely defined by constraints applied to it. FEA simulations showed that the hub easily met its required safety factor of 1.4 when machined in aluminium.

The front hub presented more of a design challenge, as the smaller outer diameter and large wheel offset due to brake packaging left a much greater scope for weight saving. Calculations showed that an aluminium design could be made to a comparable weight to a high strength steel at room temperature. However, the hub would be exposed to potentially high temperatures due to its connection to the brake rotor; the material properties of aluminium deteriorate rapidly with increasing temperature, which was enough of a concern to rule it out as a material choice. The final design, a hollow EN26 steel tube with one threaded end and mounting flanges for the wheel and brake spider, was analysed in FEA, and passed the analysis with relatively few iterations.

7.3 Brake System

Braking performance was one of the weaknesses of Monash's 2010 car; an attempt at weight reduction resulted in a brake system with insufficient thermal mass and surface area to dissipate the heat generated during driving. This boiled the hydraulic fluid after 3-4 minutes of hard driving, causing a total loss of braking power, and an accompanying reduction in the performance envelope of the car. The high temperatures generated by this lightweight system also took a toll on the components; brake pads lasted for approximately one hour of driving due to the high pad pressure and temperature, and thermal stresses generated in the rotors are thought to have contributed to their failure through cracking.



Figure 30: Failure due to cracking in a 2010 brake rotor. Several rotors failed this way.

Clearly it would be necessary to design a larger, heavier system for the 2011 car; brake reliability issues would impact crucial testing time. Ideally, this would have involved an in depth heat transfer analysis to determine the safety margin in any given system; however, the flow regime of air in contact with the brake system is very complex, given the rotor's rotation and shielded location inside a rotating wheel, with the flow around the wheel strongly influenced by the front wing. The literature on brake cooling is surprisingly sparse. Some studies have made effective use of nondimensional relationships in determining the cooling capacity of brakes; however, this was based on brakes within the wheel of a light trucks or passenger cars, and their application in this circumstance is likely very limited.

It was therefore decided to build a brake system based on components that were clearly more substantial than absolutely necessary. This was a matter of engineering judgement, based on the calculated differences in thermal properties of the old system and newer proposed designs.

7.3.1 Hydraulic Circuit, Bias Adjustment

The brake system consists of a relatively simple pair of hydraulic circuits, with a master and slave cylinder arrangement. The twin circuit arrangement is a requirement of the rules (see appendix B), providing a level of redundancy in case of a fluid leak. The pedal box was the one major part carried over from the 2010 to the 2011 car, and required the use of Tilton 77 series inclined master cylinders. The cost of these parts was very high (\$400) and the team had one spare from the 2009 car, so it was quickly decided to design the new system to reuse this component.

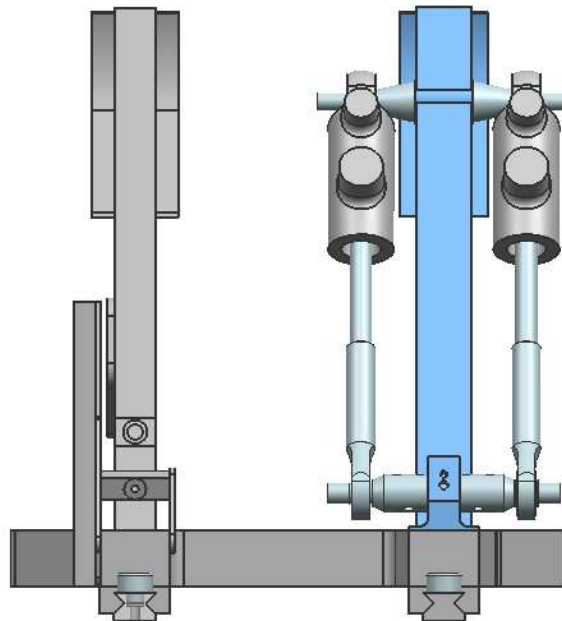


Figure 31: Pedal box as viewed from the front bulkhead, including the bias bar assembly

Brake bias is one of the fundamental tuning adjustments on the car. This was provided by mounting the forward end of the master cylinders to a bar that was free to rotate about its own centre. The bar had holes drilled along it at 5% increments of length, allowing the bias to be adjusted in a finite and repeatable way by moving the pivot point, and thus the load from the pedal reacted by each master cylinder.

The circuit was completed using standard -4 fittings. The brake pressure sensors were connected to the car's data logging system, allowing close examination of the driver's braking behaviour and consistency of brake bias.

7.3.2 Rotor Mounting

Most commercial brake systems use rotors that are fixed directly to their hubs, with either a one sided floating or opposed piston arrangement .

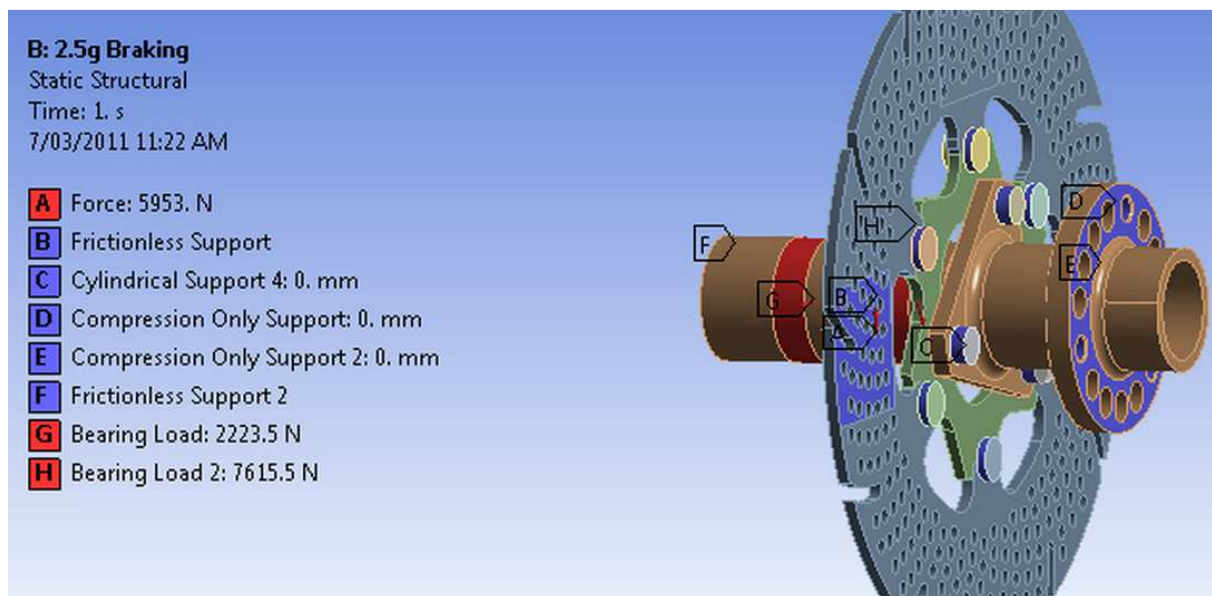
Any of these arrangements should be capable of applying an equal force to each side of a brake rotor; however, experience has shown that static friction in sliding calipers and poorly matched seals and

Final Year Project 2011
Final Report

pistons tend to bias the force to one pad. This leads to inconsistent pad wear and, more importantly in a performance car application, inconsistent brake feel as left-right pairs of calipers 'grip' the rotor to different degrees. As it was not acceptable to redesign and rebuild the brakes during the year, it was decided to use the most error tolerant arrangement - that of opposed pistons with a floating rotor.

Most OEM motorcycle floating rotors transfer torque through flanged cylinders, usually called bobbins or buttons. The usual means of installing and retaining the bobbins is through a circlip installed in a groove; this was not considered acceptable, as unpredictable side loading had caused the circlips to come unseated in 2010, and there was no apparent robust means to improve this.

To make the brake rotor mounting as robust as possible, the bobbins did not connect the rotor directly to the hub; rather, an intermediate brake 'spider' was used. This allowed the bobbins to be welded together between the rotor and spider, making the spider, bobbins and rotor a permanent assembly. The spider connected to the hub through three cap screws retained by nyloc nuts; the redundant loading between the six bobbins and three cap screws made the bolt loading very uncertain, so some time was dedicated to FEA analysis of the whole assembly, with correct contact constraints (see figure 31). This method of retaining the rotor also had the advantage that it greatly simplified the machining of the front hub flange - this could now be accomplished by milling three flats on a circular flange.



To meet the larger rotor at the front, the caliper had to be mounted some distance out from the axle line. By constraining the upright to a simple shape, the mounting options were limited). To reduce the CG height of the assembly, the caliper was mounted as low as possible within the available space. This meant the bottom mount could attach with a simple lug connected to the wall of the upright; the top mount, however, was required to bridge a significant gap.

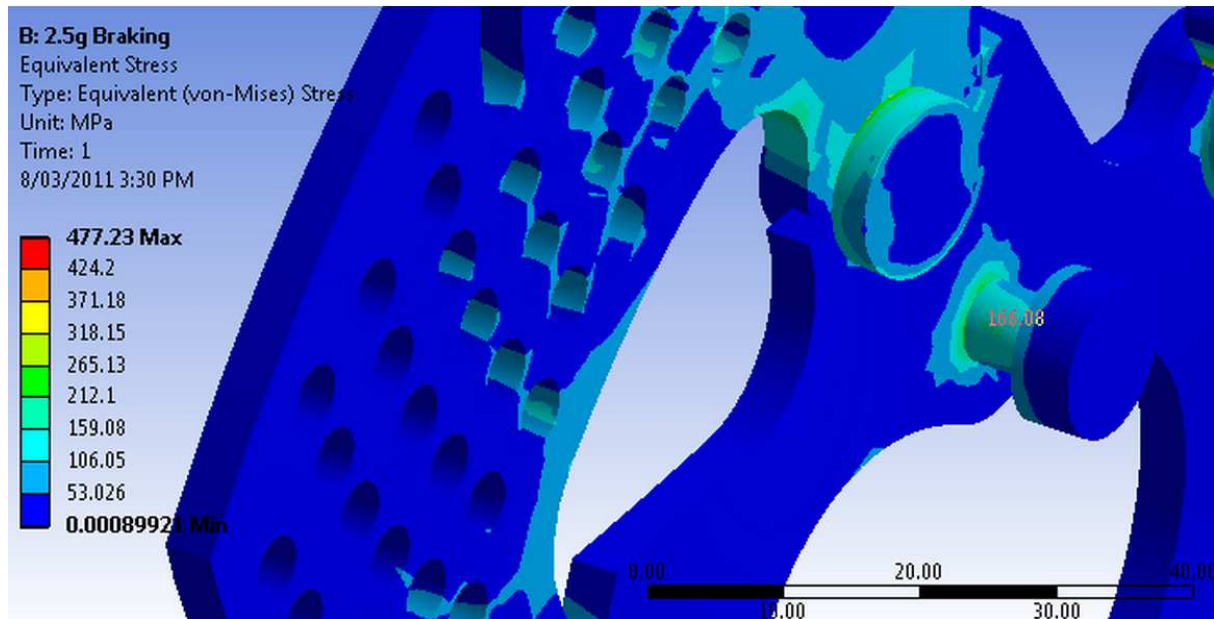


Figure 32: FEA setup and solution of the complete brake and hub assembly. Correct contact constraints were used, causing a very slow solution process.

As the two mounts caused redundant loading, it was possible to reduce the load acting in the x-z plane by reducing its stiffness; a low bending stiffness made the connection to the upright act as a pinned joint (see figure 33).

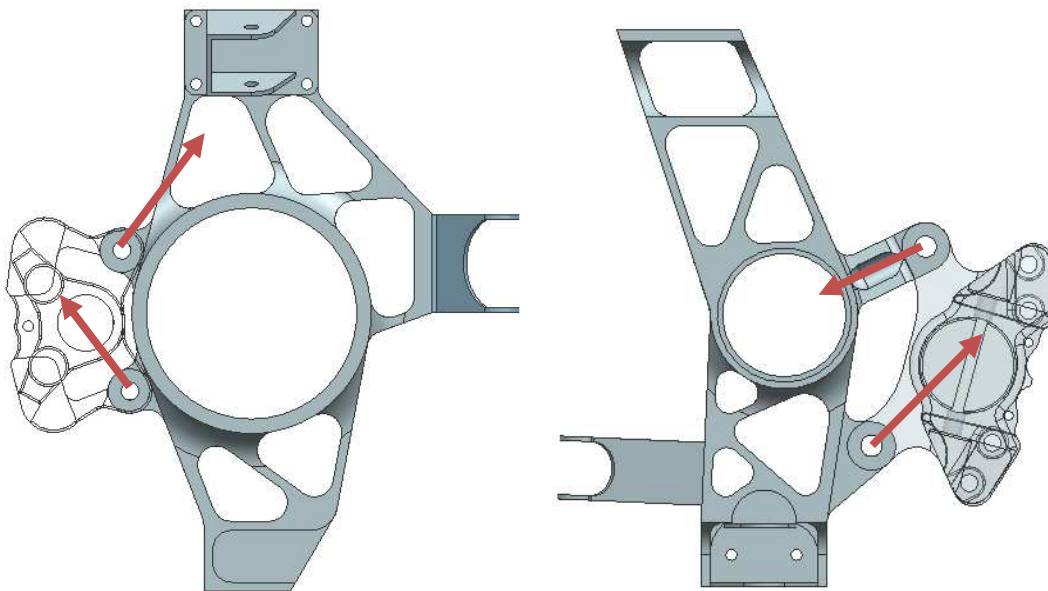


Figure 33: Forces applied to the uprights by the brake calipers

A further measure to enhance the robustness of this arrangement was an attempt to use the bobbins for lateral retention only, with torque transmitted through teeth on the spider directly to the rotor arms.

7.3.3 Caliper Selection

There are a very wide range of brake calipers available that are suitable for a Formula SAE car. OEM front calipers from sports bikes are well suited to the application, as they are designed to stop a vehicle of similar size to and FSAE car in competitive riding situation. Other suitable brakes are designed for duty as front or rear brakes on small (400-500kg) formula cars.

A range of options were assessed, and the final decision was driven mostly by cost and availability - lightweight calipers have a low thermal mass, and can detract from the performance of the system, so weight was not a strong driving consideration.

Table 7: Comparison of common caliper options.

	Brembo 4pot (typical)	Red Devil sprint	Wilwood Dynapro	KTM superduke	KTM ATV (Magura)
Cost	\$100	\$295	\$106 (or \$65 from Ohio uni)	Free	Free
Weight	700g	650g (dry, no pads)	800g (dry, no pads)	?	?
Pistons	4	4	2	4	4
Piston dia	30	31.75	44.45 or 35.0	?	26
Total piston area	2827mm ²	3166mm ²	3103mm ² (44.45)	?	2123mm ²
Mounting	Radial	Axial	Axial	Radial	Axial
Pads	\$90	\$84	\$70	\$71	\$53

The Wilwood Dynapro was selected from this list. The low price and easy availability of this caliper made it particularly attractive, and it had a strong reputation among other Formula SAE teams.

7.4 Wishbones

The wishbones are among the simplest components in a double wishbone setup. Each wishbone is the assembly of two axially loaded members, two ends constrained to the chassis and one end to the upright, and is thus able to constrain two degrees of freedom. It is usually convenient to react vertical loads through one wishbone on each corner. The M11 also uses wishbones to react the downforce generated by its wings.

For packaging reasons, the car is arranged with pullrods on the front and pushrods on the rear. These rods attach to the wishbone some distance from the upright, to clear the brake rotors through the full range of suspension movement. This imposes a large bending load on the wishbone tubes of the front upper and rear lower wishbones.

Round tube was chosen as the basis for the wishbones, due to its ready availability in higher grades of steel and ease of fabrication. Most of the design effort was focused on designing against failure. Three major failure modes were considered - failure due to yield in axial tension or compression, buckling in compression and bending. The effects of the bending and axial load were also considered together. The

useful life of a Formula SAE car is short enough that fatigue is not a major consideration; the safety factor used to account for unexpected overloads and material inconsistencies was considered large enough to eliminate this as a concern.

AISI 4130 steel was used for the tube and sheet elements. 4130 is used on several sections of the car, due to weldability similar to mild steel. The residual stresses generated in welding this material reduce the strength of the joint to significantly lower than that of the base metal; this can be offset with heat treatment. One of the teams' long term sponsors specialises in metal treatment, so a wide variety of treatments are available; post weld stress relief was used for the wishbones, as it can return most of the strength to the joints.

Using the method shown in appendix D, the maximum load in each tube was found for each load case. A range of common tube diameters and wall thicknesses were analysed, with the stress from each load case compared to the yield strength of the material to generate a minimum safety factor. A weight for each tube was also included. The results are summarised in table 8

Table 8: Steel tube used in the wishbones

	Tube Gauge	Min Safety Factor
Front Upper	3/4"x1.2mm	1.41
Front Lower	5/8"x0.9mm	2.33
Rear Upper	5/8"x0.9mm	4.20
Rear Lower	3/4"x1.2mm	1.42

A minimum safety factor of 1.4 was applied. Although this analysis showed that 1/2" (12.7mm) OD wishbones were feasible for the front lower wishbones, 5/8" tubes were specified instead due to concerns about a bending overload from a wayward cone becoming jammed between the wheel and the wishbone. This scenario occurred on the second day of testing.

The wishbones were designed with some kinematic adjustment in mind. The front lower wishbones were fitted with threaded adjustment on both ends, allowing caster adjustment and limited kingpin inclination adjustment (the wishbone must be strained to adjust kingpin inclination). A similar arrangement was used on the rear upper wishbones.

One unusual feature of the wishbones was designed with consideration of upright machining - the inclination of the front upper wishbone exceeded the angular displacement limit of the outboard spherical bearing. Normally this would require an angled clevis to be built into the upright, but this would drastically complicate the machining of the upright. The issue was solved by inclining the bearing cup on the wishbone, as shown in figure 34.



Figure 34: Inclined bearing cup arrangement on the front upper wishbone

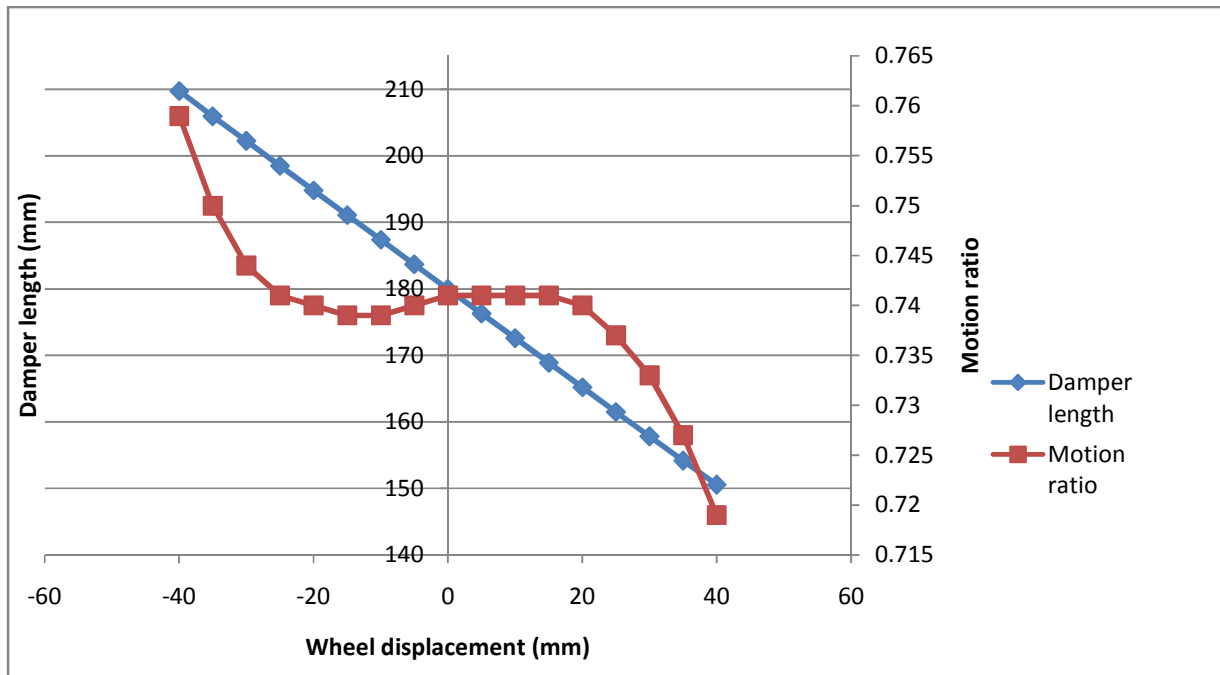
Steel on steel rod ends formed the basis of this adjustment. Threaded inserts were turned on a manual lathe and welded into the tube ends. The push and pull rods were connected to the wishbones through a laser cut sheet steel clevis, welded onto a gusset. Where adjusters weren't necessary, plain spherical bearings were used. The relatively small axial load applied to the bearings on the chassis side of the wishbones lent themselves to narrow race sphericals, retained by staking. The bearing cups for these sphericals were laser cut and welded onto the tubes, then the bore was machined in place. The outboard spherical joints, particularly on the front upper and rear lower wishbones, are subject to a more significant axial load, so wider race bearings were used in a machined bearing cup. The bearing cup included a shoulder and circlip groove for retention.

7.5 Bellcranks

The bellcranks transmit the force and motion of the spring/damper to the wishbone. The main complicating factor in their design is kinematics; for the car to respond well, the motion ratio (ratio of shock movement/wheel movement) must be nearly constant, giving a linear response, ideally with a slightly increasing value as the wheel moves in either direction from its static position (in practice, this sometimes is not possible). With the shock and wishbone pickup points largely fixed by stiffness and packaging considerations, the choice of bellcrank points was critical. Figure 11 tracks the motion of the rear wheel relative to the compression of the spring and damper with the chosen bellcrank points on the rear of the car; the motion ratio is the derivative of the nearly linear curve relating wheel and damper displacement.

On the rear of the car, the linkage including the shock pickup, pushrod, bellcrank and shock pickup are relatively in plane, and two separate aluminium plates gave sufficient out of plane stiffness. These were simply laser cut and reamed. On the front, packaging difficulties made the linkage less than ideal, with significantly more out of plane loading. These bellcranks were therefore made of fabricated 4130 sheet, with shear plates between the two sides, to increase the out of plane stiffness to an adequate level.

Figure 35: Motion of the rear bellcranks



On both the front and rear of the car, the bellcranks pivot about deep groove ball bearings.

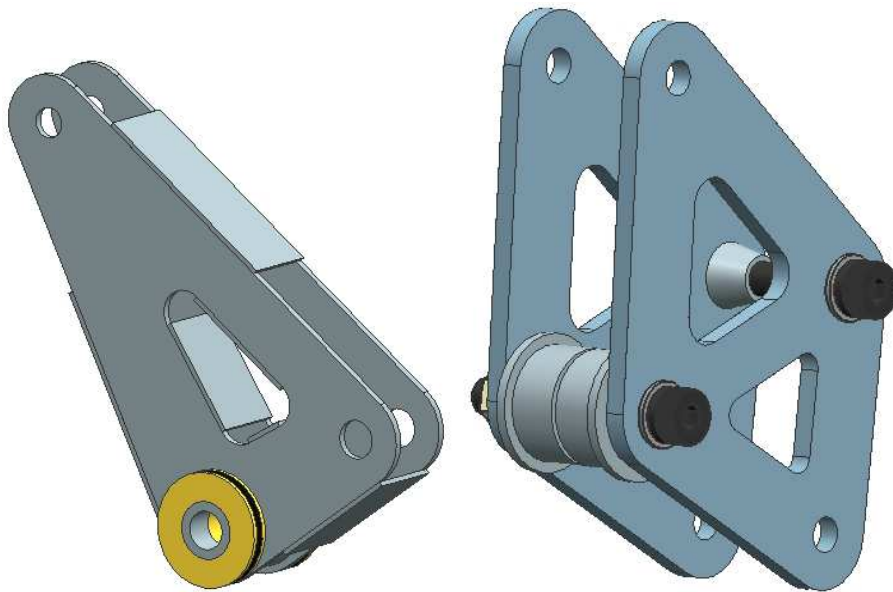


Figure 36: Front (left) and rear (right) bellcranks, with fasteners

7.6 Anti Roll Bars

The anti roll bar is a displacement sensitive suspension element that does not react to bump motion (both wheels in a pair displacing equally) but provides a restoring force to react a rolling motion (unequal wheel displacements). Many different arrangements can achieve this aim, and the design is often driven by packaging constraints as much as any other consideration.

One advantage utilising inboard damper actuation is that arguably the simplest solution - a bar bent into a u shape, connected to the suspension via drop links - could be installed relatively easily. On the rear of the car, sufficient space was available that a single bar could be used, with simple finite adjustment of the drop link location to change the effective stiffness of the bar.

The front antiroll bar was designed in a similar way. However, the front suspension and wing mounts were already competing for space between the chassis and front wheel, and finite adjustment was not possible in the same way as on the rear of the car. Instead of removing the tuning adjustment afforded by variable stiffnesses, three different bars were fabricated, all with different wall thicknesses and stiffnesses.

Both antiroll bars were mounted on manually machined aluminium bearing blocks supporting bronze bushings.



Figure 37: Components competing for packaging space around the front left wheel

8. TESTING

8.1 *Shakedown Testing*

Shakedown testing: Although all efforts had been made to build a robust car, it was expected that some failures would occur when the car was first run under power. Surprisingly, no major failures occurred on this first day of testing; the car ran for several hours without incident. The lack of suspension setup, however, was evident. The car pushed to one side under power, and one driver spun the car three times on the same lap. This led the team to set corner weights properly, and to reduce front camber, which was excessive due to incorrect wishbone lengths.

8.2 *Spring and Antiroll Bar (Steady State) Testing*

Spring/anti roll bar balance: Three test days were dedicated to establishing the oversteer/understeer balance of the car. The dampers were set to their lowest settings to minimise their effect on the behaviour of the car, and a short track was set up with two constant radius corners of 4m and 5m inside radius. Initially, soft springs (200-250lb/in) were tested, with anti roll bars and relative front and rear ride springs changed in response to driver feedback. At the same time, the development driver reported consistent understeer upon turning into the corners. Although this could have been remedied with damper settings, the team took the opportunity to lower the front roll centres - this increased the elastic weight transfer on the front of the car relative to the geometric weight transfer, and so increased the front end grip during the initial turn in stage of cornering. A reduction in front roll centre of only 10mm proved satisfactory.

8.3 *Damper Testing*

With the steady state, non winged balance achieved, improvements were sought through damper tuning. The planned dyno testing by the Holden Racing Team had to be put off due to other commitments, so this was undertaken blindly - no calculations were done on the frequency response for different settings. High speed damping was initially left at its softest setting, while low speed damping was varied on the front and rear of the car respectively. The damping was increased gradually until the point where driver feedback indicated that an optimum value had been reached and exceeded - the damper was then changed back to the previous setting.

High speed damping was then increased in a similar way. This testing regime was very efficient, and a good setting was achieved very early in the day. Spring stiffnesses were increased to give more 'baseline' setups to use when wings were added to the setup. As spring stiffness was increased from 200lb/inch on all four wheels to 350 and 450 lb/inch, the car remained very well balanced - only changes in damper settings were needed to return the car to a good setup.

9. FAILURES AND SUGGESTED IMPROVEMENTS

Until the date of writing of this report, the 2011 car had proven to be among the most reliable ever produced by the Monash team. However, due to the prototype nature of the car and the speed with which it was designed and built, it was always accepted that some part failures were inevitable.

Final Year Project 2011
Final Report

Great care was taken in designing the front hubs to withstand the significant loads applied to them. The bearing arrangement required the use of two small spacers, against which the tapered roller bearings could be preloaded. The loading of the spacers was overlooked, and they were manufactured from 2mm thick aluminium tube. Under normal driving, the whole axial force applied to the hub (i.e. the total side loading on the tyre) had to be reacted through this spacer. One end of the spacer was butted against the radius manufactured into the inner race of the bearing, leaving an even lesser thickness of material in contact.

The resulting failure is shown in figure 38. The hub spacer was crushed against the bearing, causing the aluminium to yield and forcing it into the space formed between the bearing radius and the hub. Prior to the hub and upright being disassembled, the castellated nut that applied the preload to the assembly had been tightened several times, appearing to come loose repeatedly. This should have been recognised as an issue earlier on. The fault was only detected when the three cap screws holding the brake spider to the hub made contact with the upright, causing the assembly to seize.



Figure 38: Crushed spacer being extracted from the front hub

This failure demonstrates the need to analyse all parts in an assembly, not just the large and obvious ones.

As discussed in an earlier section, the uprights were originally intended to be machined from aluminium billet. Although previous experience had shown that machined uprights tended to be very time consuming and unreliable in their manufacture, it was thought that by carefully considering toolpaths during their design, the uprights could be made from this way without these issues. By virtue of

Final Year Project 2011
Final Report

packaging constraints, the rear uprights were the simpler to make, only requiring two machine setups on a three axis mill. However, between programming, finding appropriate tools, machine setup and checking tolerances, the total time needed to manufacture these parts was estimated at 40 hours after they were finished. As the driving deadline approached and not enough NC time was available to manufacture the front uprights, a change of plan was needed; temporary uprights were designed to be laser cut from relatively thick mild steel, and were manufactured within three days of the laser cutting being finished.



Figure 39: Mild steel uprights after welding

Although twice the weight of the original NC designs, these uprights tolerated months of initial testing with no issues. They will be replaced with lighter sheet metal uprights closer to the competition date.

The details of the rear constant velocity joints have not been discussed in this report. However, one failure related to these components is relevant to the suspension design. The CV joints are of a tripod design, transmitting the engine torque through three lobes mounted on needle roller bearings. Aluminium was the only reasonably light alternative for use in the rear hub, but it was considered too soft to react the contact force of the lobes. A steel sleeve was hot wire cut and press fit into a matching shape machined into the hubs. These sleeves were originally meant to be cut from through hardened EN26 steel; this was not available before the driving deadline, so mild steel was used instead.

When exposed to shock loads from the driveline, the mild steel sleeve material was crushed, wearing a deep groove into the sleeve and forcing a large burr to form alongside it, as shown in figure 40. This was a problem for a number of reasons - the groove caused the hub and driveshaft to rotate relative to one another (ie freeplay), which led to backlash in the engagement of the limited slip differential. This may have contributed to some of the oscillatory 'hopping' behaviour observed in recent testing. The

driveshafts became jammed in the hubs, and could not be removed without an extreme degree of leverage. The force with which the burrs retained the



Figure 40: Damaged rear hub sleeve

The car was designed close to its rollover point, to take advantage of a narrow track width. During damper testing, it was shown that the CG height was slightly greater than expected, as the car began to roll several times.



Figure 41: Initiation of a full vehicle roll

Further testing with linear potentiometers attached to the wishbone arms showed that in cornering, the increase in damper length on the inside wheels was much greater than the decrease on the outside wheels - the car was jacking up, a result of roll centres that were too high. The effect was difficult to replicate, and never occurred again after the roll centres were lowered.

10. CONCLUSIONS

The 2011 suspension system represents an excellent achievement by Monash Motorsport - a complete system designed from scratch and manufactured in record time. This is a result of goal setting which acknowledged the tight timeline faced by designers.

The clear imperative to get the most out of the car through robust, reliable designs filtered down to the component design level. The few failures experienced in testing to date resulted from neglecting small issues, rather than fundamentally flawed approaches to design.

All component weights met their targets according to CAD modelling, and physically weighing the parts should confirm this. Shortly after this report is written, the car will be broken down, giving an opportunity to weigh parts and check for compliance with the targets set out in section 4.6.

The large range of adjustments built into the system has already been very well utilised, even though the team is in a relatively early stage of testing. The car as a whole shows great promise at the testing stage, and is expected to continue the success of the Monash team into the future.

11. ACKNOWLEDGEMENTS

Thanks to Scott Wordley, Steven Webb, Martin Bett, Travis Leenaerts and the new suspension recruits for their valuable contributions. Also thanks to Calspan and the FSAE TTC volunteers, for their valuable work in making tyre data available to students.

12. REFERENCES

- Kasprzak, M. E., & Gentz, D. 2006. *The Formula SAE Tire Test Consortium—Tire Testing and Data*. SAE International.
- Liu, Q., Lee, J., and Guo, K 2007 "*Analysis of Non-Steady State Tire Cornering Properties Based on String-Concept Deformation and Geometric Relationship of Contact Patch*," SAE International
- Milliken, D. & Milliken, W 1995, *Race Car Vehicle Dynamics*, SAE International
- Narasimha Rao, K., Kumar, R., and Bohara, P. 2004 "*Prediction Of Tyre Force And Moment Characteristics During Vehicle Cornering Using Finite Element Techniques*, SAE International
- Pacejka, H 2002, *Tyre and Vehicle Dynamics*, Elsevier Butterworth-Heinemann
- Smith, C. 1978, *Tune to Win*. St. Paul: Motorbooks.
- Sorniotti, A. and Velardocchia, M 2008 "*Enhanced Tire Brush Model for Vehicle Dynamics Simulation*," SAE International

Final Year Project 2011
Final Report

Staniforth, A. 1999, *Competition Car Suspension*. Somerset: Haynes Publishing.

Svendenius, J. and Gäfvert, M 2004 "A Brush-Model Based Semi-Empirical Tire-Model for Combined Slips," SAE International

Trevorrow, N. 2006, *A theoretical model and experimental investigation of racing slick tyre performance and behaviour*, Monash University Dept of Mechanical Engineering

13. APPENDICES

13.1 Appendix A: 3D Vector Force Analysis in Upright Design

Out of necessity, many spreadsheets have been produced by the Monash team to predict loads in components for the purpose of stress and deflection analysis. The suspension system is functionally a collection of linkages in three dimensions, and analysing the loads at important points using two dimensional free body diagrams requires a number of assumptions to be made. Finite element analysis is being increasingly used to predict actual stress and deflection in more complex geometries; however, the accuracy of the output of FEA analyses is fundamentally limited by the accuracy of the inputs and boundary conditions (a common phrase used to describe FEA is 'rubbish in, rubbish out').

To improve the accuracy of FEA analyses, and improve confidence in the results, a spreadsheet was developed that writes and solves a free body diagram in three dimensions, removing most of the assumptions that cause problems with two dimensional FBDs. The spreadsheet uses basic vector algebra to express the equations of static equilibrium as simultaneous equations in vector matrix form. The equations can then be solved in an automated fashion.

The underlying assumptions of this analysis are

- The free body includes the tyre, wheel, upright and hub, and is has loads applied at the contact patch, upper and lower wishbone points, and tie rod point.
- The system is in steady state, so this is a quasi-static analysis.
- The load from the contact patch is a point load, and no moment is generated by the tyre. This assumption can be corrected by moving the contact patch point back, which simulates the self aligning torque provided by the tyres.
- The wishbone point connected to the shock (in the case of the 2011 car, the front upper wishbones and rear lower wishbones) can provide a load in any direction, ie it is fully constrained.
- The other wishbones can only provide a load in their own plane - this is accurate given the degrees of freedom provided by the spherical bearings.
- The aerodynamic downforce is a vertical vector applied at the upper wishbone point
- Under acceleration, a torque is applied to the free body by the driveshaft.

Apart from the steady state and contact patch point load assumptions, very little is lost between the reality and this model of the system.

The user must provide geometrical information, in the form of suspension points and a contact patch points. These are easily obtained from the CAD model of the car. The user must also provide a contact patch load for the corner of the car in question, which can be obtained from any good vehicle dynamics textbook. The tie rod is axially loaded, so the direction of the force it applies to the free body must be in the direction of the rod orientation. This load can be expressed as the vector

$$\mathbf{F}_T = |F_T|\hat{T}_x \mathbf{i} + |F_T|\hat{T}_y \mathbf{j} + |F_T|\hat{T}_z \mathbf{k}$$

where

$$\hat{\mathbf{T}} = \hat{T}_x \mathbf{i} + \hat{T}_y \mathbf{j} + \hat{T}_z \mathbf{k} = \frac{\mathbf{T}_O - \mathbf{T}_I}{\sqrt{(T_{O,x} - T_{I,x})^2 + (T_{O,y} - T_{I,y})^2 + (T_{O,z} - T_{I,z})^2}}$$

where \mathbf{T}_O and \mathbf{T}_I refer to the outboard and inboard points of the tie rod respectively.

The forces applied to the upright by the lower and upper wishbones respectively are denoted as

$$\mathbf{F}_L = F_{L,x}\mathbf{i} + F_{L,y}\mathbf{j} + F_{L,z}\mathbf{k}, \quad \mathbf{F}_U = F_{U,x}\mathbf{i} + F_{U,y}\mathbf{j} + F_{U,z}\mathbf{k}$$

However, these expressions alone don't quite capture the behaviour of the wishbone without the push/pullrod or shock connected. An additional condition must be applied to constrain the force to be in plane with this wishbone. Assuming the upper wishbone is the one carrying the planar force,

$$\mathbf{V}_N = \mathbf{U}_F \times \mathbf{U}_A, \quad \mathbf{U}_F = (U_{o,x} - U_{f,x})\mathbf{i} + (U_{o,y} - U_{f,y})\mathbf{j} + (U_{o,z} - U_{f,z})\mathbf{k},$$

$$\mathbf{U}_L = (U_{o,x} - U_{a,x})\mathbf{i} + (U_{o,y} - U_{a,y})\mathbf{j} + (U_{o,z} - U_{a,z})\mathbf{k},$$

Where, for example, $U_{f,x}$ is the difference between the x coordinates of the outboard and fore inboard points of the upper wishbone. \mathbf{V}_N is a vector perpendicular to the plane of the wishbone.

$$\mathbf{V}_N = \begin{vmatrix} U_{o,y} - U_{f,y} & U_{o,z} - U_{f,z} \\ U_{o,y} - U_{a,y} & U_{o,z} - U_{a,z} \end{vmatrix} \mathbf{i} - \begin{vmatrix} U_{o,x} - U_{f,x} & U_{o,z} - U_{f,z} \\ U_{o,x} - U_{a,x} & U_{o,z} - U_{a,z} \end{vmatrix} \mathbf{j} + \begin{vmatrix} U_{o,x} - U_{f,x} & U_{o,y} - U_{f,y} \\ U_{o,x} - U_{a,x} & U_{o,y} - U_{a,y} \end{vmatrix} \mathbf{k}$$

The planar force condition is enforced by

$$\mathbf{V}_N \cdot \mathbf{F}_U = 0$$

The vectormatrix form of the system can now be written as (see next page)

$$\begin{bmatrix}
1 & 0 & 0 & 1 & 0 & 0 & \frac{T_{0,x} - T_{1,x}}{|\mathbf{T}_0 - \mathbf{T}_1|} \\
0 & 1 & 0 & 0 & 1 & 0 & \frac{T_{0,y} - T_{1,y}}{|\mathbf{T}_0 - \mathbf{T}_1|} \\
0 & 0 & 1 & 0 & 0 & 1 & \frac{T_{0,z} - T_{1,z}}{|\mathbf{T}_0 - \mathbf{T}_1|} \\
0 & CP_z - L_{0,z} & L_{0,y} - CP_y & 0 & CP_z - U_{0,z} & U_{0,y} - CP_y & \frac{T_{0,y} - T_{1,y}}{|\mathbf{T}_0 - \mathbf{T}_1|} (CP_z - T_{0,z}) - \frac{T_{0,z} - T_{1,z}}{|\mathbf{T}_0 - \mathbf{T}_1|} (CP_y - T_{0,y}) \\
CP_z - L_{0,z} & 0 & L_{0,x} - CP_x & CP_z - U_{0,z} & 0 & U_{0,x} - CP_x & \frac{T_{0,x} - T_{1,x}}{|\mathbf{T}_0 - \mathbf{T}_1|} (CP_z - T_{0,z}) - \frac{T_{0,z} - T_{1,z}}{|\mathbf{T}_0 - \mathbf{T}_1|} (CP_x - T_{0,x}) \\
CP_y - L_{0,y} & L_{0,x} - CP_x & 0 & CP_y - U_{0,y} & U_{0,x} - CP_x & 0 & \frac{T_{0,x} - T_{1,x}}{|\mathbf{T}_0 - \mathbf{T}_1|} (CP_y - T_{0,y}) - \frac{T_{0,y} - T_{1,y}}{|\mathbf{T}_0 - \mathbf{T}_1|} (CP_x - T_{0,x}) \\
0 & 0 & 0 & \begin{bmatrix} U_{0,y} - U_{f,y} & U_{0,z} - U_{f,z} \\ U_{0,y} - U_{a,y} & U_{0,z} - U_{a,z} \end{bmatrix} & - \begin{bmatrix} U_{0,x} - U_{f,x} & U_{0,z} - U_{f,z} \\ U_{0,x} - U_{a,x} & U_{0,z} - U_{a,z} \end{bmatrix} & \begin{bmatrix} U_{0,x} - U_{f,x} & U_{0,y} - U_{f,y} \\ U_{0,x} - U_{a,x} & U_{0,y} - U_{a,y} \end{bmatrix} & 0
\end{bmatrix}
\begin{bmatrix} F_{L,x} \\ F_{L,y} \\ F_{L,z} \\ F_{U,x} \\ F_{U,y} \\ F_{U,z} \\ |F_T| \end{bmatrix} = \begin{bmatrix} F_{CP,x} \\ F_{CP,y} \\ F_{CP,z} \\ 0 \\ 0 \\ 0 \\ 0 \end{bmatrix}$$

This can be solved for the force vector.

13.2 FEA output

Displacement - Nodal, Magnitude
 Min : 0.000e+000, Max : 3.371e-001, mm
 Deformation : Displacement - Nodal

Stress - Elemental, Von-Mises
 Min : 5.829e-003, Max : 2.266e+002, N/mm²(MPa)
 Deformation : Displacement - Nodal

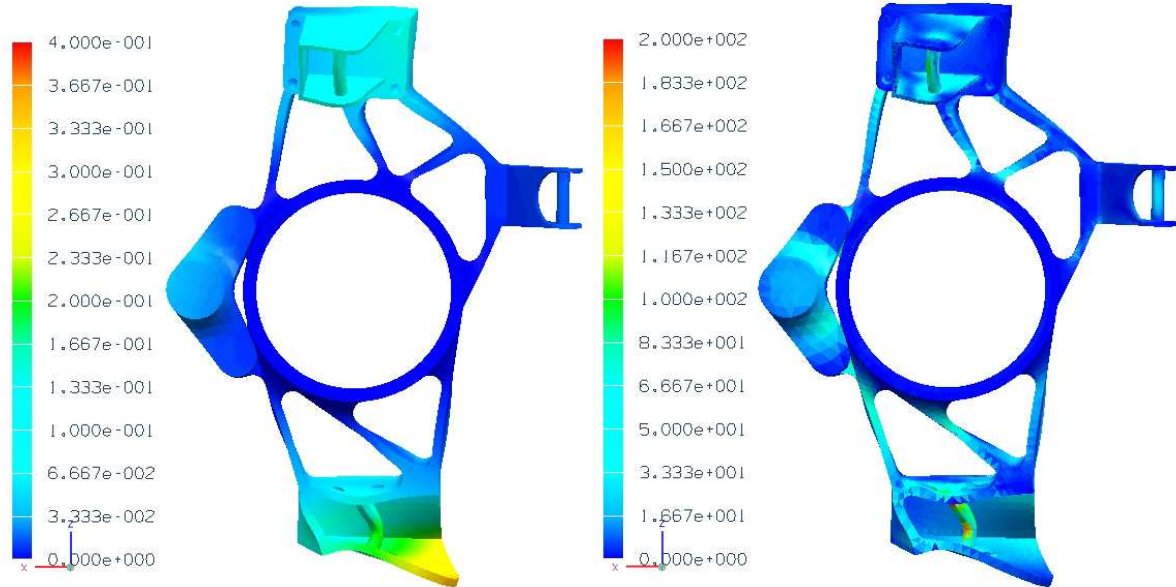


Figure 42: Combined braking/cornering

Displacement - Nodal, Magnitude
 Min : 0.000e+000, Max : 6.933e-002, mm
 Deformation : Displacement - Nodal

Stress - Elemental, Von-Mises
 Min : 3.333e-003, Max : 7.656e+001, N/mm²(MPa)
 Deformation : Displacement - Nodal

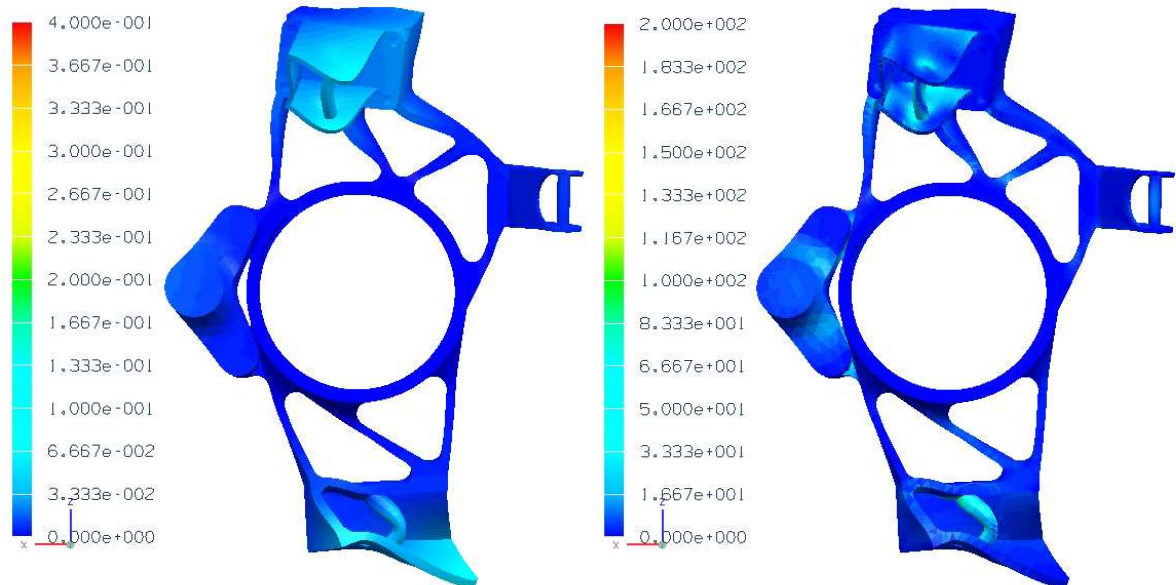


Figure 43: Braking

Final Year Project 2011
Final Report

Displacement - Nodal, Magnitude
 Min : 0.000e+000, Max : 1.364e-001, mm
 Deformation : Displacement - Nodal

Stress - Elemental, Von-Mises
 Min : 1.310e-003, Max : 9.824e+001, N/mm²(MPa)
 Deformation : Displacement - Nodal

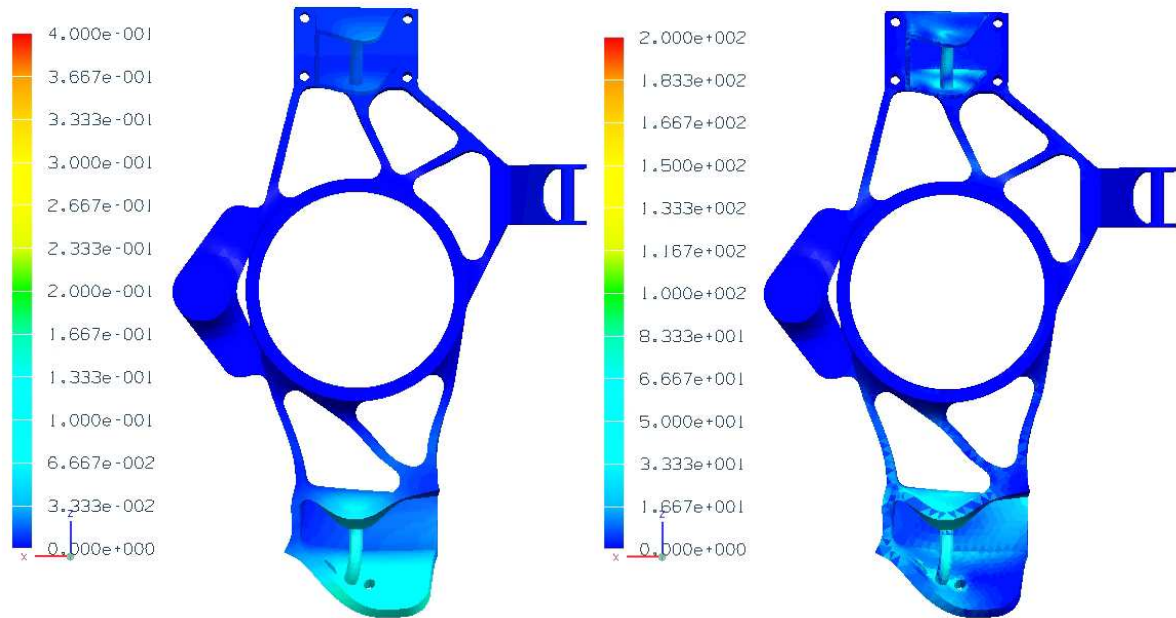


Figure 44: Bump

Displacement - Nodal, Magnitude
 Min : 0.000e+000, Max : 4.620e-001, mm
 Deformation : Displacement - Nodal

Stress - Elemental, Von-Mises
 Min : 1.264e-002, Max : 2.767e+002, N/mm²(MPa)
 Deformation : Displacement - Nodal

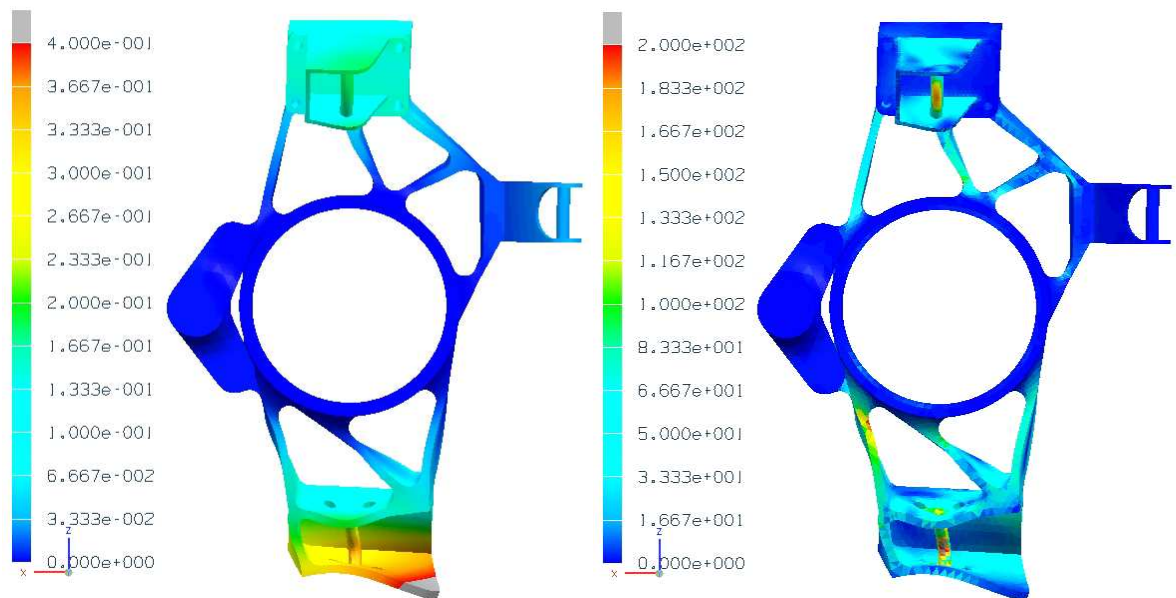


Figure 45: Cornering

13.3 Appendix B: Formula SAE Rules Relevant to Suspension Design

The following is a complete list of the rules from the 2011 Formula SAE rulebook that directly affect the design of suspension components:

B2.3 Wheelbase

The car must have a wheelbase of at least 1525 mm (60 inches). The wheelbase is measured from the center of ground contact of the front and rear tires with the wheels pointed straight ahead.

B2.4 Vehicle Track

The smaller track of the vehicle (front or rear) must be no less than 75% of the larger track.

B6.1 Suspension

B6.1.1 The car must be equipped with a fully operational suspension system with shock absorbers, front and

rear, with usable wheel travel of at least 50.8 mm (2 inches), 25.4 mm (1 inch) jounce and 25.4 mm (1 inch) rebound, with driver seated. The judges reserve the right to disqualify cars which do not represent a serious attempt at an operational suspension system or which demonstrate handling inappropriate for an autocross circuit.

B6.1.2 All suspension mounting points must be visible at Technical Inspection, either by direct view or by removing any covers.

B6.2 Ground Clearance

There is no minimum ground clearance requirement. However, teams are reminded that under Rule D1.1.2 any vehicle condition which could, among other things, "... compromise the track surface" is a valid reason for exclusion from an event. Any vehicle contact that creates a hazardous condition or which could damage either the track surface or the timing system is cause for declaring a vehicle DQ.

B6.3 Wheels

B6.3.1 The wheels of the car must be 203.2 mm (8.0 inches) or more in diameter.

B6.3.2 Any wheel mounting system that uses a single retaining nut must incorporate a device to retain the nut

and the wheel in the event that the nut loosens. A second nut ("jam nut") does not meet these requirements.

B6.3.3 Standard wheel lug bolts are considered engineered fasteners and any modification will be subject to

extra scrutiny during technical inspection. Teams using modified lug bolts or custom designs will be required to provide proof that good engineering practices have been followed in their design.

B6.3.4 Aluminum wheel nuts may be used, but they must be hard anodized and in pristine condition.

B6.4 Tires

B6.4.1 Vehicles may have two types of tires as follows:

- **Dry Tires** – The tires on the vehicle when it is presented for technical inspection are defined as its "Dry Tires". The dry tires may be any size or type. They may be slicks or treaded.
- **Rain Tires** – Rain tires may be any size or type of treaded or grooved tire provided:

Final Year Project 2011
Final Report

1. The tread pattern or grooves were molded in by the tire manufacturer, or were cut by the tire manufacturer or his appointed agent. Any grooves that have been cut must have documentary proof that it was done in accordance with these rules.

2. There is a minimum tread depth of 2.4 mms (3/32 inch).

Note: Hand cutting, grooving or modification of the tires by the teams is specifically prohibited.

B6.4.2 Within each tire set, the tire compound or size, or wheel type or size may not be changed after static

judging has begun. Tire warmers are not allowed. No traction enhancers may be applied to the tires after the static judging has begun.

B6.7 Rollover Stability

B6.7.1 The track and center of gravity of the car must combine to provide adequate rollover stability.

B6.7.2 Rollover stability will be evaluated on a tilt table using a pass/fail test. The vehicle must not roll when

tilted at an angle of sixty degrees (60°) to the horizontal in either direction, corresponding to 1.7 G's.

The tilt test will be conducted with the tallest driver in the normal driving position.

ARTICLE 7: BRAKE SYSTEM

B7.1 Brake System - General

The car must be equipped with a braking system that acts on all four wheels and is operated by a single control.

B7.1.1 It must have two independent hydraulic circuits such that in the case of a leak or failure at any point in

the system, effective braking power is maintained on at least two wheels. Each hydraulic circuit must have its own fluid reserve, either by the use of separate reservoirs or by the use of a dammed, OEMstyle reservoir.

B7.1.2 A single brake acting on a limited-slip differential is acceptable.

B7.1.3 The brake system must be capable of locking all four (4) wheels during the test specified below.

B7.1.4 "Brake-by-wire" systems are prohibited.

B7.1.5 Unarmored plastic brake lines are prohibited.

B7.1.6 The braking systems must be protected with scatter shields from failure of the drive train (see B.8.13)

or from minor collisions.

B7.1.7 In side view no portion of the brake system that is mounted on the sprung part of the car can project

below the lower surface of the frame or the monocoque, whichever is applicable.

B7.1.8 The brake pedal shall be designed to withstand a force of 2000 N without any failure of the brake system or pedal box. This may be tested by pressing the pedal with the maximum force that can be exerted by any official when seated normally.

B7.1.9 The brake pedal must be fabricated from steel or aluminum or machined from steel, aluminum or titanium.

B7.2 Brake Test

The brake system will be dynamically tested and must demonstrate the capability of locking all four

(4) wheels and stopping the vehicle in a straight line at the end of an acceleration run specified by the brake inspectors.

B7.3 Brake Over-Travel Switch

B7.3.1 A brake pedal over-travel switch must be installed on the car. This switch must be installed so that in

the event of brake system failure such that the brake pedal over travels, the switch will be activated and will stop the engine from running. This switch must kill the ignition and cut the power to any electrical fuel pumps.

B7.3.2 Repeated actuation of the switch must not restore power to these components, and it must be designed

so that the driver cannot reset it.

B7.3.3 The switch must be implemented with analog components, and not through recourse to programmable

logic controllers, engine control units, or similar functioning digital controllers.

B7.4 Brake Light

B7.4.1 The car must be equipped with a red brake light of at least 15 watts, or equivalent, clearly visible from

the rear. If an LED brake light is used, it must be clearly visible in very bright sunlight.

B7.4.2 This light must be mounted between the wheel centerline and driver's shoulder level vertically and approximately on vehicle centerline laterally.

13.4 Appendix C: MATLAB Tyre Data Treatment

The full MATLAB code used to produce the tyre diagrams throughout the report are shown below. The coding was relatively simple and inefficient, representing the limited programming skills of the author:

```
clear all

%Load free rolling data file
load('B1320run18')

%The following loop generates an array of normal loads, approximating the
%measured normal loads from the test rig as the closest nominal applied
%load. This array is used as a signpost in other parts of the code, so
%the data can be grouped as needed

NominalFZ=zeros(size(FZ));
lb_N=0.45359237*9.8;
for counter2=1:size(FZ)
    check50=sqrt((50*lb_N+FZ(counter2))^2);
    check100=sqrt((100*lb_N+FZ(counter2))^2);
    check150=sqrt((150*lb_N+FZ(counter2))^2);
    check250=sqrt((250*lb_N+FZ(counter2))^2);
    check350=sqrt((350*lb_N+FZ(counter2))^2);
    closest=min([check50 check100 check150 check250 check350]);
    if closest==check50, NominalFZ(counter2)=50*lb_N;
        elseif closest==check100, NominalFZ(counter2)=100*lb_N;
            elseif closest==check150, NominalFZ(counter2)=150*lb_N;
                elseif closest==check250,
NominalFZ(counter2)=250*lb_N;
                    elseif closest==check350,
NominalFZ(counter2)=350*lb_N;
                        end
                    end
                end
            end
        end
    end

%Same function as the previous loop, this time for inclination angle

NominalIA=zeros(size(IA));
for counter3=1:size(IA)
    check0=sqrt((0-IA(counter3))^2);
    check1=sqrt((1-IA(counter3))^2);
    check2=sqrt((2-IA(counter3))^2);
    check3=sqrt((3-IA(counter3))^2);
    check4=sqrt((4-IA(counter3))^2);
    closest=min([check0 check1 check2 check3 check4]);
    if closest==check0, NominalIA(counter3)=0;
        elseif closest==check1, NominalIA(counter3)=1;
            elseif closest==check2, NominalIA(counter3)=2;
                elseif closest==check3, NominalIA(counter3)=3;
                    elseif closest==check4, NominalIA(counter3)=4;
                        end
                    end
                end
            end
        end
    end

%Arrays are initialised as empty arrays; their size will not be known
until the next loop is executed.
```

Final Year Project 2011
Final Report

```
FY_FZ50=[];
FY_FZ100=[];
FY_FZ150=[];
FY_FZ250=[];
FY_FZ350=[];
SA_FZ50=[];
SA_FZ100=[];
SA_FZ150=[];
SA_FZ250=[];
SA_FZ350=[];
FZ_FZ50=[];
FZ_FZ100=[];
FZ_FZ150=[];
FZ_FZ250=[];
FZ_FZ350=[];

%The following loop sorts the data according to normal load, forming
%new arrays with names including normal load labels

for counter5=1:size(SA)
    if NominalIA(counter5)==2
        if NominalFZ(counter5)==50*lb_N
            SA_FZ50(size(SA_FZ50)+1)=SA(counter5);
            FY_FZ50(size(FY_FZ50)+1)=FY(counter5);
            FZ_FZ50(size(FZ_FZ50)+1)=FZ(counter5);
        elseif NominalFZ(counter5)==100*lb_N
            SA_FZ100(size(SA_FZ100)+1)=SA(counter5);
            FY_FZ100(size(FY_FZ100)+1)=FY(counter5);
            FZ_FZ100(size(FZ_FZ100)+1)=FZ(counter5);
        elseif NominalFZ(counter5)==150*lb_N
            SA_FZ150(size(SA_FZ150)+1)=SA(counter5);
            FY_FZ150(size(FY_FZ150)+1)=FY(counter5);
            FZ_FZ150(size(FZ_FZ150)+1)=FZ(counter5);
        elseif NominalFZ(counter5)==250*lb_N
            SA_FZ250(size(SA_FZ250)+1)=SA(counter5);
            FY_FZ250(size(FY_FZ250)+1)=FY(counter5);
            FZ_FZ250(size(FZ_FZ250)+1)=FZ(counter5);
        elseif NominalFZ(counter5)==350*lb_N
            SA_FZ350(size(SA_FZ350)+1)=SA(counter5);
            FY_FZ350(size(FY_FZ350)+1)=FY(counter5);
            FZ_FZ350(size(FZ_FZ350)+1)=FZ(counter5);
        end
    end
end

%The following section fits a magic formula curve to each set of
%normal loads, slip angles and resultant forces. For each fit, the
%code extracts peak forces, corresponding angles and cornering
%stiffnesses

%Forms an evenly spaced array for use in fitting
SlipArray=-13:0.01:13;
%Increases the number of iterations allowed in the fitting function;
%the default value is too low
options = optimset('MaxFunEvals',10^10, 'MaxIter', 10^10);
```

Final Year Project 2011
Final Report

```
%The fminsearch function attempts to minimise the square of the
residuals in the external function "PacejkaUnknowns";
%Symm_Coeff are the four coefficients needed to define the magic
%formula that is symmetrical about the x and y axes. Shift_Coeff
%have to be found separately, as fminsearch produces poor fits with
%more than four degrees of freedom. Initial guesses are all 1 and 0,
%then the output from each fit is carried over to the next normal
%load - this improves the output.

Symm_Coeff=fminsearch(@PacejkaUnknowns,[1 1 1 1], options,
FY_FZ50,SA_FZ50);
Shift_Coeff=fminsearch(@PacejkaShift,[0
0],options,Symm_Coeff,FY_FZ50,SA_FZ50);
%Applies the coefficients to the magic formula, giving a fitted
%array
Fitted_50=Symm_Coeff(3)*sin(Symm_Coeff(2)*atan(Symm_Coeff(1)*(1-
Symm_Coeff(4))*(SlipArray-
Shift_Coeff(1))*(pi/180)+(Symm_Coeff(4)/Symm_Coeff(1))*atan(Symm_Coeff(1)*(Sl
ipArray-Shift_Coeff(1))*(pi/180))))+Shift_Coeff(2);
%Finds the cornering stiffness as the gradient at zero slip angle
CStiff_50=abs((Fitted_50(ceil(max(size(SlipArray))/2))-
Fitted_50(ceil(max(size(SlipArray))/2)-1))/(SlipArray(2)-SlipArray(1)));
[Peak_50,CorrSlipID]=max(Fitted_50);
CorrSlip_50=SlipArray(CorrSlipID);
MuY_50=Peak_50/(50*lb_N);

Symm_Coeff=fminsearch(@PacejkaUnknowns,Symm_Coeff, options,
FY_FZ100,SA_FZ100);
Shift_Coeff=fminsearch(@PacejkaShift,[0
0],options,Symm_Coeff,FY_FZ100,SA_FZ100);
Fitted_100=Symm_Coeff(3)*sin(Symm_Coeff(2)*atan(Symm_Coeff(1)*(1-
Symm_Coeff(4))*(SlipArray-
Shift_Coeff(1))*(pi/180)+(Symm_Coeff(4)/Symm_Coeff(1))*atan(Symm_Coeff(1)*(Sl
ipArray-Shift_Coeff(1))*(pi/180))))+Shift_Coeff(2);
CStiff_100=abs((Fitted_100(ceil(max(size(SlipArray))/2))-
Fitted_100(ceil(max(size(SlipArray))/2)-1))/(SlipArray(2)-SlipArray(1)));
[Peak_100,CorrSlipID]=max(Fitted_100);
CorrSlip_100=SlipArray(CorrSlipID);
MuY_100=Peak_100/(100*lb_N);

Symm_Coeff=fminsearch(@PacejkaUnknowns,Symm_Coeff, options,
FY_FZ150,SA_FZ150);
Shift_Coeff=fminsearch(@PacejkaShift,[0
0],options,Symm_Coeff,FY_FZ150,SA_FZ150);
Fitted_150=Symm_Coeff(3)*sin(Symm_Coeff(2)*atan(Symm_Coeff(1)*(1-
Symm_Coeff(4))*(SlipArray-
Shift_Coeff(1))*(pi/180)+(Symm_Coeff(4)/Symm_Coeff(1))*atan(Symm_Coeff(1)*(Sl
ipArray-Shift_Coeff(1))*(pi/180))))+Shift_Coeff(2);
CStiff_150=abs((Fitted_150(ceil(max(size(SlipArray))/2))-
Fitted_150(ceil(max(size(SlipArray))/2)-1))/(SlipArray(2)-SlipArray(1)));
[Peak_150,CorrSlipID]=max(Fitted_150);
CorrSlip_150=SlipArray(CorrSlipID);
MuY_150=Peak_150/(150*lb_N);

Symm_Coeff=fminsearch(@PacejkaUnknowns,Symm_Coeff, options,
FY_FZ250,SA_FZ250);
```

Final Year Project 2011
Final Report

```

Shift_Coeff=fminsearch(@PacejkaShift,[0
0],options,Symm_Coeff,FY_FZ250,SA_FZ250);
Fitted_250=Symm_Coeff(3)*sin(Symm_Coeff(2)*atan(Symm_Coeff(1)*(1-
Symm_Coeff(4))*(SlipArray-
Shift_Coeff(1))*(pi/180)+(Symm_Coeff(4)/Symm_Coeff(1))*atan(Symm_Coeff(1)*(Sl
ipArray-Shift_Coeff(1))*(pi/180))))+Shift_Coeff(2);
CStiff_250=abs((Fitted_250(ceil(max(size(SlipArray))/2))-
Fitted_250(ceil(max(size(SlipArray))/2)-1)))/(SlipArray(2)-SlipArray(1)));
[Peak_250,CorrSlipID]=max(Fitted_250);
CorrSlip_250=SlipArray(CorrSlipID);
MuY_250=Peak_250/(250*lb_N);

Symm_Coeff=fminsearch(@PacejkaUnknowns,Symm_Coeff, options,
FY_FZ350,SA_FZ350);
Shift_Coeff=fminsearch(@PacejkaShift,[0
0],options,Symm_Coeff,FY_FZ350,SA_FZ350);
Fitted_350=Symm_Coeff(3)*sin(Symm_Coeff(2)*atan(Symm_Coeff(1)*(1-
Symm_Coeff(4))*(SlipArray-
Shift_Coeff(1))*(pi/180)+(Symm_Coeff(4)/Symm_Coeff(1))*atan(Symm_Coeff(1)*(Sl
ipArray-Shift_Coeff(1))*(pi/180))))+Shift_Coeff(2);
CStiff_350=abs((Fitted_350(ceil(max(size(SlipArray))/2))-
Fitted_350(ceil(max(size(SlipArray))/2)-1)))/(SlipArray(2)-SlipArray(1)));
[Peak_350,CorrSlipID]=max(Fitted_350);
CorrSlip_350=SlipArray(CorrSlipID);
MuY_350=Peak_350/(350*lb_N);

%Plots raw and fitted data for output
plot(SA_FZ50,FY_FZ50,'g.',SlipArray,Fitted_50,'r.', SA_FZ100,
FY_FZ100, 'g.',SlipArray, Fitted_100, 'c.',SA_FZ150,FY_FZ150,'g.',
SlipArray,Fitted_150,'m.',SA_FZ250,FY_FZ250,'g.',SlipArray,Fitted_250,'y.',SA
_FZ350,FY_FZ350,'g.',SlipArray,Fitted_350,'b.')

Load_Array=[50*lb_N 100*lb_N 150*lb_N 250*lb_N 350*lb_N];
Peak_Array=[Peak_50 Peak_100 Peak_150 Peak_250 Peak_350];
CorrSlip_Array=[CorrSlip_50 CorrSlip_100 CorrSlip_150 CorrSlip_250
CorrSlip_350];
CStiff_Array=[CStiff_50 CStiff_100 CStiff_150 CStiff_250 CStiff_350];
MuY_Array=[MuY_50, MuY_100, MuY_150, MuY_250, MuY_350];

%Removes all original data for the new file to be loaded
clear AMBTMP ET FX FY FZ IA MX MZ N NFX NFY P RE RL RST SA SL SR TSTC
TSTI TSTO V testid tireid
%Loads the combined brake/driving/cornering data file
load('Bl320run99')

%Sorts data for the second file
NominalFZ=zeros(size(FZ));
lb_N=0.45359237*9.8;
for counter2=1:size(FZ)
check50=sqrt((50*lb_N+FZ(counter2))^2);
check150=sqrt((150*lb_N+FZ(counter2))^2);
check250=sqrt((250*lb_N+FZ(counter2))^2);
check350=sqrt((350*lb_N+FZ(counter2))^2);
closest=min([check50 check150 check250 check350]);
if closest==check50, NominalFZ(counter2)=50*lb_N;

```

Final Year Project 2011
Final Report

```

        elseif closest==check150, NominalFZ(counter2)=150*lb_N;
        elseif closest==check250, NominalFZ(counter2)=250*lb_N;
        elseif closest==check350,
NominalFZ(counter2)=350*lb_N;
        end
    end

NominalIA=zeros(size(IA));
for counter3=1:size(IA)
check0=sqrt((0-IA(counter3))^2);
check2=sqrt((2-IA(counter3))^2);
check4=sqrt((4-IA(counter3))^2);
closest=min([check0 check2 check4]);
    if closest==check0, NominalIA(counter3)=0;
    elseif closest==check2, NominalIA(counter3)=2;
    elseif closest==check4, NominalIA(counter3)=4;
    end
end

NominalSA=zeros(size(SA));
for counter4=1:size(SA)
check0=sqrt((0+SA(counter4))^2);
check3=sqrt((3+SA(counter4))^2);
check6=sqrt((6+SA(counter4))^2);
closest=min([check0 check3 check6]);
    if closest==check0, NominalSA(counter4)=0;
    elseif closest==check3, NominalSA(counter4)=-3;
    elseif closest==check6, NominalSA(counter4)=-6;
    end
end

%This nested loop performs a magic formula curve fit for each
%combination of normal load, slip angle and inclination angle - 36
%in total.
m=1;
Symm_Coeff=[1 1 1 1];
for Nom_FZ=lb_N*[50 150 250 350]
    for Nom_IA=[0 2 4]
        for Nom_SA=[0 -3 -6]
            n=1;
            for dataIndex=1:size(SR)
                if NominalFZ(dataIndex)==Nom_FZ
                    if NominalIA(dataIndex)==Nom_IA
                        if NominalSA(dataIndex)==Nom_SA
                            FX_temp(n)=FX(dataIndex);
                            FY_temp(n)=FY(dataIndex);
                            SR_temp(n)=SR(dataIndex);
                            n=n+1;
                        end
                    end
                end
            end
            SlipArray=-0.2:0.0001:0.2;

            options = optimset('MaxFunEvals',10^10, 'MaxIter',
10^10);

```

Final Year Project 2011
Final Report

```

        Symm_Coeff=fminsearch(@PacejkaUnknowns,[Symm_Coeff],
options, FX_temp,SR_temp);
        Shift_Coeff=fminsearch(@PacejkaShift,[0
0],options,Symm_Coeff,FX_temp,SR_temp);

Fitted_FX=Symm_Coeff(3)*sin(Symm_Coeff(2)*atan(Symm_Coeff(1)*(1-
Symm_Coeff(4))*(SlipArray-
Shift_Coeff(1))*(pi/180)+(Symm_Coeff(4)/Symm_Coeff(1))*atan(Symm_Coeff(1)*(Sl
ipArray-Shift_Coeff(1))*(pi/180))))+Shift_Coeff(2);

        %The following if statement neglects the contribution
        %of lateral force if it represents less than 5% of the
        %maximum load at the spindle. Failing to do this can
        %generate FY curve fits with a single extreme peak,
        %skewing the results.

        if max(abs(FY_temp))>0.05*max(FX_temp)
            %Second order hyperbolic function is used to fit
            %the FY data, as this has all the necessary
            %features to match the data. The magic formula was
            %a very poor fit for FY in the combined case.
            Hyp_Coeff=fminsearch(@HyperbUnknowns,[1 1 1 1], options,
FY_temp,SR_temp);

Fitted_FY=1./(Hyp_Coeff(1)*SlipArray.^2+Hyp_Coeff(2)*SlipArray+Hyp_Coeff(3))+
Hyp_Coeff(4);
            else Fitted_FY=zeros(size(Fitted_FX));
            end

            %Plots the two curve fits
            plot(SR_temp, FY_temp, '.g',SlipArray,
Fitted_FY, '.b',SR_temp, FX_temp, '.c', SlipArray,
Fitted_FX, 'r.',SlipArray,sqrt(Fitted_FX.^2+Fitted_FY.^2), '.m')

            Fitted=sqrt(Fitted_FX.^2+Fitted_FY.^2);

            if Fitted(1)>Fitted(2)
                Peak_Force_Array_x(m)=Fitted_FX(1);
                Peak_Force_Array_y(m)=Fitted_FY(1);
                m=m+1;
            end

            for q=2:(max(size(Fitted))-1)
                if Fitted(q-1)<Fitted(q)
                    if Fitted(q+1)<Fitted(q)
                        Peak_Force_Array_x(m)=Fitted_FX(q);
                        Peak_Force_Array_y(m)=Fitted_FY(q);
                        m=m+1;
                    end
                end
            end

            if Fitted(max(size(Fitted)))>Fitted(max(size(Fitted))-1)
                Peak_Force_Array_x(m)=Fitted_FX(max(size(Fitted)));

```


Final Year Project 2011
Final Report

```

        Peak_Force_Array_y(m)=Fitted_FY(max(size(Fitted)));
        m=m+1;
    end

    pause(0.01);
    %Clears data so the arrays can be rebuilt with the next
    %combination of conditions
    clear FX_temp FY_temp SR_temp

end
end

%This if loop sorts peaks according to load, so the effect of
%normal load can be clearly seen on the friction ellipses
if Nom_FZ==50*lb_N
    Peak_Force_Array_x(m)=0;
    Peak_Force_Array_y(m)=max(Fitted_50);
    Peak_Force_Array_x_50=Peak_Force_Array_x;
    Peak_Force_Array_y_50=Peak_Force_Array_y;
    k_50=convhull(Peak_Force_Array_x_50,Peak_Force_Array_y_50);
elseif Nom_FZ==150*lb_N
    Peak_Force_Array_x(m)=0;
    Peak_Force_Array_y(m)=max(Fitted_150);
    Peak_Force_Array_x_150=Peak_Force_Array_x;
    Peak_Force_Array_y_150=Peak_Force_Array_y;

k_150=convhull(Peak_Force_Array_x_150,Peak_Force_Array_y_150);
elseif Nom_FZ==250*lb_N
    Peak_Force_Array_x(m)=0;
    Peak_Force_Array_y(m)=max(Fitted_250);
    Peak_Force_Array_x_250=Peak_Force_Array_x;
    Peak_Force_Array_y_250=Peak_Force_Array_y;

k_250=convhull(Peak_Force_Array_x_250,Peak_Force_Array_y_250);
elseif Nom_FZ==350*lb_N
    Peak_Force_Array_x(m)=0;
    Peak_Force_Array_y(m)=max(Fitted_350);
    Peak_Force_Array_x_350=Peak_Force_Array_x;
    Peak_Force_Array_y_350=Peak_Force_Array_y;

k_350=convhull(Peak_Force_Array_x_350,Peak_Force_Array_y_350);
end
m=1;

end

%Plots the friction ellipse
plot(Peak_Force_Array_y_50(k_50),Peak_Force_Array_x_50(k_50),'b.-
',Peak_Force_Array_y_50,Peak_Force_Array_x_50,'b.',Peak_Force_Array_y_150(k_1
50),Peak_Force_Array_x_150(k_150),'g.-
',Peak_Force_Array_y_150,Peak_Force_Array_x_150,'g.',Peak_Force_Array_y_250(k
_250),Peak_Force_Array_x_250(k_250),'r.-
',Peak_Force_Array_y_250,Peak_Force_Array_x_250,'r.',Peak_Force_Array_y_350(k
_350),Peak_Force_Array_x_350(k_350),'m.-
',Peak_Force_Array_y_350,Peak_Force_Array_x_350,'m.')

```

13.5 Appendix D: Wishbone Stress Calculations

The wishbones had to be designed against three failure modes; axial overload, buckling and bending failure. The axial stress in each tube is easily calculated from the axial force applied to tube (found using method in Appendix C and the tube geometry.

$$\sigma_A = F_A \cdot \frac{D_o^2 - D_i^2}{4I}$$

The bending moment causing the peak bending stress is the product of the vertical component of the push/pull rod load and the difference in y-coordinate of the push/pull rod and outboard wishbone point. Using the same notation as in appendix C,

$$M_{max} = F_{O,z} \cdot (L_{O,z} - P_{O,z})$$

$$\sigma_B = \frac{16 \cdot M_{MAX} \cdot D_o}{\pi(D_o^4 - D_i^4)}$$

This assumes that the bending stress is distributed equally between the two tubes. The tensile and compressive stresses caused by this bending load can be added directly to the axial stresses, ie

$$\sigma_{max} = \sigma_A + \sigma_B$$

This peak stress can then be compared to the yield stress of the material.

Each tube is considered safe with regards to buckling if the peak axial load is less than the limit imposed by the Euler buckling equation,

$$F_A < \frac{\pi^2 EI}{l^2}$$

$$F_A < \frac{\pi^3 E(D_o^4 - D_i^4)}{64((U_{O,x} - U_{F,x})^2 + (U_{O,y} - U_{F,y})^2 + (U_{O,z} - U_{F,z})^2)}$$

The full output of the spreadsheet based on these calculations is tabulated below. All outputs are given in terms of safety factor, to aid the decisionmaking process

	15.875	5/8						
<i>Front Upper Fore</i>								
Length	356.22	<u>1.30</u>	<u>1.20</u>	<u>1.10</u>	<u>1.00</u>	<u>0.89</u>	<u>0.80</u>	<u>0.70</u>
Weight		165.39	153.72	141.87	129.84	116.41	105.27	92.72
I		1593.20	1499.24	1400.99	1298.34	1180.18	1079.30	962.65
Bending SF		1.27	1.19	1.12	1.03	0.94	0.86	0.77
Axial SF		5.98	5.56	5.13	4.70	4.21	3.81	3.35
Buckling SF		5.81	5.47	5.11	4.74	4.31	3.94	3.51

*Final Year Project 2011
Final Report*

Combined SF 1.05 0.98 0.92 0.85 0.77 0.70 0.62

15.875 **0.63**

*Front Upper
Aft*

Length	281.00	<u>1.30</u>	<u>1.20</u>	<u>1.10</u>	<u>1.00</u>	<u>0.89</u>	<u>0.80</u>	<u>0.70</u>
Weight		130.47	121.26	111.91	102.43	91.83	83.04	73.14
I		1593.20	1499.24	1400.99	1298.34	1180.18	1079.30	962.65
Bending SF		1.27	1.19	1.12	1.03	0.94	0.86	0.77
Axial SF		22.30	20.72	19.13	17.51	15.70	14.19	12.50
Buckling SF		34.81	32.76	30.61	28.37	25.79	23.58	21.03
Combined SF		1.20	1.13	1.05	0.98	0.89	0.81	0.72

15.875 **0.63**

Front Lower Fore

Length	459.15	<u>1.30</u>	<u>1.20</u>	<u>1.10</u>	<u>1.00</u>	<u>0.89</u>	<u>0.80</u>	<u>0.70</u>
Weight		213.18	198.13	182.86	167.36	150.05	135.69	119.52
I		1593.20	1499.24	1400.99	1298.34	1180.18	1079.30	962.65
Bending SF		0.00	0.00	0.00	0.00	0.00	0.00	0.00
Axial SF		5.36	4.98	4.60	4.21	3.77	3.41	3.00
Buckling SF		5.99	5.64	5.27	4.88	4.44	4.06	3.62

15.875 **0.63**

*Front Lower
Aft*

Length	423.00	<u>1.30</u>	<u>1.20</u>	<u>1.10</u>	<u>1.00</u>	<u>0.89</u>	<u>0.80</u>	<u>0.70</u>
Weight		196.40	182.53	168.46	154.18	138.24	125.01	110.11
I		1593.20	1499.24	1400.99	1298.34	1180.18	1079.30	962.65
Bending SF		0.00	0.00	0.00	0.00	0.00	0.00	0.00
Axial SF		4.57	4.25	3.92	3.59	3.22	2.91	2.56
Buckling SF		3.15	2.96	2.77	2.56	2.33	2.13	1.90

15.875 **0.63**

*Rear Upper
Fore*

Length	561.37	<u>1.30</u>	<u>1.20</u>	<u>1.10</u>	<u>1.00</u>	<u>0.89</u>	<u>0.80</u>	<u>0.70</u>
Weight		260.64	242.25	223.57	204.62	183.46	165.90	146.12
I		1593.20	1499.24	1400.99	1298.34	1180.18	1079.30	962.65
Bending SF		14.45	13.60	12.71	11.78	10.71	9.79	8.73
Axial SF		17.83	16.57	15.29	14.00	12.55	11.35	10.00
Buckling SF		6.97	6.56	6.13	5.68	5.17	4.72	4.21
Combined SF		7.98	7.47	6.94	6.40	5.78	5.26	4.66

Final Year Project 2011
Final Report

15.875	0.63							
<i>Rear Upper Aft</i>								
Length	254.28	<u>1.30</u>	<u>1.20</u>	<u>1.10</u>	<u>1.00</u>	<u>0.89</u>	<u>0.80</u>	<u>0.70</u>
Weight		118.06	109.73	101.27	92.68	83.10	75.14	66.19
I		1593.20	1499.24	1400.99	1298.34	1180.18	1079.30	962.65
Bending SF		14.45	13.60	12.71	11.78	10.71	9.79	8.73
Axial SF		9.82	9.13	8.43	7.71	6.91	6.25	5.51
Buckling SF		97.25	91.51	85.52	79.25	72.04	65.88	58.76
Combined SF		5.85	5.46	5.07	4.66	4.20	3.82	3.38

15.875	0.63							
<i>Rear Lower Fore</i>								
Length	595.96	<u>1.30</u>	<u>1.20</u>	<u>1.10</u>	<u>1.00</u>	<u>0.89</u>	<u>0.80</u>	<u>0.70</u>
Weight		276.70	257.17	237.34	217.23	194.76	176.12	155.13
I		1593.20	1499.24	1400.99	1298.34	1180.18	1079.30	962.65
Bending SF		3.61	3.40	3.18	2.94	2.68	2.45	2.18
Axial SF		21.17	19.68	18.16	16.62	14.90	13.48	11.87
Buckling SF		7.35	6.92	6.46	5.99	5.44	4.98	4.44
Combined SF		3.09	2.90	2.70	2.50	2.27	2.07	1.84

15.875	0.63							
<i>Rear Lower Aft</i>								
Length	343.55	<u>1.30</u>	<u>1.20</u>	<u>1.10</u>	<u>1.00</u>	<u>0.89</u>	<u>0.80</u>	<u>0.70</u>
Weight		159.51	148.25	136.82	125.23	112.28	101.53	89.43
I		1593.20	1499.24	1400.99	1298.34	1180.18	1079.30	962.65
Bending SF		3.61	3.40	3.18	2.94	2.68	2.45	2.18
Axial SF		7.70	7.16	6.61	6.05	5.42	4.90	4.32
Buckling SF		8.05	7.57	7.08	6.56	5.96	5.45	4.86
Combined SF		2.46	2.30	2.15	1.98	1.79	1.63	1.45

19.05	3/4							
<i>Front Upper Fore</i>								
Length	356.22	<u>1.30</u>	<u>1.20</u>	<u>1.10</u>	<u>1.00</u>	<u>0.89</u>	<u>0.80</u>	<u>0.70</u>
Weight		201.42	186.97	172.35	157.56	141.08	127.44	112.12
I		2870.26	2692.24	2507.69	2316.45	2098.16	1913.25	1700.97
Bending SF		1.90	1.79	1.66	1.54	1.39	1.27	1.13
Axial SF		7.29	6.76	6.23	5.70	5.10	4.61	4.06
Buckling SF		10.47	9.82	9.15	8.45	7.65	6.98	6.21
Combined SF		1.51	1.41	1.31	1.21	1.09	1.00	0.88

19.05 **0.75**

Final Year Project 2011
Final Report

Front Upper
 Aft

Length	281.00	<u>1.30</u>	<u>1.20</u>	<u>1.10</u>	<u>1.00</u>	<u>0.89</u>	<u>0.80</u>	<u>0.70</u>
Weight		158.89	147.49	135.96	124.29	111.29	100.53	88.45
I		2870.26	2692.24	2507.69	2316.45	2098.16	1913.25	1700.97
Bending SF		1.90	1.79	1.66	1.54	1.39	1.27	1.13
Axial SF		27.16	25.21	23.24	21.24	19.02	17.18	15.12
Buckling SF		62.72	58.83	54.79	50.61	45.85	41.80	37.17
Combined SF		1.78	1.67	1.55	1.43	1.30	1.18	1.05

19.05 **0.75**

Rear Lower
 Fore

Length	595.96	<u>1.30</u>	<u>1.20</u>	<u>1.10</u>	<u>1.00</u>	<u>0.89</u>	<u>0.80</u>	<u>0.70</u>
Weight		336.98	312.81	288.35	263.59	236.03	213.21	187.58
I		2870.26	2692.24	2507.69	2316.45	2098.16	1913.25	1700.97
Bending SF		5.42	5.09	4.74	4.38	3.96	3.61	3.21
Axial SF		25.78	23.93	22.06	20.17	18.06	16.31	14.35
Buckling SF		13.24	12.42	11.57	10.68	9.68	8.82	7.85
Combined SF		4.48	4.19	3.90	3.60	3.25	2.96	2.63

19.05 **0.75**

Rear Lower Aft

Length	343.55	<u>1.30</u>	<u>1.20</u>	<u>1.10</u>	<u>1.00</u>	<u>0.89</u>	<u>0.80</u>	<u>0.70</u>
Weight		194.26	180.33	166.22	151.95	136.06	122.91	108.14
I		2870.26	2692.24	2507.69	2316.45	2098.16	1913.25	1700.97
Bending SF		5.42	5.09	4.74	4.38	3.96	3.61	3.21
Axial SF		9.38	8.71	8.03	7.34	6.57	5.94	5.22
Buckling SF		14.50	13.60	12.67	11.70	10.60	9.66	8.59
Combined SF		3.44	3.21	2.98	2.74	2.47	2.25	1.99

25.4 **1**

Front Upper Fore

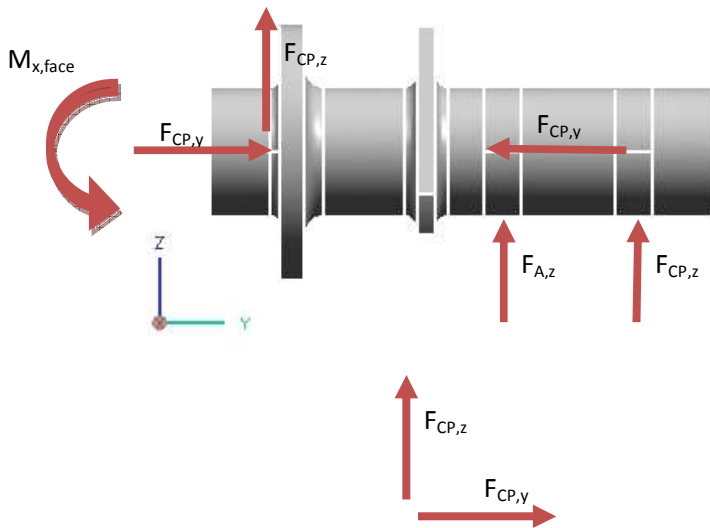
Length	356.22	<u>1.30</u>	<u>1.20</u>	<u>1.10</u>	<u>1.00</u>	<u>0.89</u>	<u>0.80</u>	<u>0.70</u>
Weight		273.47	253.49	233.32	212.98	190.41	171.78	150.92
I		7166.65	6695.05	6210.98	5714.24	5152.90	4681.82	4145.70
Bending SF		3.57	3.33	3.09	2.84	2.56	2.33	2.06
Axial SF		9.89	9.17	8.44	7.70	6.89	6.21	5.46
Buckling SF		26.14	24.42	22.66	20.85	18.80	17.08	15.12

Final Year Project 2011
Final Report

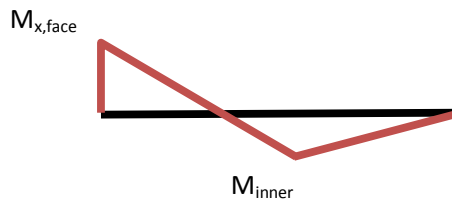
Combined SF		2.62	2.44	2.26	2.08	1.87	1.69	1.50
	25.40	1.00						
Front Upper								
Aft								
Length	281.00	<u>1.30</u>	<u>1.20</u>	<u>1.10</u>	<u>1.00</u>	<u>0.89</u>	<u>0.80</u>	<u>0.70</u>
Weight		215.73	199.96	184.06	168.01	150.21	135.51	119.06
I		7166.65	6695.05	6210.98	5714.24	5152.90	4681.82	4145.70
Bending SF		3.57	3.33	3.09	2.84	2.56	2.33	2.06
Axial SF		36.87	34.18	31.46	28.71	25.67	23.16	20.35
Buckling SF		156.59	146.29	135.71	124.86	112.59	102.30	90.58
Combined SF		3.25	3.04	2.81	2.59	2.33	2.12	1.87

13.6 Appendix E: Hub Calculations

To find the loading on each bearing and the maximum stress in the hub, the load from the contact patch must be analysed in two planes. In the x-z plane,



The bending moment diagram will take the shape



For this geometry, the larger bending moment is always found at the hub face. The maximum resulting stress is

The axial stress can be added directly to this peak value,

This can be repeated in the x-y plane, and the results added trigonometrically to determine a peak total stress.

13.7 Appendix F: Brake Calculations

Measuring the effect of different pedal ratios, master cylinders, calipers and rotors is relatively straightforward. The brake system is a simple hydraulic circuit.

The distribution of the force applied by the pedal to the brake master cylinders is determined by the position of the brake master cylinder. This is quantified here as B, representing the percentage front brake bias.

$$F_{master,front} = F_{pedal} \cdot \frac{B}{100}, \quad F_{master,rear} = F_{pedal} \cdot \frac{(1 - B)}{100}$$

$$P = \frac{F_{master}}{A_{master}}$$

$$F_{piston} = P \cdot A_{piston}$$

This gives the force applied by each piston in the caliper. There are two possible arrangements for the piston; single or double sided. For the case of a single sided caliper, the clamping force is equivalent to the piston force multiplied by the number of pistons. For a double sided caliper, the clamping force is half this value. It's easy to overlook that the brake force is applied to both sides of the caliper. Continuing for a dual sided caliper,

$$F_{clamp} = \frac{n_{pistons} \cdot F_{piston}}{2}$$

$$T_{rotor} = 2 \cdot F_{clamp} \cdot r_{mid} \cdot \mu_{pad}$$

$$F_{cp} = \frac{T_{rotor}}{r_{wheel}}$$

Where T_{rotor} is the torque applied to the rotor by the system, r_{mid} is the mid rotor radius, μ_{pad} is the pad/rotor coefficient of friction, and F_{cp} is the force applied to the road at the tyre contact patch. This value can be compared to the maximum force that the contact patch can generate, the product of the normal load on the tyre and the tyre's coefficient of friction. The result is a measure of how close each wheel is to locking.